APPLYING TWO-DIMENSIONAL KALMAN FILTERING TECHNIQUES TO DIGITAL ELEVATION MODELS FOR TERRAIN SURFACE MODELLING

PING WANG

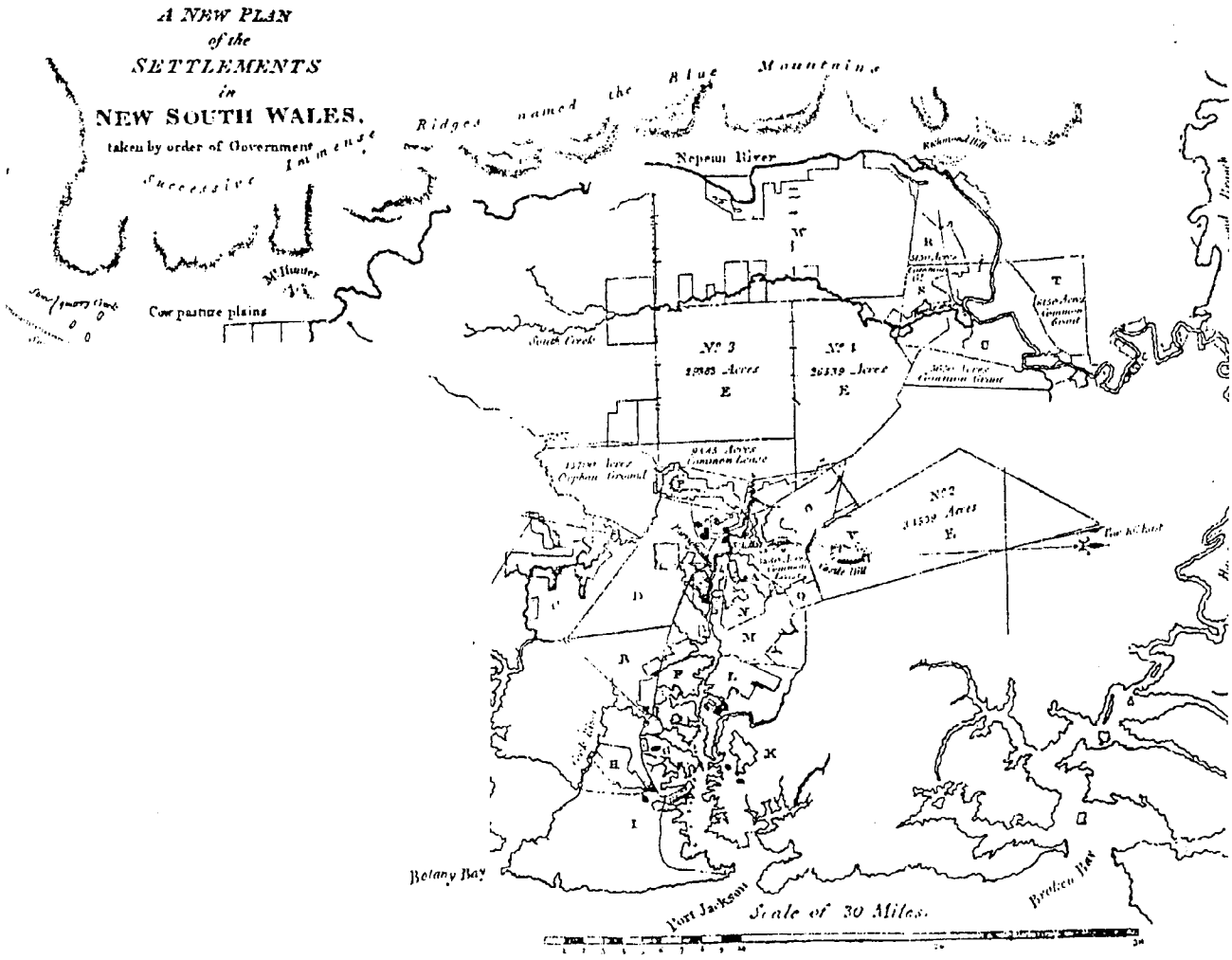

UNISURV S-67, 2001

Reports from

SCHOOL OF SURVEYING
AND SPATIAL INFORMATION SYSTEMS

THE UNIVERSITY OF NEW SOUTH WALES UNSW SYDNEY NSW 2052 AUSTRALIA

UNISURV REPORT S-67, 2001

APPLYING TWO-DIMENSIONAL KALMAN FILTERING TECHIQUES TO DIGITAL ELEVATION MODELS FOR TERRAIN SURFACE MODELLING

PING WANG

Received: October 2001
Accepted: November 2001

SCHOOL OF SURVEYING AND SPATIAL INFORMATION SYSTEMS
(formerly GEOMATIC ENGINEERING)
UNIVERSITY OF NEW SOUTH WALES
UNSW SYDNEY NSW 2052
AUSTRALIA

UNISURV REPORTS

Series Editor: Dr. J. M. Rüeger

National Library of Australia

Card No. and ISBN 0 - 7334 - 1857 - 0

FOREWORD

The determination of digital elevation models has been a continuing research topic in the area of photogrammetry and remote sensing at UNSW for a number of years, including image matching on satellite images and aerial photography. The results of these studies and others undertaken elsewhere, have demonstrated that there are residual errors in the elevations determined by these methods, that can only be eliminated by manual intervention. A more automatic method of locating and filtering the errors in the data is desirable. In addition, since many DEMs used for terrain modelling by geographers and land specialists are derived from various sources, such as digitising maps and secondary processing of photogrammetric data, these DEMs are often subject to systematic errors that lead to so-called 'sinks' and 'mounds' in the data. Methods of overcoming these errors are often only marginally unsuccessful.

To overcome these problems, Dr Ping Wang has developed unique methods of filtering and smoothing DEM data based on a two-dimensional Kalman filtering algorithm for her PhD thesis, jointly within the Schools of Geography and Surveying and Spatial Information Systems. Since the theory of Kalman filtering is primarily based on a one-dimensional algorithm, she had to develop new algorithms and procedures to implement a Kalman filter for the two-dimensional DEM data. The procedures have led to efficient methods of filtering and smoothing DEM data, as well as error detection and correction. The results of tests using this algorithm have been very favourably compared with other algorithms commonly used for the filtering of DEM data for terrain modelling.

This thesis is a contribution to the research on an intelligent procedure for DEM determination from satellite and aerial images, funded by the Australian Research Council, and being undertaken jointly by Professor Trinder (UNSW) and Professor Kurt Kubik from the University of Queensland.

Em. Professor John Trinder
November 2001

ABSTRACT

Digital Elevation Models (DEMs) have been increasingly used to model topographic characteristics of the terrain surface in geographical, hydrological, and biological studies. Elevation information, together with the first and second order partial derivatives of the elevation derived from a DEM, are the most important terrain variables for terrain modelling. In this thesis, a new method of applying a two-dimensional (2-D) Kalman filtering technique over a grid DEM for terrain surface modelling is developed consisting of three major components: the 2-D Kalman filter, the method for DEM outlier detection and removal, and a 2-D Kalman smoother.

The 2-D Kalman filter establishes dynamic and functional models for a grid DEM to produce optimal estimates of terrain attributes of a DEM point using the relevant DEM observations, and the predictions derived from its orthogonal neighbouring DEM points. This 2-D recursive process is shown to be ideal for handling DEM random noise during the terrain modelling process. The method for DEM outlier detection and removal is an extra function that is added to the 2-D Kalman filter developed in this research. It uses the dispersions between the predicted estimates of elevation and the relevant elevation observations to detect outliers. These are removed by amplifying the relevant observation variance of that point while deriving the updated estimates of elevation in the 2-D Kalman filtering process. The reliability of outlier detection relates to the level of confidence selected. It is suitable for applications in smooth terrain surfaces where the accuracy of the predictions of elevations is high. The 2-D Kalman smoother is a linear combination of four 2-D Kalman filtering results, derived on the basis of different orientations, that further improves the accuracy of the 2-D Kalman filtering process.

The methods are applied experimentally on a simulated and a real world DEM. The results show that the 2-D Kalman filtering algorithm developed in this research is capable of detecting and removing DEM outliers with a high degree of accuracy and reliability, and is more efficient in reducing the effect of DEM random noise, compared to the commonly used terrain modelling methods.

TABLE OF CONTENTS

LIST OF TABLES

Table

LIST OF FIGURES

Figure

ACKNOWLEDGEMNETS

My supervisor, Professor John C. Trinder, School of Geomatic Engineering, first introduced me to the topic of the Digital Elevation Models and photogrammetry. His advice and suggestions throughout four and half years were of invaluable help in improving my work and developing a thorough understanding of the topic. I would like to thank him for his guidance and also for his efforts in procuring financial support during my studies.

Professor Barry Garner, School of Geography, has acted as a second supervisor since August 1997. Since then he has offered critical and valuable suggestions for improving this thesis and I am very grateful for his advice on research strategies and particularly for his help in editing drafts.

Professor Andrew Skidmore, now with ITC in the Netherlands, was my first supervisor in the School of Geography from March to June 1996. Professor Skidmore initially introduced me to terrain modelling. He was at the time working together with Professor Trinder on an Australian Research Council funded research project. I would like to thank him for his encouragement and assistance while he was at UNSW.

Professor Qiming Zhou, now at the Hong Kong Baptist University, assumed responsibility as my supervisor in the School of Geography for the period July 1996 to July 1997. His expertise in hydrological models and drainage patterns had an important influence on my work. I thank him for sharing his experiences with me and for helping me formulate my ideas while he was at UNSW.

I would like to thank the Faculty of Applied Science, UNSW, for awarding me an Overseas Postgraduate Research Scholarship and additional scholarship moneys that enabled me to study at UNSW. I also thank the many friends, colleagues, and staff in the Schools of Geography and Geomatic Engineering for their friendship, help and kindness. Special thanks are given to Mr. Brian Donnelly, School of Geomatic

Engineering, and Mr. John Owen and Mr. Yanni Zakaria, School of Geography for their technical support during the last four and half years.

Last, but not least, my deepest appreciation is given to my family, especially my parents, my parents-in-law, my son Jeff and baby daughter Jenny, for their love, encouragement and understanding during my studies. Finally, I especially thank my husband, Dr. Shaowei Han, Senior Lecturer in the School of Geomatic Engineering, for his unfailing support and valuable suggestions on the development of the 2-D Kalman filtering algorithm.

CHAPTER 1

INTRODUCTION

1.1 Digital Elevation Models (DEMs)

The morphology of the surface of the earth plays an important role in understanding the physical, chemical, and biological processes that occur within the landscape. The shape of the terrain influences many phenomena of the physical environment, such as the flow of surface water, transport of sediment and pollutants, climate both at local and regional scales, as well as nature and distribution of plants and animals, and the migration pattern of many animal species (Blaszczynski 1997). Knowledge of terrain morphology is also important for many engineering or land-management endeavors that affect or disturb the surface of the land.

The morphology of a terrain surface is defined directly by the relief of the terrain. In the digital domain, terrain relief is represented as Digital Elevation Models (DEMs), which have been extensively studied for more than three decades in photogrammetry (Ackermann 1994). Grid-structured DEMs are widely applied in different fields, which are also chosen as the default DEM format of this thesis. Grid DEMs can be generated from contour maps, photogrammetric stereo models, and other active remote sensing systems, such as radar and laser scanners. Among the existing DEM generation approaches, the conventional analytical photogrammetric method is a standard procedure with high quality standards (Ackermann 1994). Advanced digital photgrammetric methods, based on Digital Photogrammetric Workstation (DPW), can now produce highly accurate elevations.

Researchers have become increasingly concerned with the use of grid DEMs for automatically modelling terrain features, such as slope and aspect (Hodgson 1995, Bolstad and Stowe 1994, Skidmore 1989), topographic features (Lee 1994), radiance and

hillshading (Giles and Franklin 1996, Lapen and Martz 1993, Zhou 1992), soil wetness (O'Loughlin 1986), surface/volume approximation (Kalmar *et al* 1995), accuracy assessment (Rieger 1996, Wolock and McCade 1995, Kraus 1994, Freeman 1991), valley/ridge identification (Tribe 1991, Haralick 1983), drainage basin delineation (Freeman 1991, Lammers and Band 1990, Martz and Jong 1988, Mark 1984), and drainage network extraction (Meisels *et al* 1995, Holmgren 1994, Martz and Garbrecht 1992, Chorowicz *et al* 1992, Quinn *et al* 1991, Qian *et al* 1990, Smith *et al* 1990, Seemuller 1990, Band 1986, O'Callaghan and Mark 1984).

The modelling of terrain surface by DEMs has gradually evolved into a major constituent of Geographical Information Systems (GIS) technology (Brändli 1996). In conjunction with the two dimensional functions of a GIS, the integration of digital terrain modelling (DTM) and GIS provides a powerful and flexible basis for the display, analysis, and modelling of phenomena related to the topography of terrain surfaces.

1.2 Terrain Surface Modelling

Automated extraction of new information from grid DEMs, i.e. terrain surface modelling techniques, has achieved three levels of complexity in current GIS (Blaszczynski 1997). The first and fundamental level of terrain surface modelling is to compute terrain topographic attributes, such as slope and aspect, from DEM data. These attributes can be used as geomorphological parameters for environmental studies. The second level is to delineate watershed boundaries or steepest flow paths over the terrain surface of DEM mapping area. The modelling at this level is generally based on the further analysis of terrain topography and geometry, and usually does not need additional information other than the DEM. A third level of terrain surface modelling undertaken in GIS is to integrate the first and second level of terrain surface modelling with other parameters to further model the relevant geomorphological processes, which occur over the landscape.

However, it is not a simple task to monitor terrain topographic attributes from DEMs, since it uses discretely grid-structured data to model the continuity of real landscapes.

Although digital terrain modelling using grid DEMs has been studied more than two decades, there are still significant limitations in the terrain modelling methods developed to date. Some of these are:

- they use deterministic terrain models, and do not count the errors that the models may generate;

- they use a fix-sized modelling window, such as 3 by 3 or 2 by 2 window, for digital terrain modelling, and this cannot be changed for different types of landscapes.

- they use limited DEM measurements (up to 9 measurements) to derived the relevant terrain topographic attributes of each DEM point, no matter how large the DEM data set is, and this is inefficient in reducing the effect of DEM random errors, and

- none of the existing terrain modelling methods, to the author's knowledge, have developed procedures for DEM outlier detection and removal.

In summary, the limitations arise mainly from an insufficient understanding of terrain topographic characteristics defined by discrete grid DEMs, and the lack of the theoretical means to systematically process DEMs to generate accurate terrain topographic attributes.

1.3 The Kalman Filtering Technique

Kalman filtering is a linear estimator suitable for random process (Kalman 1960). A Kalman filter for a particular application is developed based on a so-called dynamic model, and functional model. Kalman filters use a stochastic model to model the unknown parameters of a random process between adjacent neighbours. The dynamic model established in a Kalman filter is able to generate the predictions of the unknown parameters. These predictions are used as another source of information, other than the observations, to produce the optimal estimates of the random process. Furthermore, the Kalman filter is a recursive process. All the predictions and the observations of the

processed points of the random process are used for the processing of the next DEM point to be processed. Or in another words, besides the adjacent processed points, the filter uses all previously processed points to derive the optimal estimates of the point being processed, with unequal importance, which is controlled by their variance-covariance factors. The contributions from closer neighbouring points would be greater than those from remote points, where the correlation is weak. Kalman filters can also be applied in vector form with multiple unknown parameters. The scalar Kalman filtering is only a special case of a Kalman filter. It is able to handle large data sets in an efficient way through its recursive process. In addition, it is capable of providing the variance-covariance information for the processing, which can be used for further error analysis. That is why the Kalman filter has been widely and successfully adopted in different disciplines for on-line (real-time) or off-line random processes since its introduction.

1.4 Aims and Objectives

Applying Kalman filtering techniques on grid DEMs for terrain surface modelling may overcome the shortcomings of the current DTM techniques in the following respects:

- The terrain modelling method will be based on a stochastic rather than a deterministic model. In this way, the terrain model will be less affected by errors in DEM observations, as well as the differences in the terrain model itself;

- The terrain modelling methods will not be limited to a certain fix-sized modelling window, such as 3 by 3 window, instead it will use the whole DEM as an observation sequence of a random process;

- The derived terrain topographic attributes will be the optimal estimates of the relevant random process by minimizing DEM observation errors and model errors in the sense of minimum-mean-square-error.

- It would be possible to introduce other statistical tools for DEM outlier detection and removal during the terrain modelling process. At each DEM point, the *a priori*

estimates of terrain attributes are generated by the Kalman filtering, as well as the associated variance-covariance matrix of the estimates. It is possible to establish a test statistic for DEM outlier detection and develop the relevant removal procedures;

- The use of Kalman filtering techniques in terrain surface modelling permits a recursive computing process, which would be significant for handling DEMs for terrain modelling applications.

- Using DEMs for terrain surface modelling is often an off-line process, so theoretically there are no processing limitations as occur for Kalman real-time applications. If a Kalman smoother was developed, it will be possible to use all DEM measurements to derive the terrain attributes for each DEM point. Therefore, the efficiency of DEM random error treatment would therefore be greatly improved.

The innovative use of Kalman filtering techniques on grid DEMs for terrain surface modelling therefore will overcome the limitations of current terrain models, and create more accurate and reliable terrain topographic attributes.

1.5 Methodology

However, the application of Kalman filtering techniques on DEMs for terrain modelling is a challenge, since it has not been applied in terrain surface modelling. In addition, from the aspect of the Kalman filtering techniques, it involves the development of a method of Kalman filtering in two-dimensions.

The key problems in the development of 2-D Kalman filters for terrain modelling are the establishment of a stochastic terrain model, and a truly recursive process over the 2-D DEMs. In this study, the elevation, and two first partial derivatives of elevation along the two orthogonal axes of a DEM were chosen as the topographic attributes to be determined from a DEM. The stochastic terrain model, which is also used as the dynamic model of the Kalman filtering, is formed as a linear function of the three terrain attributes between the adjacent DEM points. The observations at each point are assumed to be

linear in terms of terrain attributes to form the functional model. Based on the dynamic and the functional models, particular 2-D Kalman recursive equations will be developed, which consists of more than five equations to make it suitable for applications in terrain modelling.

The method for DEM outlier detection and removal will be developed based on the relevant results of the 2-D Kalman filter and the detection theory in statistics. The method will detect outliers based on the differences between the *a priori* estimates of elevation of a DEM and the relevant DEM observations. The binary hypothesis testing and the Neyman-Pearson strategy will be used to investigate the reliability of outlier detection. If an outlier is detected, the algorithm will remove the effect of the outlier by generating the estimate of elevation of the DEM point using mainly the prediction.

The developed 2-D Kalman smoother is a linear combination of four Kalman filtering results, which is applied over the same DEM at four different orientations. This algorithm enables the use of the full DEM to estimate terrain attributes of a single DEM point, and therefore further improve the accuracy of the derivation of terrain attributes.

1.6 Thesis Outline

This thesis consists of eight chapters.

Following the introduction, Chapter 2 reviews and compares current terrain surface modelling techniques using grid DEMs. The DEM acquisition techniques and products are summarized. The characteristics of DEM errors and their impact on DEM applications, the effect of DEM resolution on DEM applications are reviewed. The current terrain surface modelling techniques are compared, and their limitations are investigated.

Chapter 3 introduces the Kalman filtering techniques, including the theory of one-dimensional (1-D) Kalman filter for filtering and smoothing problems, a comparison of

Kalman filtering with the conventional least squares method, and the developed 2-D Kalman filter and its limitations.

Chapter 4 presents the first part of the development of the new 2-D Kalman filtering algorithm for terrain surface modelling. It covers the establishment of the dynamic and functional model of the 2-D Kalman filter, and the derivation of 2-D Kalman recursive equations. Computational considerations including the boundary conditions and the determination of stochastic models are also addressed. Experiments over the simulated terrain surfaces are described, and the relevant results are compared with those derived using other terrain models.

Chapter 5 presents the second part of the 2-D Kalman filtering algorithm, i.e. a method for DEM outlier detection and removal. A brief introduction of statistical hypothesis testing is given at the beginning of the Chapter. The method for outlier detection and removal is presented, and the reliability of outlier detection is further discussed in terms of internal and external reliability. Experimental results for outlier detection and removal are presented, followed by pertinent comparisons with other terrain models.

Chapter 6 presents the third part of the 2-D Kalman filtering algorithm, i.e. a Kalman smoother, based on the developments of Chapters 4 and 5. The results of the testing of the 2-D Kalman smoother are given, as well as a comparison of the smoothing results with the Kalman filtering results. A summary of the 2-D Kalman filtering algorithm for terrain surface modelling is presented.

Chapter 7 presents experimental results of the developed algorithm applied to real DEM data. The efficiency of DEM random noise reduction and outlier detection and removal of the 2-D Kalman filtering algorithm are investigated. The impacts of terrain characteristics and DEM resolution on the filtering or smoothing results are analysed.

Chapter 8 summarizes findings, draws conclusions, and makes recommendation on topics for further research. Some points related to the applications of the 2-D Kalman filtering

algorithm for terrain surface modelling using grid DEMs and further potential are also addressed.

1.7 Contributions

This is the first time that a digital signal processing technique, i.e. Kalman filtering, has been systematically applied to terrain surface modelling. This study develops a completely new approach to modelling terrain topographic attributes from grid-structured DEMs. The innovation of the 2-D Kalman filtering algorithm in terrain surface modelling exist not only in terrain surface modelling but also in the 2-D Kalman filtering technique.

- A new 2-D Kalman filtering algorithm for terrain modelling is developed. It establishes dynamic functional models over a grid DEM for terrain modelling, and develops a recursive process in two dimensions.

- The technique includes a function for DEM outlier detection and removal , which has not been addressed in the existing terrain modelling methods.

- A 2-D Kalman smoother is developed. The four-step filtering strategy developed in the smoother enables an effective establishment of a 2-D Kalman smoothing procedure that further improves the accuracy of the derivation of terrain topographic attributes.

CHAPTER 2

ACQUSITION AND APPLICATION OF DEMS FOR TERRAIN SURFACE MODELLING

2.1 DEM Acquisition and DEM Products

2.1.1 DEM acquisition

DEM data may be acquired from existing maps, from photogrammetric stereo models, from ground surveys, or from other systems, such as radar or laser altimeters and sensors carried in aircraft and spacecraft, and active remote sensing systems.

Generating DEM from ground surveys

Data derived by field survey involves the measurement of traverses with additional radiations or measurement of offsets (equivalent to radiations at right angles to a traverse). Either method results in vector data, which can be recorded by manual means in tabular or graphical form, with modern electronic equipment, for example by a data logger which can be plugged directly into a computer (Trinder 1996).

Generating DEM from existing maps

The two most commonly used techniques of acquiring DEM from existing maps are manually digitizing contour lines (line following), and map scanning. Manual digitizing involves the tracing of features on a map with a digitizing cursor. It has a high probability of either duplicating or omitting information (Doyle 1978). Raster scanning, a computer controlled operation, which creates a digital image of the source maps, is now used extensively. The resultant image is composed of a number of raster lines each composed of a number of image elements, i.e. pixels (Faust 1987, Sircar and Cebrian 1991). This image can be converted to vector by raster-vector conversion software. Significant editing may be required subsequently to obtain correct vector data.

Generating DEMs from stereo models

DEMs may be acquired from photogrammetric observations of aerial photos or satellite imagery on analytical or digital stereoplotters. The generation of DEMs using analytical photogrammetry is a standard and well established task (Ackermann 1994), involving data sampling and interpolation. In the sampling, a dense network of points is measured, the location of which will be dependent on the roughness of terrain. Many sampling methods have been developed to provide 'good' solutions to the selection of DEM point location, including selective sampling, adaptive sampling, and progressive sampling. Further details of DEM sampling are given in Makarovic (1973, 1976, 1977), Ayeni (1982), Balce (1987), and Burrough and McDonnell (1998). Data interpolation is also an important issue, since the measurements sampled from a stereo model are often inadequate and irregularly distributed. The problem of determining 'what is between the sample points measured' affects the quality of the final DEM. Many interpolation algorithms are designed to minimise the RMS-error (standard derivation of elevation discrepancies) of a DEM (Torlegård *et al* 1986). On the other hand, some interpolation algorithms are designed to preserve terrain texture, such as stream lines, ridge lines, maxima and minima points, sometimes at the cost of altimetric accuracy (Polidori and Chorowicz 1993). There is an extensive literature on interpolation including contributions by Kraus and Mikhail (1972), Briggs (1973), Schut (1976), Kubik and Botman (1976), Peucker (1980), Sibson (1980), Lam (1983), Yoeli (1984), Watson and Philip (1985), Hutchinson (1984, 1989), Polidori and Chorowicz (1993), Nery *et al* (1994), Todini and Ferraresi (1996) and Burrough and McDonnell (1998).

DEMs can be extracted using digital photogrammetry by image matching techniques from overlapping digital photographs. Extracting DEMs from a digital stereo model comprises two major operations, image matching and calculation of the three dimensional coordinates of each matched point of the DEM (Trinder *et al* 1994). Image matching is a difficult task since variations exist in the radiometric and geometric properties of a given object in the image pair. Matching algorithms have been developed mainly based on the comparison of the similarity or differences of corresponding areas (image patch) of two photographs, or features (significant points, lines, regions, structures) (Baltsavias 1991). The image matching approach is developed for DEM generation since it enables the operator to carry out a number of automatic operations, such as automatic target location and elevation computation, with sub-pixel matching

accuracy (Trinder *et al* 1994, Ackermann 1994). There are a number of digital photogrammetric systems available, which have different levels of performance and interactive operations (Madani 1993, Heipke 1993, Al-garnl 1995, Molnar *et al* 1996, Shear and Allen 1996, Baltsavias and Käser 1998, Bacher 1998).

Generating DEMs from active sensors

DEM can also be acquired from active remote sensing systems, such as Radar (RAdio Detection And Ranging) and laser scanners. The sensors emit their own energy which is reflected by the terrain and recorded by the systems. Radar systems have a particular advantage in those parts of the world where significant cloud or haze problems severely limit the opportunities for visible/infrared image acquisition (Wise 1989), and theoretically can be operated in any season and at any time (day and night). Elevation can be determined by radargrammetry from two overlapping radar images, or by radar interferometry, which uses the phase difference between the received radar radiation on two antennas, typically separated on an aircraft or spacecraft (RSMAS 1995). The Shuttle Radar Topographical Mission (SRTM) of NASA permitted the generation of global high resolution digital topographic data, with 30 metre x 30 metre spatial sampling with 16 metre absolute vertical height accuracy, 10 metre relative vertical height accuracy, covering 80% of earth's land mass (between 60°N and 56°S). However, currently there are technical difficulties with this approach, such as low coherence over the surfaces of complex topography, atmospheric artefacts, and effects of vegetation, which limit the application of interferometric Synthetic Aperture Radar (SAR) DEMs (RSMAS 1995, Crosetto and Crippa 1998).

Laser scan techniques determine terrain elevations by measuring the distance from the aircraft to the terrain surface in scan lines normal to the flight path. Position and tilts of the aircraft must be accurately determined by Global Positioning Systems (GPS) and Inertial Navigation Systems (INS). In a pilot study of using airborne laser data to determine terrain elevation over difficult terrain surfaces, such as vegetation covered areas, can be found in Kraus and Pfeifer (1998).

2.1.2 DEM products

The choice of methods of collecting a DEM is a matter of accuracy and cost. For example, the DEM derived by ground survey is the most accurate method, but centimetre accuracy is achieved at relatively high cost. Compared to ground surveys, the photogrammetric method would be cost effective for a large area. The accuracy of digitizing existing maps will vary according to the scale of a map used and other factors. The accuracy specifications for mapping in Australia set by the National Mapping Council require that 90% of well defined points on the map must be within 0.8 mm for map scale greater than 1:20,000, and 0.5mm for map scales less than or equal to 1:20,000 for planimetry, and within 0.5 contour interval for heights. The currency of the data will depend on the age of the map, but elevations will not be significantly affected, because they do not normally change with time.

Another important issue is the lineage of a DEM data, that is, the processes used on the data since its original derivation, which may affect the DEM accuracy. The DEM user should be aware of where the DEM data has came from, and how it was produced. A DEM with long lineage may be subject to significant errors introduced by each subsequent process since its original derivation, while a DEM with short lineage, such as one derived from ground survey, may be more accurate, since it is subject to fewer subsequent processes.

DEM data are produced by authorized government agencies and private sectors. In Australia, the Australian Surveying and Land Information Group (AUSLIG) and some state mapping agencies produce and distribute national DEM products. The available digital elevation data from AUSLIG includes DEM-9S (approximately 250m grid spacing), 18" (approximately 500m) and 3" (approximately 100m) grid DEM, 50m and 20m spacing contours, and irregular points of spot height and Critical Aeronautical Heights (http://www.auslig.gov.au). The accuracy of the DEM-9S makes it suitable for the applications that require data from map scales of 1:250,000. Results of some accuracy tests on the data can be found in
http://www.auslig.gov.au/products/digidat/dem9s/00000017.htm (June 2000).

The U.S. Geological Survey (USGS) is a major DEM producer in USA. It provides 7.5-minute with 30m grid spacing, 15-minute, 30-minute and 1-degree DEM data, covering the American national land surface, generated by digitizing the source of contour maps or aerial photographs (Source: http://edcwww.cr.usgs.gov/glis/hyper/guide/usgs_dem, July 1999). A 7.5-minute DEM data spans 7.5 minutes of latitude and longitude. The accuracy of USGS' DEMs are obtained by comparing a minimum of test points with ground control values, and is documented with the data. For example, the vertical accuracy of USGS 7.5-minute DEM is reported to be equal to or better than 15 metres, and can support applications to a level of detail similar for manual interpretation of information on printed maps at scales not larger than 1:24,000 scale.

2.2 DEM Accuracy

2.2.1 DEM errors and their characteristics

Spatial data is subject to errors, which generally result from four major causes (Maffini *et al* 1989):

- the inherent properties of nature. These are not always distinct and clear, but frequently gradual and fuzzy.
- the nature of measurement. That acquired by observers with instruments inevitably introduces errors. The capability of the person using the measuring device can also clearly influence the range of errors.
- the data model that is used to communicate the measurements. The very structure of the data model, such as raster or vector, can be a source of error.
- the data processing and transformation. The more times a set of measurements are transformed through one process or another, the more likely new errors or uncertainties will be introduced into the derivative products.

The quality of a DEM depends firstly on the data acquisition: density, distribution and quality of measured points, the representation of spatial morphological features (break lines, etc.); and secondly relates to data processing: interpolation and special operational processes (filtering, etc.) (Ackermann 1978). Theobald (1989) has indicated that DEM errors may be caused by inadequacies in the source documents and instruments. Torlegård *et al* (1986) show that the accuracy of a DEM depends on a series of

parameters, such as terrain type, density of measured points, type of measurements (selective, profiles, contours, grids, progressive), interpolation method, DEM sampling interval, instrument and operator precision, number, location and accuracy of control ponts, quality of photographs, and flying height. Carter (1988) has pointed out that the representation of the terrain by a DEM in grid format may poorly define the land form in areas of gentle slope or complex relief because the grid spatial resolution cannot be varied. Therefore, the applications of DEM data should be governed by the resolution, accuracy, and precision of the DEM. The experiments by Li (1994) further confirm that DEMs derived from different source data achieve different levels of accuracy.

DEM errors can be classified as systematic errors, random noise and outliers. Systematic DEM errors are the biases and artefacts resulting from deterministic systems which, if known, may be represented by certain functional relationships (Thapa and Bossler 1992). Torlegård *et al* (1986) examined systematic DEM errors derived by analytical photogrammetric methods and summarised their causes as being due to the reconstruction of the stereo model, the interpolation algorithms, and effects of vegetation height. Brown and Bara (1994) attempted to recognise the systematic errors in the USGS 7.5-Minute DEMs using the anisotropy of semivariograms and fractal dimensions. Garbrecht and Starks (1995) noted the systematic errors in USGS 7.5-Minute Level 1 DEM, and believed that they relate to the manual profiling technique used during the data generation.

DEM random noise refers to randomly distributed errors with high frequency characteristics in the spectral domain, normally with zero mean and a certain variance (Tempfli 1980). Random noise reduces DEM precision but does not introduce systematic bias. Precision is defined as the degree of variation about a mean, while accuracy refers to the degree with which an estimated mean differs from the true mean. Random noise in DEMs are likely to be introduced in all steps of DEM processing from the original source data through to data processing. Schwarz (1982) had shown that stereoscopic observations of topographic features result in height measurement precision varying from 0.07-0.15‰ of the flying height. Tests of stereoscopic observations on black and white aerial photographs revealed that standard deviations of height measurement could be improved to 0.03‰ of flying height (Trinder 1984). The tests by Torlegård *et al* (1986) showed that the standard error in photogrammetrically

measured DEMs is in the range of 0.2-0.4‰ of flying height in flat or moderately undulating terrain. In very hilly terrain the standard error increases to approximately 1-2‰ of flying height. The accuracy of DEMs, derived from photogrammetrically measured contours, is reported to be as much as 1/3 to 1/5 of the contour interval. Depending on the characteristics of the terrain topography, it can be further improved to 1/6 to 1/14 of the contour interval if additional information about specific features is available (Li 1994). The accuracy of DEMs produced by digital photogrammetric means, using least squares matching, is typically of the order of 0.2 to 0.3 pixel (Trinder *et al* 1992). Using feature based image matching, the accuracy is in the order of 0.3 to 0.4 pixel level (Ackermann 1994).

Outliers are another kind of error in DEMs. The definition of an outlier is 'an observation which deviates so much from other observations as to arouse suspicions that it is generated by a different mechanism' (Hawkins 1980). An inspection of a sample containing outliers would reveal some large discrepancies between the observations of outliers and the other data, as measured on some suitable standardized scale. In photogrammetrically derived DEMs, errors may occur more frequently in a difficult than smooth terrain, which can vary from 0% to 3% of the observations of a DEM with 0.5% median value (Torlegård *et al* 1986).

2.2.2 Impact of DEM errors on terrain surface modelling

The impact of DEM random errors on the extraction of terrain features is significant. Lee *et al* (1992) demonstrated that the magnitudes and the spatial patterns of the random errors in a DEM significantly affect the results of terrain analysis. An evaluation of SPOT derived DEMs showed that they were unreliable for computing the derivative topographic variables (Giles and Franklin 1996). Bolstad and Stowe (1994) evaluated the DEM accuracy of the USGS-7.5 Minute DEMs, as well as SPOT derived DEMs, and found statistically significant errors in slopes and aspects in the SPOT DEM. Huss and Pumar (1997) investigated the effects of errors on the estimates of intervisibility, and indicated that heights at the nodes of an uniform grid spacing over a specified geographical area may differ from the true height at the specified grid point on the earth.

Some researchers have attempted to use different means to monitor the effect of DEM random noise in the modelling of terrain topography. Tempfli (1980) tried to use spectra to describe DEM random noise and terrain relief in the study of the different interpolation methods and the influence of sampling density. Kraus (1994) analysed the effects of random noise on DEM surfaces and their derivatives, and used the accuracy of elevation and the relevant maximum slope to model the accuracy of isolines, such as contours and slope lines. Hunter and Goodchild (1997) declared that errors in slope and aspect depend on the spatial structure of DEM errors, and developed an error propagation model for slope and aspect, based on DEM standard deviations. Rieger (1996) developed a DEM error propagation model for slope and aspect calculation, based on different algorithms to derive the slope and aspect from a DEM.

Some researchers, for example Giles and Franklin (1996), have suggested that an appropriate method of correction or filtering a raw DEM must be applied to reduce the effect of the DEM noise before the derivatives of the DEM can be calculated. However, few attempts could be found to develop a particular method to efficiently reduce the effect of DEM random noise in terrain surface modelling.

The effect of DEM outliers on terrain surface modelling is also significant, especially in the modelling of their neighbouring DEM points. Experiments conducted by Wang (1998) and Wang *et al* (1998b) illustrated the significant influence of DEM outliers on the derivation of terrain topographic attributes. However, few other studies have documented a quantitative evaluation of the impact of outliers or methods of detecting and removing them in digital terrain modelling.

The impact of DEM systematic errors on terrain surface modelling is dependent on the characteristics of DEM systematic errors. If the systematic errors have a linear relationship with the observations, they may mainly affect the absolute values of elevation, and usually have little influence on the quality of DEM derivations, such as gradients, slope, aspect, etc. which are obtained from local height differences. However, if the systematic errors are nonlinear, the impact will be more complex.

One of the important objectives of this study, therefore, is to develop efficient methods to reduce the effects of DEM random noise and detect and remove DEM outliers for

terrain surface modelling. However, this research will not involve the study of DEM systematic errors, which may need additional tools and more investigations on their characteristics.

2.2.3 DEM resolution and its impact on its applications

An inherent property of geographic phenomena is their resolution dependency, which means that the characteristics of geographic patterns under observation vary with the sampling interval of the data describing them. Resolution in a DEM is the smallest interval between adjacent DEM positions or posts. When an elevation grid is sub-sampled to obtain another grid at a coarser resolution, not only are the fine resolution features removed, but also the number of grid cells describing the surface is reduced.

The sampling interval utilized to create DEMs is critical to their capability to portray the landscape, particularly in complex and rugged terrain. High sampling frequency of information represented in DEMs better represents landscape terrain for the user (Pike 1988, Walsh 1989). In theory, the minimum DEM sampling rate needed to preserve all the information content of a particular terrain surface should be twice the highest signal frequency. However, this is hard to achieve in practice, since the interpretation of the characteristics of terrain in the spectral domain is difficult. Empirical recommendations may be applied in practice. Kubik (1985) recommended that using 5m DEM sampling intervals for plateau and hilly terrain would be suitable from stereo models with 1:25,000 photo scale, while in the rolling downland terrain, the sampling interval should be 8m over the stereo models with a 1:78,000 photo scale.

Some researchers have investigated the impact of DEM resolutions on terrain modelling. Chang and Tsai (1991) show that the accuracy of slope and aspect decreases with lower DEM resolution. Zhang and Montgomery (1994) stated that, in the context of catchment simulation, DEM resolution significantly affects computed topographic parameters and influences physically based models of runoff generation and surface processes. Band *et al* (1995) indicated that DEM resolution appears to have more impact on simulated hydrographs of a TOPMODEL-based watershed model.

Fractals provide an important approach in describing and modelling the resolution effects of spatial data (Cao and Lam 1997, Xia and Clarke 1997). Nakano (1984) found a systematic increase of fractal dimension with elevation over short distances along the Pacific coast in Japan. Both Klinkenberg (1988) and Xia (1993) confirmed that the variation of fractal dimension of elevations depends on the landform characteristics of different geographic areas. Unfortunately, the applications of fractals in DEM-related terrain modelling is still limited. Nevertheless, many fundamental questions about fractals remain to be answered before their full potential can be exploited. More extensive empirical studies are needed to reveal the wide range of uses and practical limitations of fractal geometry in terrain modelling (Xia and Clarke 1997).

2.3 Digital Terrain Surface Modelling Techniques

2.3.1 Terrain topographic attributes and their geomorphological significance

Terrain topographic attributes that can be derived directly from a DEM and which are geomorphologically significant are summarised in Table 2-1 (Moore *et al* 1993).

Among these, slope is defined by a plane tangent to the surface as modelled by the DEM at any point and comprises two components: gradient, the maximum rate of change of elevation; and aspect, the compass direction of this maximum rate of change (Burrough and McDonnell 1998). Gradient is usually measured in per cent, degrees or radians, and aspect in degrees (converted to a compass bearing). Convexity is defined as the rate of change of slope or aspect, measured in degrees per unit of distance, e. g. degrees per 100 m. Profile convexity is the rate of change of slope, and plane convexity is the rate of change of aspect. Concavity is negative convexity. A point on a straight and planar slope has zero convexity. The importance of profile and plan convexities rest in their control of acceleration/deceleration and convergence/divergence of near-surface flows, and their effect on shelter or exposure to the wind, radar scanners and the human eye. They also affect the distribution of stresses in the ground and snow or ice cover. High values of plan convexity hinder overland movement (Evans 1972, 1980).

Table 2-1 Terrain attributes derived from DEM data (after Moore *et al* 1993)

Attribute	Definition	Significance
Altitude	Elevation	Climate, vegetation, potential energy
Upslope height	Mean height of upslope area	Potential energy
Aspect	Slope azimuth	Solar insolation, evapotranspiration, flora and fauna distribution, and abundance
Slope	Gradient	Overland and subsurface flow velocity and runoff rate, precipitation, vegetation, geomorphology, soil water content, land capability class
Upslope slope	Mean slope of upslope area	Runoff velocity
Dispersal slope	Mean slope of dispersal area	Rate of soil drainage
Catchment slope	Average slope over the catchment	Time of concentration
Upslope area	Catchment area above a short length of contour	Runoff volume, steady-state runoff rate
Dispersal area	Area downslope from a short length of contour	Soil drainage rate
Catchment area	Area draining to catchment outlet	Runoff volume
Specific catchment area	Upslope area per unit width of contour	Runoff volume, steady-state runoff, soil characteristics, soil water content, geomorphology
Flow path length	Maximum distance of water flow to a point in the catchment	Erosion rates, sediment yield, time of concentration
Upslope length	Mean length of flow paths to a point in the catchment	Flow acceleration, erosion rates
Dispersal length	Distance from a point in the catchment to the outlet	Impedance of soil drainage
Catchment length	Distance from highest point to outlet	Overland flow attenuation
Profile curvature	Slope profile curvature	Flow acceleration, erosion/deposition rate, geomorphology
Plan curvature	Contour curvature	Converging/diverging flow, soil water content, soil characteristics

Based on these attributes, terrain hydrological, geomorphological and biological significance can be further modelled, by combining the indices that describe or characterise the spatial variability of specific processes occurring in the landscape (Moore *et al* 1991), for example, soil water content distribution and surface saturation zones, calculation of precipitation and soil erosion, and monitoring of solar radiation dependent processes.

2.3.2 Terrain surface modelling techniques

Elevation and its partial derivatives, i.e. gradient along the X and Y mapping axes, are the most important terrain topographic attributes to be derived from a grid DEM, since all other terrain attributes can be expressed as functions of these. From this point of view, Evans (1972) has suggested using elevation at a point, and its two first partial derivatives, as a unifying concept to rebuild general geomorphometry. Many of the developed terrain surface modelling methods actually attempt to optimally model the first partial derivatives of elevation, i.e. gradients, from a grid-structured DEM.

A variety of digital models of terrain attributes using grid DEMs have been developed. Some commercial GIS, such as Arc/Info, and terrain modelling software, such as SCOP, also include modules of terrain modelling. The reviews of terrain modelling techniques can be found in Skidmore (1989), Chang and Tsai (1991), Srinivasan and Engel (1991), Guth (1995) and Florinsky (1998). The current terrain modelling methods can be classified into the maximum value, weighted elevation difference and the surface fitting approaches.

The maximum value approach

This approach is the simplest but coarsest method. It uses the maximum values within a DEM neighborhood to approximate the real values of the relevant terrain attributes of the point of interest (Travis *et* al 1975, Beasley and Huggins 1982, Shanholtz *et al* 1990).

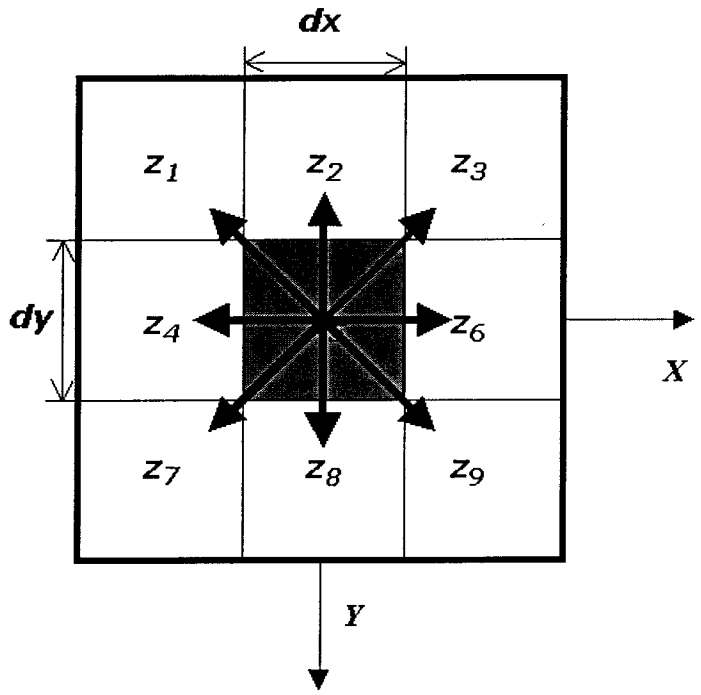

Figure 2-1 The maximum value approach

Travis *et al* (1975) used a 3 by 3 window to model the gradient and aspect of each DEM point shown in Figure 2-1. The gradient of a DEM point is defined as the maximum chnage from the central point to the eight nearest points, and the relevant aspect of the point is the direction of the maximum gradient:

$$G(i,j) = max((z_5 - z_k)) \quad while \quad k = 1,2,3,4,6,7,8,9 \qquad 2\text{-}1$$

where $G(i,j)$ is the gradient of the central point of the window, i.e. DEM point (i,j) and z_1 to z_9 are the DEM measurements of the corresponding points in the window.

Shanholtz *et al* (1990) developed a method for slope using the maximum gradient within a 3 by 3 neigbourhood. The slope of the central point of the window is calculated with respect to its eight neighbours:

$$S(i,j) = max|z_5 - z_k|/100L \quad while \quad k = 1,2,3,4,6,7,8,9 \qquad 2\text{-}2$$

where L is the distance from the centre point to its neighbours, evaluated for the DEM sampling interval dx or dy for the four adjacent points, and $\sqrt{(dx)^2 + (dy)^2}$ for the diagonal points.

Beasley and Huggins (1982) also presented a method to estimate the average slope from the maximum value of the linear combinations of the four neighbours.

The weighted elevation difference approach

This approach is more accurate and more commonly used than the maximum value approach. The terrain attributes are determined using the elevation differences along the X and Y-axes and a weighting factor, which is normally based on the distance between the neighbouring points and the point of interest within a neighbourhood. The approach can be further classified into the second-order finite difference and third-order finite difference method, depending on whether or not it only uses four immediately adjacent DEM points or all eight surrounding DEM points.

Dozier and Strahler's (1983) method simply chose the closest two adjacent DEM points in the X or Y-axes to determine the gradients of point (i, j) of these two directions, as shown in Figure 2-2:

$$G_x(i,j) = (z_6 - z_4)/2dx \qquad 2\text{-}3$$

$$G_y(i,j) = (z_8 - z_2)/2dy \qquad 2\text{-}4$$

Where $G_x(i,j)$ and $G_y(i,j)$ are the gradient along the X and Y-axes.

The slope and aspect of the centre point are determine from:

$$S(i,j) = \arctan\sqrt{(G_x(i,j))^2 + (G_y(i,j))^2} \qquad 2\text{-}5$$

$$A(i,j) = \arctan\frac{G_y(i,j)}{G_x(i,j)} \qquad 2\text{-}6$$

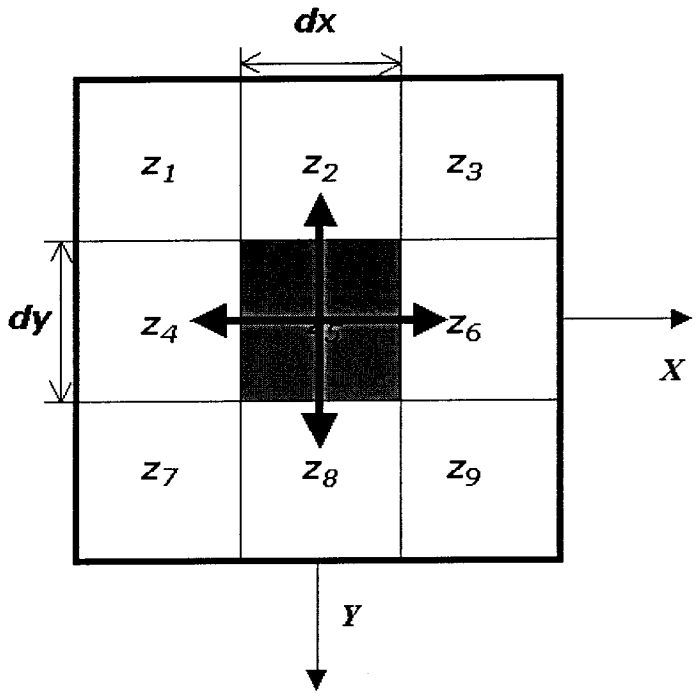

Figure 2-2 The second-order finite difference method

Ritter's (1987) slope and aspect model is essentially the same as that developed by Dozier and Strahler (1983), but they used different units in the slope calculation. Ritter uses per cent as the unit for slope calculation, while Dozier and Strahler (1983) uses radians:

$$S(i,j) = 100\frac{\sqrt{(z_6 - z_4)^2 + (z_8 - z_2)^2}}{2d} \qquad 2\text{-}7$$

where d is the DEM sampling interval. A slope of 100 percent, for example, represents a 45 degree slope, when the rise and run are equal.

The terrain attribute models developed by Dozier and Strahler (1983) and Ritter (1987) are a good compromise between accuracy and computational complexity. Precision is lost, since the contributions from the diagonally adjacent points are ignored when calculating the slope and aspect. However, they are more accurate than the algorithms that produce slope and aspect from only two points, which is the case for the method of the maximum value method. It is also a relatively simple and easily implemented algorithm in practice.

The algorithms presented in Sharpnack and Akin (1969) and Horn (1981) are able to use not only the adjacent, but diagonal DEM points to predict the terrain variables of the centre point of the 3 by 3 window (see Figure 2-3). Sharpnack and Akin (1969) even use the six surrounding DEM points to compute each gradient of the centre point:

$$G_x(i,j)=[(z_9+z_6+z_3)-(z_7+z_4+z_1)]/6dx \qquad 2\text{-}8$$

$$G_y(i,j)=[(z_9+z_8+z_7)-(z_3+z_2+z_1)]/6dy \qquad 2\text{-}9$$

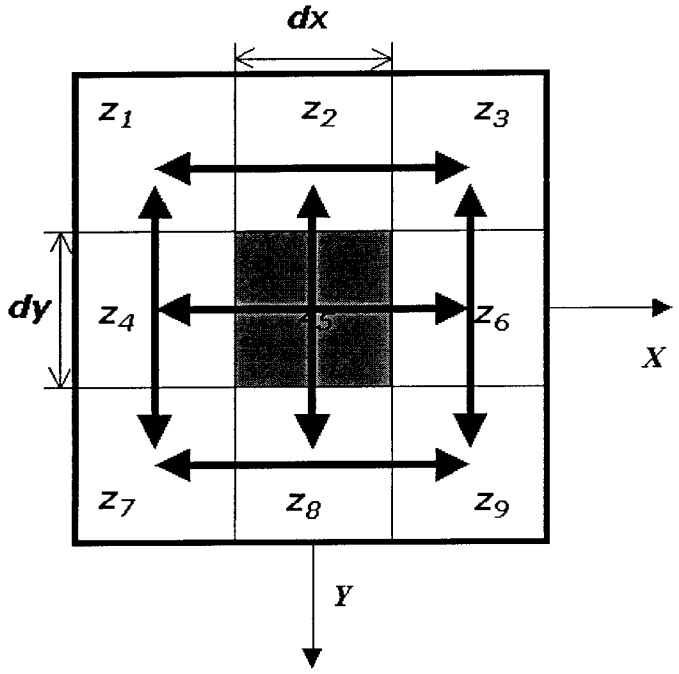

Figure 2-3 The third-order finite difference method

The derived gradients are used to compute the slope and aspect of the same point using the same equations as Eq. 2-5 and 2-6.

Based on the method of Sharpnack and Akin (1969), Horn (1981) introduced different weight factors for different surrounding points. It gives double weight to the two immediate adjacent points in the derivation of gradients, for they are closer to the centre point than those in the diagonal direction:

$$G_x(i,j)=[(z_9+2z_6+z_3)-(z_7+2z_4+z_1)]/8dx \qquad 2\text{-}10$$

$$G_y(i,j)=[(z_9+2z_8+z_7)-(z_3+2z_2+z_1)]/8dy \qquad 2\text{-}11$$

One important thing to be noticed is that, in this approach, the elevation at the centre (i,j) is never considered for estimating the terrain attributes: only its neighbours are considered. This leads to inaccurate estimation of average slope values if the elevation data have small pits or ridges. Hence, a function to smooth the elevation data sets is normally used before calculating the slopes, thereby eliminating small pits or ridges (Srinivasan and Engel 1991).

The surface fitting approach

The third terrain attribute modelling approach uses a surface fit to the 3 by 3 window. The resolved parameters of the fitted surface are used to derive the terrain topographic attributes of the central point of the window (see Figure 2-4).

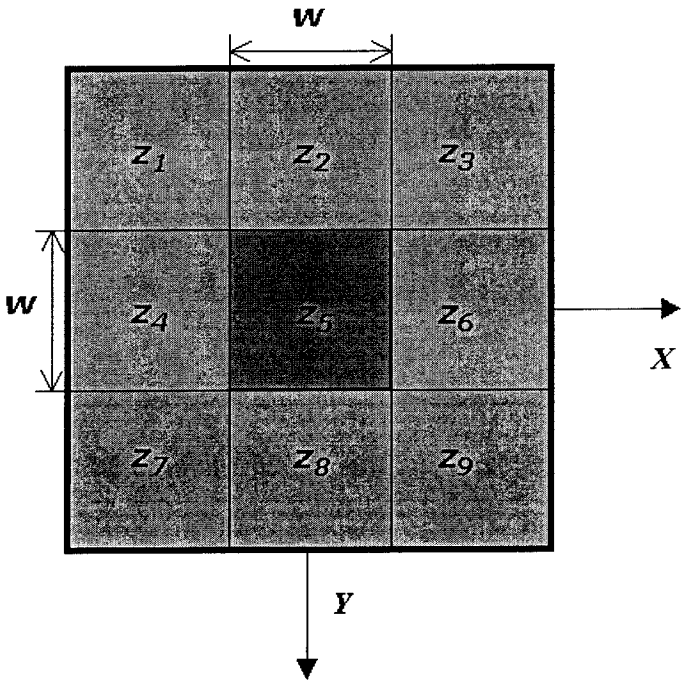

Figure 2-4 The surface fitting approach

The polynomial used in Evans (1980) to fit to the 3 by 3 window is a six-parameter quadratic equation:

$$z = ax^2 + by^2 + cxy + dx + ey + f \qquad 2\text{-}12$$

Where a, b, c, d, e and f are the unknown parameters, (x, y, z) is the coordinate of a DEM point.

The mathematical definitions of the terrain attributes gradient, slope, aspect, profile and plan curvature, are expressed as the functions of the unknown parameters of Eq. 2-12 (Pennock *et al* 1987):

$$G_x(i,j) = d \qquad 2\text{-}13$$

$$G_y(i,j) = e \qquad 2\text{-}14$$

$$S(i,j) = \sqrt{d^2 + e^2} \qquad 2\text{-}15$$

$$A(i,j) = \arctan\left(\frac{e}{d}\right) \qquad 2\text{-}16$$

$$PlC(i,j) = \frac{-2\left(bd^2 + ae^2 - cde\right)}{\sqrt[3]{\left(e^2 + d^2\right)^2}} \qquad 2\text{-}17$$

$$PrC(i,j) = \frac{-2\left(ad^2 + be^2 + cde\right)}{\left(e^2 + d^2\right)\sqrt[3]{\left(1 + d^2 + e^2\right)^2}} \qquad 2\text{-}18$$

In order to obtain these coefficients, a least squares technique is applied by fitting Eq. 2-12 to the nine DEM points of the window:

$$\mathbf{Z} + \mathbf{V} = \mathbf{AX} \qquad 2\text{-}19$$

where $\mathbf{Z} = \begin{bmatrix} z_1 \\ z_2 \\ z_3 \\ z_4 \\ z_5 \\ z_6 \\ z_7 \\ z_8 \\ z_9 \end{bmatrix}$, $\mathbf{V}$ is the residual vector, $\mathbf{A} = \begin{bmatrix} x_1^2 & y_1^2 & x_1y_1 & x_1 & y_1 & 1 \\ x_2^2 & y_2^2 & x_2y_2 & x_2 & y_2 & 1 \\ x_3^2 & y_3^2 & x_3y_3 & x_3 & y_3 & 1 \\ x_4^2 & y_4^2 & x_4y_4 & x_4 & y_4 & 1 \\ x_5^2 & y_5^2 & x_5y_5 & x_5 & y_5 & 1 \\ x_6^2 & y_6^2 & x_6y_6 & x_6 & y_6 & 1 \\ x_7^2 & y_7^2 & x_7y_7 & x_7 & y_7 & 1 \\ x_8^2 & y_8^2 & x_8y_8 & x_8 & y_8 & 1 \\ x_9^2 & y_9^2 & x_9y_9 & x_9 & y_9 & 1 \end{bmatrix}$ and

$\mathbf{X} = [a \quad b \quad c \quad d \quad e \quad f]$. (x_i, y_i, z_i) are the coordinates of the nine points within the window illustrated in Figure 2-4. Therefore, unknown parameters are solved as:

$$\mathbf{X} = \left(\mathbf{A}^{\mathbf{T}}\mathbf{A}\right)^{-1}\mathbf{A}^{\mathbf{T}}\mathbf{Z} \qquad 2\text{-}20$$

Rewriting the above equation in another form (Pennock *et al* 1987):

$$a = \frac{[z_1 + z_3 + z_4 + z_6 + z_7 + z_9 - 2(z_2 + z_5 + z_8)]}{6w^2} \qquad 2\text{-}21$$

$$b = \frac{[z_1 + z_2 + z_3 + z_7 + z_8 + z_9 - 2(z_4 + z_5 + z_6)]}{6w^2} \qquad 2\text{-}22$$

$$c = \frac{[z_3 + z_7 - z_1 - z_9]}{4w^2} \qquad 2\text{-}23$$

$$d = \frac{[z_3 + z_6 + z_9 - z_1 - z_4 - z_7]}{6w} \qquad 2\text{-}24$$

$$e = \frac{[z_1 + z_2 + z_3 - z_7 - z_8 - z_9]}{6w} \qquad 2\text{-}25$$

$$f = \frac{[5z_1 + 2(z_2 + z_4 + z_6 + z_8) - (z_1 + z_3 + z_7 + z_9)]}{9} \qquad 2\text{-}26$$

where w is the DEM sampling interval.

Moving the 3 by 3 window along the DEM, the gradients, slope, aspect, plan and profile curvatures of all points of DEM can be calculated.

The Evans method (1980) is the most accurate terrain modelling method among the existing algorithms, for it is able to use redundant measurements and least squares to estimate the unknown parameters of the assumed polynomial (Florinsk 1998). It is also claimed that it produces more terrain attributes, such as plan and profile curvatures, compared with the methods of the weighted elevation difference approach.

Shary's (1995) method is actually the same as the Evans (1980) method, except one more constraint is added to the polynomial fitting. It requires the polynomial to pass exactly through the central point of the window, to make it easier for the solution of the parameters:

$$z = \frac{ax^2}{2} + \frac{by^2}{2} + cxy + dx + ey + z_5 \qquad 2\text{-}27$$

This method yields the same values for the unknown parameters as Evans (1980), with small modifications for a and b. If aims at providing a fast algorithm to derive DEM attributes.

$$a = \frac{[z_1 + z_3 + z_7 + z_9 - 2(z_4 + z_6) + 3(z_2 + z_8) - 6z_5]}{5w^2} \qquad 2\text{-}28$$

$$b = \frac{[z_1 + z_3 + z_7 + z_9 - 2(z_2 + z_8) + 3(z_4 + z_6) - 6z_5]}{5w^2} \qquad 2\text{-}29$$

Heerdegen and Beran's method (1981) is the same as Shary's, using the relevant elevation values of the eight neighbouring points. It assumes that z_5 is zero, and all other eight points in Figure 2-4 have height values relatative to it. The polynomial used to fit the 3 by 3 window in Heerdegen and Beran's method (1981) is represented in Eq, 2-30:

$$z = ax^2 + by^2 + cxy + dx + ey \qquad 2\text{-}30$$

Therefore, the methods of Heerdegen and Beran (1982) and Shary (1995) are the special cases of the Evans method.

Zevenbergen and Thorne (1987) use a Lagrangian polynomial with nine unknown parameters. The method assumes that the fitted surface passes exactly through all DEM points of the search window. The appropriate surface is produced by the partial quartic equation:

$$z = ax^2y^2 + bx^2y + cxy^2 + dx^2 + ey^2 + fxy + gx + hy + i \qquad 2\text{-}31$$

where a through f are the unknown parameters.

The relationship between the nine unknown parameters a through f of Eq. 2-31 are derived by using the nine DEM observations of the 3 by 3 window shown in Figure 2-4:

$$a = \frac{[(z_1 + z_3 + z_7 + z_9)/4 - (z_2 + z_4 + z_6 + z_8)/2 + z_5]}{w^4} \qquad 2\text{-}32$$

$$b = \frac{[(z_1 + z_3 - z_7 - z_9)/4 - (z_2 - z_8)/2]}{w^3} \qquad 2\text{-}33$$

$$c = \frac{[(-z_1 + z_3 - z_7 + z_9)/4 + (z_4 - z_6)/2]}{w^3} \qquad 2\text{-}34$$

$$d = \frac{[(z_4 + z_6)/2 - z_5]}{w^2} \qquad 2\text{-}35$$

$$e = \frac{[(z_2 + z_8)/2 - z_5]}{w^2} \qquad 2\text{-}36$$

$$f = \frac{[-z_1 + z_3 - z_7 + z_9]}{4w^2} \qquad 2\text{-}37$$

$$g = \frac{(-z_4 + z_6)}{2w} \qquad 2\text{-}38$$

$$h = \frac{(z_2 - z_8)}{2w} \qquad 2\text{-}39$$

$$i = z_5 \qquad 2\text{-}40$$

The terrain topographic indices are found by differentiating Eq. 2-27 and solving for the central point of the 3 by 3 window in Zevenbergen and Thorne (1987) as:

$$S(i,j)=\sqrt{g^2+h^2} \qquad 2\text{-}37$$

$$A(i,j)=\arctan\left(\frac{-h}{-g}\right) \qquad 2\text{-}38$$

$$PlC(i,j)=\frac{2\left(dh^2+eg^2-fgh\right)}{g^2+h^2} \qquad 2\text{-}39$$

$$PrC(i,j)=\frac{-2\left(dg^2+eh^2+fgh\right)}{g^2+h^2} \qquad 2\text{-}40$$

A comparison of the methods of surface fitting is listed in Table 2-2. Compared with the method of Zevenbergen and Thorne (1987), the Evans (1980) method is more flexible in the use of DEM measurements within the window. It uses nine DEM observations to determine six unknown parameters of the polynomial, while the Zevenbergen and Thorne (1987) method uses nine observations to solve nine unknown parameters. Hence, the Evans method (1980) is able to use redundant observations and the least squares method to improve the accuracy, although the actual improvement is limited. Evans' (1980) method is also more accurate than that of Heerdegen and Beran (1982) and Shary (1995) methods in the sense that it is more general, and does not include specific constraints as defined in the two latter methods.

2.4 The Limitations in Terrain Surface Modelling Methods

The review of the existing terrain surface methods indicates that there are limitations in all three approaches. As mentioned in Section 2.2, DEMs are subject to systematic errors, random noise and outliers, no matter what method is used to acquire it. DEM errors may significantly affect the derivation of terrain surface methods. However, most of the developed terrain surface methods ignore these facts in almost all steps of terrain modelling, from terrain model design through to the DEM processing.

Table 2-2 Comparison of different surface fitting methods

Model	Fitted surface	Unknown parameters of the surface	Redundant DEM observations involved	Central point used in the window	Least squares
Evans	$z = ax^2 + by^2 + cxy + dx + ey + f$	6	yes	Same as other 8 DEM points	yes
Shary	$z = \frac{ax^2}{2} + \frac{by^2}{2} + cxy + dx + ey + z_5$	5	yes	Specially used	yes
Heerdegen and Beran	$z = ax^2 + by^2 + cxy + dx + ey$	5	yes	Specially used	yes
Zevenbergen and Thorne	$z = ax^2y^2 + bx^2y + cxy^2 + dx^2 + ey^2 + fxy + gx + hy + i$	9	no	Same as other 8 DEM points	no

Most terrain modelling methods determine terrain models in a deterministic manner, ignoring DEM observation errors as well as model errors. For example, the gradient model in Dozier and Strahler (1983), the slope model in Ritter (1987), the gradient, slope, aspect and curviture models in Zevenbergen and Thorne (1987) are all deterministic. Only Evans (1980) attempted to establish a stochastic observation model over DEM measurements while estimating the unknown parameters (see Eq. 2-19). However, its efficiency in terms of reducing DEM noise is affected by the use of limited number of DEM points.

All the developed terrain surface methods use a 3 by 3 window to process DEMs. This ignores other neighbouring DEM points during the derivations of the terrain attributes of the point of interest. To reduce DEM random noise in a DEM, the more DEM points that are involved, the more accurate will be the derived terrain attributes. Skidmore (1989) declared that methods using eight or nine neighbouring points to predict terrain

attributes are more suitable than those that use four points. Florinsky (1998) confirms that Evans' (1980) method is the most accurate algorithm among those existing, since it is able to adopt additional elevation measurements, and therefore leads to improvements in the accuracy and tolerance of terrain modelling. Moreover, some of the terrain modelling methods that do use the nine points of the window will be even worse. Some only use eight surrounding points (Sharpnack and Akin 1969, Horn 1981, Shanholtz *et al* 1990), and others even only four points in the window (Travis *et al* 1975, Beasley and Huggins 1982, Dozier and Strahler 1983, Ritter 1987). No modelling technique has been developed yet to incorporate more points than that in the 3 by 3 window.

The weighting factors used in the weighted elevation difference approach and the least squares technique introduced in the Evans method (1980) are inefficient in reducing DEM random noise. The weighting factors used in the weighted elevation difference approach act as low pass filters that may smooth DEM random noise, but the efficiency of the smoothing is not ideal, and pre-processing of DEM data, such as a smoothing or filtering, is normally still required before applying the terrain modelling algorithm on the DEM (Papo and Gelbman 1984, Srinivasan and Engel 1991). Though the most accurate, Evans' (1980) introduces the least squares technique to estimate terrain attributes, its efficiency is reduced by its inability to handle more than nine DEM data points. Furthermore, none of the developed terrain modelling methods can detect and remove DEM outliers.

CHAPTER 3

A STUDY OF KALMAN FILTERING TEHCNIQUES

3.1 Introduction

From the digital signal processing point of view, a DEM can be considered as a 2-D random (stochastic) process, which is interpreted in terms of a family of random signals, since it is subject to random noise as discussed in Chapter 2. The Kalman filtering is an application of statistical estimation theory, which is concerned with techniques for optimally estimating the value of a set of unknown parameters **x** from a set of observations **y** containing information about **x** (Minkler and Minkler 1993) (see Figure 3-1).

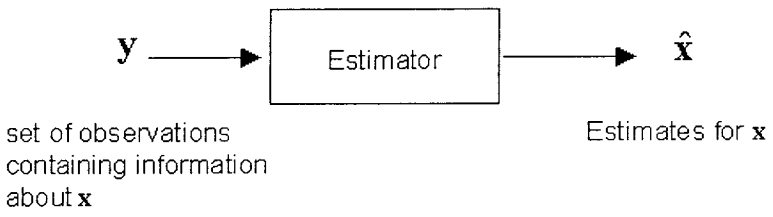

Figure 3-1 Estimating unknown parameters x from a set of observations y

An estimation filter is a system that collects the components that interact with each other, and is an environment to perform some purposeful behaviour. The relationship between a set of unknown parameters and a set of observed variables of a system, can usually be presented as a mathematical formula. The Kalman filter is a linear estimator initially introduced in 1960 (Kalman 1960), which is governed by differential (continuous-time Kalman filtering) or difference (discrete-time Kalman filtering) equations by using the 'state' concept. The state of a system is the minimum information about the past and present, needed to determine all future responses of a system, given the future input (Padulo and Arbib 1974). In a certain random case, it can be considered as the minimum amount of information about past and present estimates,

needed to determine an optimal casual estimate of future responses given future noisy observations (Woods and Radewan 1977).

Due to the advantages of Kalman recursive solutions of the discrete-data linear filtering, which can be implemented in real-time applications using computer technology, the one-dimensional (1-D) Kalman filtering technique has achieved great success in a wide range of applications. Developments in extending Kalman filtering into two dimensions, especially for image processing, have also been reported. However, the two-dimensional Kalman filtering algorithm for digital terrain modelling developed in this thesis extends 1-D Kalman filtering theory in a new way, rather than adopting the existing 2-D Kalman filters used in image processing (Woods and Radewan 1977). This is due to the characteristics of the terrain surface model as well as the limitations of the current 2-D Kalman techniques. To introduce the 2-D Kalman algorithm developed in this research, a review of some important aspects of Kalman filtering techniques is given in this Chapter.

3.2 One Dimensional Kalman Filtering Technique

3.2.1 Dynamic model and functional model

Kalman filtering is well established for the one-dimensional case. According to Brown and Hwang (1992), the dynamic model is given as:

$$\mathbf{X}_{k+1} = \Psi_k \mathbf{X}_k + \mathbf{W}_k \qquad 3\text{-}1$$

The observation of the process is assumed to occur at discrete points in time in accordance with the linear relationship:

$$\mathbf{Z}_k = \mathbf{H}_k \mathbf{X}_k + \mathbf{V}_k \qquad 3\text{-}2$$

Where

$\mathbf{X}_k$ $(n \times 1)$ process state vector at time k

Ψ_k $(n \times n)$ matrix relating $\mathbf{X}_k$ to $\mathbf{X}_{k+1}$ in the absence of a forcing function

$\mathbf{W}_k$ $(n \times 1)$ vector, assumed to be a white noise sequence with known covariance structure $\mathbf{Q}_k$

$\mathbf{Z}_k$ $(m \times 1)$ measurement vector at time k

$\mathbf{H}_k$ $(m \times n)$ matrix giving the ideal (noiseless) connection between the measurement and the state vector at time k, and

$\mathbf{V}_k$ $(m \times 1)$ measurement error, assumed to be a white noise sequence with known covariance structure, and having zero crosscorrelation with the $\mathbf{W}_k$ sequence.

The covariance matrices for the $\mathbf{W}_k$ and $\mathbf{V}_k$ vectors are given by:

$$E[\mathbf{W}_i \mathbf{W}_j^T] = \begin{cases} \mathbf{Q}_k & i = j = k \\ 0 & i \neq j \end{cases} \qquad 3\text{-}3$$

$$E[\mathbf{V}_i \mathbf{V}_j^T] = \begin{cases} \mathbf{R}_k & i = j = k \\ 0 & i \neq j \end{cases} \qquad 3\text{-}4$$

$$E[\mathbf{W}_i \mathbf{V}_j^T] = 0 \quad for \quad all \quad i \quad and \quad j \qquad 3\text{-}5$$

3.2.2 Derivation of Kalman equations

It is assumed at this point that an initial estimate of the process is known at some point in time k, and that this estimate is based on all knowledge about the process prior to k. This prior (or *a priori*) estimate will be denoted as $\mathbf{X}_k^-$ where the "super minus" is a reminder that this is the best prediction prior to assimilating the measurement at k. The error matrix associated with $\mathbf{X}_k^-$ is also assumed known, which is defined as:

$$\mathbf{e}_k^- = \mathbf{X}_k - \mathbf{X}_k^- \qquad 3\text{-}6$$

and the associated error covariance matrix is:

$$\mathbf{P}_k^- = E\left[\mathbf{e}_k^- \mathbf{e}_k^{-T}\right] = E\left[\left(\mathbf{X}_k - \mathbf{X}_k^-\right)\left(\mathbf{X}_k - \mathbf{X}_k^-\right)^T\right] \qquad 3\text{-}7$$

With the assumption of a prior estimate $\mathbf{X}_k^-$, the use of the measurement $\mathbf{Z}_k$ will be sought to improve the prior estimate. A linear blending of the noisy measurement and the prior estimate is chosen in accordance with the equation:

$$\mathbf{X}_k^+ = \mathbf{X}_k^- + \mathbf{K}_k\left(\mathbf{Z}_k - \mathbf{H}_k\mathbf{X}_k^-\right) \qquad 3\text{-}8$$

where

$\mathbf{X}_k^+$ updated estimate

$\mathbf{K}_k$ Blending factor (yet to be determined)

The problem is now to find the particular blending factor $\mathbf{K}_k$ that yields an updated estimate that is optimal in some sense. Here "minimum mean-square error" is used as the performance criterion. The expression for the error covariance matrix associated with the updated (*a posteriori*) estimate is formed:

$$\mathbf{P}_k^+ = E\left[\mathbf{e}_k \mathbf{e}_k^T\right] = E\left[\left(\mathbf{X}_k - \mathbf{X}_k^+\right)\left(\mathbf{X}_k - \mathbf{X}_k^+\right)^T\right] \qquad 3\text{-}9$$

Now, Eq. 3-2 is substituted into Eq. 3-8 and then the resulting expression is substituted for $\mathbf{X}_k^+$ into Eq. 3-9. The result is:

$$\mathbf{P}_k^+ = E\left\{\left[\left(\mathbf{X}_k - \mathbf{X}_k^-\right) - \mathbf{K}_k\left(\mathbf{H}_k\mathbf{X}_k + \mathbf{V}_k - \mathbf{H}_k\mathbf{X}_k^-\right)\right]\right.$$
$$\left.\left[\left(\mathbf{X}_k - \mathbf{X}_k^-\right) - \mathbf{K}_k\left(\mathbf{H}_k\mathbf{X}_k + \mathbf{V}_k - \mathbf{H}_k\mathbf{X}_k^-\right)\right]^T\right\} \qquad 3\text{-}10$$

Performing the indicated expectation and noting that $\left(\mathbf{X}_k - \mathbf{X}_k^-\right)$ is the *a priori* estimation error that is uncorrelated with the measurement error $\mathbf{V}_k$:

$$\mathbf{P}_k^+ = (\mathbf{I} - \mathbf{K}_k\mathbf{H}_k)\mathbf{P}_k^-(\mathbf{I} - \mathbf{K}_k\mathbf{H}_k)^T + \mathbf{K}_k\mathbf{R}_k\mathbf{K}_k^T \qquad 3\text{-}11$$

Notice here that Eq. 3-11 is a perfectly general expression for the updated error covariance matrix, and it applies for any gain $\mathbf{K}_k$, suboptimal or otherwise.

In order to find the particular $\mathbf{K}_k$ that minimizes the individual terms along the major diagonal of $\mathbf{P}_k^+$, since these terms represent the estimation error variances for the elements of the state vector being estimated, the differential calculus approach is used here and to do so two matrix differential formulas are used:

$$\frac{d[trace(\mathbf{AB})]}{d\mathbf{A}} = \mathbf{B}^T \qquad 3\text{-}12$$

$$\frac{d\left[trace\left(\mathbf{ACA}^T\right)\right]}{d\mathbf{A}} = 2\mathbf{AC} \qquad 3\text{-}13$$

where $\mathbf{A}$ and $\mathbf{B}$ matrix must be square, and $\mathbf{C}$ must be symmetric.

The derivative of a scalar with respect to a matrix is defined as:

$$\frac{ds}{d\mathbf{A}} = \begin{bmatrix} \frac{ds}{da_{11}} & \frac{ds}{da_{12}} & \Lambda \\ \frac{ds}{da_{21}} & \frac{ds}{da_{22}} & \Lambda \\ \mathrm{M} & & \end{bmatrix} \qquad 3\text{-}14$$

Eq. 3-11 is expanded and rewritten in the following form, temporarily dropping the subscripts in the $\mathbf{P}_k^+$ expression:

$$\mathbf{P}^{+} = \mathbf{P}^{-} - \mathbf{KHP}^{-} - \mathbf{P}^{-}\mathbf{H}^{T}\mathbf{K}^{T} + \mathbf{K}\left(\mathbf{HP}^{-}\mathbf{H}^{T} + \mathbf{R}\right)\mathbf{K}^{T} \qquad 3\text{-}15$$

The second and third terms are linear in $\mathbf{K}$, and the fourth term is quadratic in $\mathbf{K}$. The two matrix differentiation formulas may now be applied to Eq. 3-15. It is desirable to minimize the trace of $\mathbf{P}^{+}$ because it is the sum of the mean-square errors in the estimates of all the elements of the state vector. The argument can be used that the individual mean-square errors are also minimized when the total is minimized, provided that there are enough degrees of freedom in the variation of $\mathbf{K}$, which is the case. The trace of $\mathbf{P}^{+}$ is differentiated with respect to $\mathbf{K}$. Note that the trace of $\mathbf{P}^{-}\mathbf{H}^{T}\mathbf{K}^{T}$ is equal to the trace of its transpose $\mathbf{KHP}^{-}$. The result is:

$$\frac{d\left(trace\mathbf{P}^{+}\right)}{d\mathbf{K}} = -2\left(\mathbf{HP}^{-}\right)^{T} + 2\mathbf{K}\left(\mathbf{HP}^{-}\mathbf{H}^{T} + \mathbf{R}\right) \qquad 3\text{-}16$$

Setting the derivative equal to zero and solving for the optimal gain, the result is:

$$\mathbf{K}_{k} = \mathbf{P}_{k}^{-}\mathbf{H}_{k}^{T}\left(\mathbf{H}_{k}\mathbf{P}_{k}^{-}\mathbf{H}_{k}^{T} + \mathbf{R}_{k}\right)^{-1} \qquad 3\text{-}17$$

This particular $\mathbf{K}_{k}$, namely the one that minimises the mean-square estimation error, is called the Kalman gain.

The variance matrix associated with the optimal estimate may now be computed. Referring to Eq. 3-11, the variance matrix is:

$$\begin{aligned}\mathbf{P}_{k}^{+} &= \left(\mathbf{I} - \mathbf{K}_{k}\mathbf{H}_{k}\right)\mathbf{P}_{k}^{-}\left(\mathbf{I} - \mathbf{K}_{k}\mathbf{H}_{k}\right)^{T} + \mathbf{K}_{k}\mathbf{R}_{k}\mathbf{K}_{k}^{T} \\ &= \mathbf{P}_{k}^{-} - \mathbf{K}_{k}\mathbf{H}_{k}\mathbf{P}_{k}^{-} - \mathbf{P}_{k}^{-}\mathbf{H}_{k}^{T}\mathbf{K}_{k}^{T} + \mathbf{K}_{k}\left(\mathbf{H}_{k}\mathbf{P}_{k}^{-}\mathbf{H}_{k}^{T} + \mathbf{R}_{k}\right)\mathbf{K}_{k}^{T}\end{aligned} \qquad 3\text{-}18$$

Routine substitution of the optimal gain expression, Eq. 3-1, into Eq. 3-18 leads to:

$$\mathbf{P}_k^+ = \mathbf{P}_k^- - \mathbf{P}_k^- \mathbf{H}_k^T \left(\mathbf{H}_k \mathbf{P}_k^- \mathbf{H}_k^T + \mathbf{R}_k \right)^{-1} \mathbf{H}_k \mathbf{P}_k^- \qquad 3\text{-}19$$

or

$$\mathbf{P}_k^+ = \mathbf{P}_k^- - \mathbf{K}_k \left(\mathbf{H}_k \mathbf{P}_k^- \mathbf{H}_k^T + \mathbf{R}_k \right) \mathbf{K}_k^T \qquad 3\text{-}20$$

or

$$\mathbf{P}_k^+ = (\mathbf{I} - \mathbf{K}_k \mathbf{H}_k) \mathbf{P}_k^- \qquad 3\text{-}21$$

Of the three expressions for $\mathbf{P}_k^+$, the latter one given in Eq. 3-21 is the simplest, so it is used more frequently than the others.

A means is now available for assimilating the measurement at t_k using Eq. 3-8, with $\mathbf{K}_k$ set equal to the Kalman gain as given by Eq. 3-17. The updated estimated $\mathbf{X}_k^+$ is easily projected ahead via the transition matrix. The contribution of $\mathbf{W}_k$ in Eq. 3-1 is ignored because it has zero mean and is not correlated with any of the previous $\mathbf{W}'s$. Thus:

$$\mathbf{X}_{k+1}^- = \Psi_k \mathbf{X}_k^+ \qquad 3\text{-}22$$

The error covariance matrix associated with $\mathbf{X}_{k+1}^-$ is obtained by first forming the expression for the *a priori* error:

$$\begin{aligned} \mathbf{e}_{k+1}^- &= \mathbf{X}_{k+1} - \mathbf{X}_{k+1}^- \\ &= \left(\Psi_k \mathbf{X}_k + \mathbf{W}_k \right) - \Psi_k \mathbf{X}_k^+ \\ &= \Psi_k \mathbf{e}_k + \mathbf{W}_k \end{aligned} \qquad 3\text{-}23$$

$\mathbf{W}_k$ and $\mathbf{e}_k$ have zero crosscorrelation, because $\mathbf{W}_k$ is the process noise for the step ahead of t_k. Thus the expression of $\mathbf{P}_{k+1}^-$ can be written as:

$$\mathbf{P}_{k+1}^- = E\left[\mathbf{e}_{k+1}^- \mathbf{e}_{k+1}^{-T}\right] = E\left[(\Psi_k \mathbf{e}_k + \mathbf{W}_k)(\Psi_k \mathbf{e}_k + \mathbf{W}_k)^T\right] \qquad 3\text{-}24$$
$$= \Psi_k \mathbf{P}_k^+ \Psi_k^T + \mathbf{Q}_k$$

Now the needed quantities at time t_{k+1} are derived, and the measurement $\mathbf{Z}_{k+1}$ can be assimilated just as in the previous step.

Equations 3-8, 3-17, 3-21, 3-22, and 3-24 comprise the Kalman filter recursive equations. It should be clear that once the loop is entered, it can be continued indefinitely.

3.2.3 Recursive processing

Assume a sequence of noisy measurements $\mathbf{Z}_k$ taken at unit intervals, and it is required to determine the optimal estimate of the process at the sample time $k = 0,1,2,3,\Lambda$, etc. Given the initial predicted estimate $\mathbf{X}_0^-$ at $k = 0$, and its covariance matrix $\mathbf{P}_0^-$, the Kalman loop is entered at $k = 0$, and the sequence is processed as shown in Figure 3-2. Firstly, the Kalman gain $\mathbf{K}_0$ at time $k = 0$ is computed using Eq. 3-17. Secondly, the first measurement $\mathbf{Z}_0$ is used to improve the initial predicted estimate $\mathbf{X}_0^-$ through Eq. 3-8, resulting in the updated estimate of $\mathbf{X}_0^+$ at $k = 0$. Then, the associated covariance matrix of $\mathbf{X}_0^+$, ie. $\mathbf{P}_0^+$, is computed using Eq. 3-21. Finally, the 'project ahead' estimate, ie. $\mathbf{X}_1^-$ and its covariance matrix $\mathbf{P}_1^-$, are computed using Eq. 3-22 and Eq. 3-24, which are the prediction for the process at the next sample time $k = 1$. It will be used as input to enter the Kalman loop again for processing at the sample time $k = 1$. From this recursive procedure, it is clear that once the Kalman loop is entered at $k = 0$, the process can be carried on indefinitely. As time goes on, the Kalman filter depends more and more on the measurements and less on the initial assumptions.

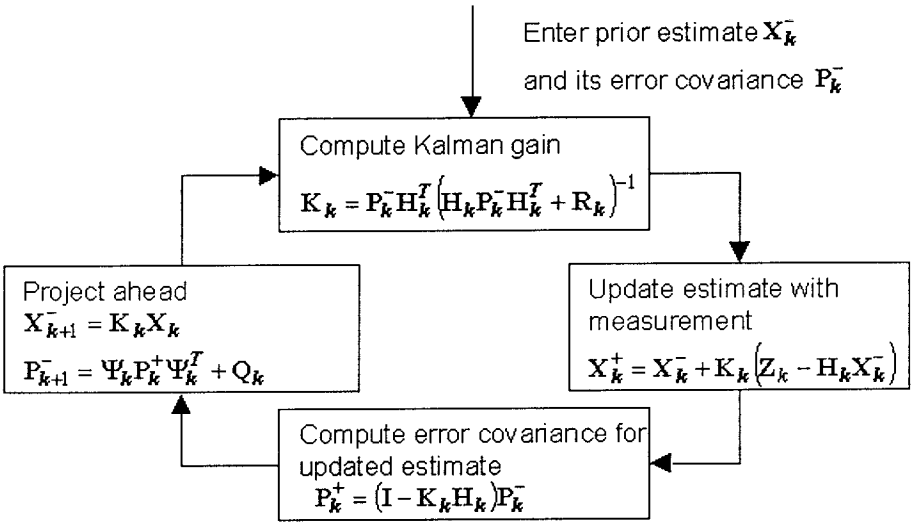

Figure 3-2 Kalman loop

3.2.4 Perspectives of Kalman filtering

Brown and Hwang (1992) summarise the perspective of Kalman filter as:

- It is intended to be used for estimating random processes. Any application in a nonrandom setting must be viewed with caution.

- It is model dependent. That is to say, it is assumed that the *a priori* model parameters are known. These, in turn, come from the second-order "statistics" of the various processes involved in the application at hand. Therefore, in its most primitive form, the Kalman filter is not adaptive or self-learning.

- It is a linear estimator. When all the processes involved are Gaussian, the filter is optimal in the minimum-mean-square-error sense within a class of all estimators, linear and non linear.

- It has various Kalman filter recursive algorithms. All of these yield identical results (assuming perfect arithetic).

- It yields the same result obtained from deterministic least-squares, under certain special circumstances.

- It is especially useful as an analysis tool in offline error analysis studies. The filter error covariance equation can be propagated recursively without actual (or simulated) measurement data.

3.3 Comparison of Kalman Filtering with Deterministic Least Squares

Kalman filtering is sometimes referred to simply as least squares filtering. This is, however, somewhat an oversimplification, because the criterion for optimization is minimum mean-square error and not the squared error in a deterministic sense. There is, however, a coincidental connection between Kalman filtering and deterministic least squares (Brown and Hwang 1992), and this will now be demonstrated.

Consider a set of m linear equations in $\mathbf{x}$ specified in matrix form by:

$$\mathbf{Mx} = \mathbf{b} \qquad 3\text{-}25$$

In Eq. 3-25 $\mathbf{M}$ and $\mathbf{b}$ are considered as given, $\mathbf{x}$ is $(n \times 1)$, $\mathbf{b}$ is $(m \times 1)$, and thus $\mathbf{M}$ is $(m \times n)$. Assume that $m > n$, and $\mathbf{x}$ is overdetermined by the system of equations represented by Eq. 3-25. Thus no solution for $\mathbf{x}$ will satisfy all equations. In such cases it is logical to find the best solution to fit all the equations. The term 'best' must be defined and it is frequently formulated as the particular $\mathbf{x}$, say $\mathbf{x}_{opt}$, that minimizes the sum of the squared residuals. That is, move $\mathbf{b}$ to the left side of Eq. 3-25 and substitute $\mathbf{x}_{opt}$ for $\mathbf{x}$. This yields a residual vector $\mathbf{v}$ given by:

$$\mathbf{Mx}_{opt} - \mathbf{b} = \mathbf{v} \qquad 3\text{-}26$$

and $\mathbf{x}_{opt}$ is chosen such that $\mathbf{v}^T\mathbf{v}$ is minimized. A perfect fit, of course, would make $\mathbf{v}^T\mathbf{v}=0$.

To generalise the problem at this point, a weighted sum of squared residuals is considered, which is specified by:

$$\mathbf{v}^T\mathbf{W}\mathbf{v}=\left(\mathbf{M}\mathbf{x}_{opt}-\mathbf{b}\right)^T\mathbf{W}\left(\mathbf{M}\mathbf{x}_{opt}-\mathbf{b}\right) \qquad 3\text{-}27$$

The weighting matrix $\mathbf{W}$ is assumed symmetric and positive definite and so is its inverse. If equal weighting of the residuals is required, $\mathbf{W}$ will simply be the identity matrix. The problem now is to find the particular $\mathbf{x}$ (i.e., $\mathbf{x}_{opt}$) that minimises the weighted sum of the residuals. Towards this end, the expression given by Eq. 3-27 may be expanded and differentiated and then set equal to zero. This leads to:

$$\begin{aligned}&\frac{d}{d\mathbf{x}_{opt}}\left[\mathbf{x}_{opt}^T\left(\mathbf{M}^T\mathbf{W}\mathbf{M}\right)\mathbf{x}_{opt}-\mathbf{b}^T\mathbf{W}\mathbf{M}\mathbf{x}_{opt}-\mathbf{x}_{opt}^T\mathbf{M}^T\mathbf{W}\mathbf{b}+\mathbf{b}^T\mathbf{b}\right]\\&=2\left(\mathbf{M}^T\mathbf{W}\mathbf{M}\right)\mathbf{x}_{opt}-\left(\mathbf{b}^T\mathbf{W}\mathbf{M}\right)^T-\mathbf{M}^T\mathbf{W}\mathbf{b}=0\end{aligned} \qquad 3\text{-}28$$

Eq. 3-28 may be solved for $\mathbf{x}_{opt}$. The result is:

$$\mathbf{x}_{opt}=\left[\left(\mathbf{M}^T\mathbf{W}\mathbf{M}\right)^{-1}\mathbf{M}^T\mathbf{W}\right]\mathbf{b} \qquad 3\text{-}29$$

and this is the solution of the deterministic least-squares problem.

Next, consider the Kalman filter solution for the same measurement situation. The vector $\mathbf{x}$ is assumed to be a random constant, so the differential equation for $\mathbf{x}$ is:

$$\dot{\mathbf{x}}=0 \qquad 3\text{-}30$$

The corresponding discrete model is then:

$$\mathbf{x}_{k+1} = \mathbf{I}\mathbf{x}_k + 0 \qquad 3\text{-}31$$

The measurement equation is:

$$\mathbf{z}_k = \mathbf{H}_k\mathbf{x}_k + \mathbf{v}_k \qquad 3\text{-}32$$

where $\mathbf{z}_k$ and $\mathbf{H}_k$ play the same roles as $\mathbf{b}$ and $\mathbf{M}$ in the deterministic problem. Since time is of no consequence, it is assumed that a prior knowledge of $\mathbf{x}$ is not available, so the initial $\mathbf{x}_0^-$ will be zero and its associated error covariance will be ∞. Therefore, using the alternative form of Kalman filter (Brown and Hwang 1992, pp259-261), the following equation is derived:

$$\begin{aligned}\mathbf{P}_0^{-1} &= (\infty)^{-1} + \mathbf{H}_0^T\mathbf{R}_0^{-1}\mathbf{H}_0 \\ &= \mathbf{H}_0^T\mathbf{R}_0^{-1}\mathbf{H}_0\end{aligned} \qquad 3\text{-}33$$

The Kalman gain is then:

$$\mathbf{K}_0 = \left(\mathbf{H}_0^T\mathbf{R}_0^{-1}\mathbf{H}_0\right)^{-1}\mathbf{H}_0^T\mathbf{R}_0^{-1} \qquad 3\text{-}34$$

and the Kalman filter estimate of $\mathbf{x}$ at $t = 0$ is

$$\mathbf{x}_0^+ = \left[\left(\mathbf{H}_0^T\mathbf{R}_0^{-1}\mathbf{H}_0\right)^{-1}\mathbf{H}_0^T\mathbf{R}_0^{-1}\right]\mathbf{z}_0 \qquad 3\text{-}35$$

This is the identical expression obtained from $\mathbf{x}_{opt}$ in the deterministic least-squares problem with $\mathbf{R}_0^{-1}$ playing the role of the weighting matrix $\mathbf{W}$, while $\mathbf{H}_0$ for $\mathbf{M}$.

The conditions under which the Kalman filter estimate coincides with the deterministic least-squares estimates will be reviewed. First, the system state vector was assumed to

be a random constant (dynamics are thus trivial). Second, the measurement sequence was assumed to yield an overdetermined system of linear equations, otherwise $\left(\mathbf{H}_0^T \mathbf{R}_0^{-1} \mathbf{H}_0\right)^{-1}$ will not exist. Finally, it is assumed that no prior knowledge about the constant vector being estimated is avaliable. The latter assumption is unusual because in many situations at least some *a priori* knowledge of the process being estimated is available. One of the aspects that distinguishes Kalman filter from other estimators is the conditions of the recursive process. Of course, if there is truly no prior knowledge to use, the Kalman filter advantages are lost (in this aspect), and it degenerates to a least-squares fit under the conditions just stated.

The coincidence of the deterministic least-squares and Kalman filtering estimates is really rather remarkable. One solution was obtained by posing a deterministic optimisation problem; the other by posing a similar stochastic problem. There is no reason to think these two approaches would lead to identical solutions. They do under certain circumstances, which may be generalised somewhat from those of this example, but not to the complete extent of the general process model used in the Kalman filter. Thus this happy coincidence in the two solutions will not always exist.

3.4 Applying Kalman Filtering to Smoothing Problems

3.4.1 About smoothing

The emphasis in the preceding sections on Kalman filtering has been on the filtering problem, that is, the estimation of the system $\mathbf{X}$, at a time t_E, based on the input measurements from t_0 to t_M, for the cases where t_M is either strictly greater than or less than t_E. When t_M is greater than t_E, the estimation filter is called a smoothing filter (Minkler and Minkler 1993). The smoothing problem is more difficult and usually leads to a more complicated expression for the Fourier transform and the recursive algorithm than occurs in the corresponding filter or prediction problem (Brown and Hwang 1992). Optimal smoothing by Kalman filtering solution is an extension of Kalman filtering.

3.4.2 Discrete Kalman smoothing – the forward-backward smoothing algorithm

An algorithm for problems of one-dimensional discrete fixed-interval smoothing, under the assumptions and conditions in Section 3.2 for the discrete-time Kalman filter, is introduced here to illustrate the smoothing process. This algorithm was initially presented by Fraser and Potter (1969) for fixed interval smoothing problems. The approach was to filter the measurement data from both ends to the interior point of interest, and then the two filter estimates were combined to obtain the optimal smoothed estimate (illustrated in Figure 3-3). The simplified derivation for the discrete case presented here is developed by Brown and Hwang (1992, pp342-349).

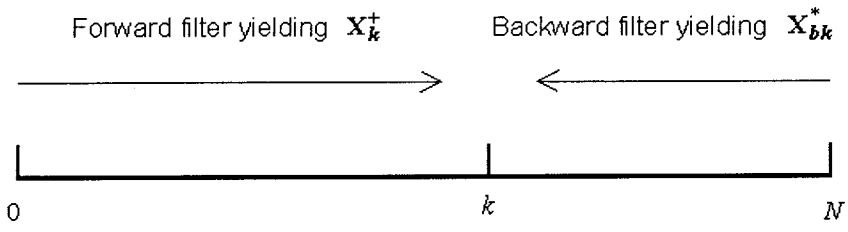

Figure 3-3 Forward-backward smoothing

Consider a fixed-length interval containing $N+1$ measurements shown in Figure 3-3. These will be indexed in ascending order $\mathbf{Z}_0$, $\mathbf{Z}_1$, ..., $\mathbf{Z}_N$. The assumptions relative to the process and measurement models are the same as for the 1-D discrete Kalman filter problem. The computational procedure for the smoothing algorithm consists of a forward recursive sweep and a backward sweep. The algorithm is entered as usual at time $t=0$ with the initial conditions $\mathbf{X}_0^-$ and $\mathbf{P}_0^-$. Then the process is swept forward using the conventional Kalman filter algorithm. With each step of the forward sweep, *a priori* and *a posteriori* estimates associated with their associated $\mathbf{P}$ matrices must have been computed. Then the process is repeated backward by starting from $t=N$ towards $t=0$, and *a priori* and *a posteriori* estimates and their associated $\mathbf{P}$ matrices are computed. The forward filter is assumed to have been stopped ahead recursively at the estimation point, say $t=k$, and the end result is *a posteriori* estimate $\mathbf{X}_k^+$ and an associated $\mathbf{P}_k^+$. The backward filter steps backward from the end point N, and it stops

at $t = k+1$ where it assimilates the $\mathbf{Z}_{k+1}$ measurement. It then projects this estimate one more step to obtain a predicted estimate $\mathbf{X}_{bk}^{*}$ and its associated $\mathbf{P}_{bk}^{*}$. It does not assimilate the $\mathbf{Z}_k$ measurement, because this has already been used in the forward filter. Finally, the forward and backward estimates are blended together using the equation:

$$\hat{\mathbf{X}}(k \mid N) = \mathbf{P}(k \mid N)\left[\mathbf{P}_k^{+\,-1}\mathbf{X}_k^{+} + \mathbf{P}_{bk}^{*\,-1}\mathbf{X}_{bk}^{*}\right] \qquad 3\text{-}36$$

Where

$$\mathbf{P}(k \mid N) = \left[\mathbf{P}_k^{+\,-1} + \mathbf{P}_{bk}^{*\,-1}\right]^{-1} \qquad 3\text{-}37$$

The notation of $\hat{\mathbf{X}}(k \mid N)$ represents the "estimate of $\mathbf{X}$ at time $t = k$ given all the measurement data up through time $t = N$".

3.5 Kalman Filtering in Two Dimensions

The extension of Kaman filtering to two-dimensions resulted from the interest in the problem of two-dimensional recursive filtering with particular application to images (Woods 1981). In fact, a straightforward extension of the 1-D Kalman filter techniques results in a number of state variables proportional to N for filtering an $N \times N$ digital image. Early attempts to achieve a truly recursive 2-D Kalman filter were of only limited success due to both the difficulty in establishing a suitable 2-D model and also the high dimensionality of the resulting state vector. In the following sections, a close look is taken at the problems caused by the nature of two dimensions on the establishment of the state, as well as available solutions of the problem.

3.5.1 Problems of extending Kalman filtering into two dimensions

Consider a particular raster scanning of 2-D discrete data with $N \times N$ regularly spaced points, i.e. left to right, top to bottom, illustrated in Figure 3-4. Thus, at any point in the picture, some points will be the "past", one point will be the "present", and remaining points will be the "future".

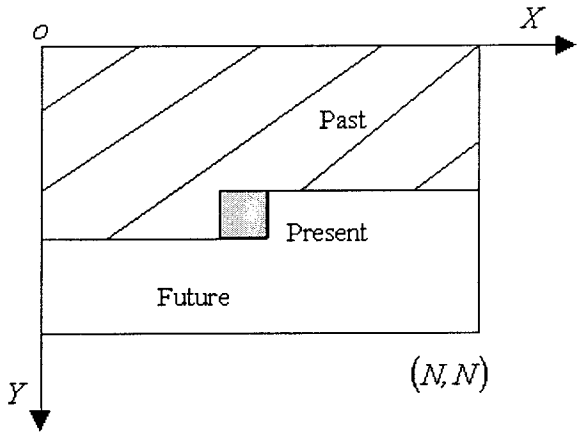

Figure 3-4 Scalar scanning rectangular region using raster scanning

Suppose the dynamic model and observation model, as those mentioned in Section 3.2, are available for the 2-D data shown in Figure 3-4:

$$\mathbf{s}(m) = \mathbf{C}\mathbf{s}(m-1) + \mathbf{w}(m) \qquad 3\text{-}38$$

$$\mathbf{r}(m) = \mathbf{H}\mathbf{s}(m) + \mathbf{v}(m) \qquad 3\text{-}39$$

where $\mathbf{s}$ is the signal state vector, $\mathbf{r}$ is the observation or received signal, $\mathbf{v}$ is the observation noise, and $\mathbf{w}$ is the random process. The matrices $\mathbf{C}$ and $\mathbf{H}$ are, respectively, the system and observation matrix. $\mathbf{v}$ and $\mathbf{w}$ are uncorrelated, with Gaussian, zero-mean noise sources:

$$E\left[\mathbf{w}(m)\mathbf{w}^T(k)\right] = \mathbf{Q}_w \delta_{mk} \qquad 3\text{-}40$$

$$E\left[\mathbf{v}(m)\mathbf{v}^T(k)\right] = \mathbf{Q}_v \delta_{mk} \qquad 3\text{-}41$$

$$E\left[\mathbf{w}(m)\mathbf{v}^T(k)\right]=0 \qquad 3\text{-}42$$

where $\mathbf{Q}_w$ and $\mathbf{Q}_v$ are correlation matrices and δ_{mk} is the Kronecker delta function, which equals 1 when $m=k$; or equals to zero when $m\neq k$. The Kalman filtering equations for this model are:

$$\mathbf{s}^-(m)=\mathbf{C}\mathbf{s}^+(m-1) \qquad 3\text{-}43$$

$$\mathbf{P}^-(m)=\mathbf{C}\mathbf{P}^+(m-1)\mathbf{C}^T+\mathbf{Q}_w \qquad 3\text{-}44$$

$$\mathbf{K}(m)=\mathbf{P}^-(m)\mathbf{H}^T\left(\mathbf{H}\mathbf{P}^-(m)\mathbf{H}^T+\mathbf{Q}_v\right)^{-1} \qquad 3\text{-}45$$

$$\mathbf{s}^+(m)=\mathbf{s}^-(m)+\mathbf{K}(m)\left[\mathbf{r}(m)-\mathbf{H}\mathbf{s}^-(m)\right] \qquad 3\text{-}46$$

$$\mathbf{P}^+(m)=\left[\mathbf{I}-\mathbf{K}(m)\mathbf{H}\right]\mathbf{P}^-(m) \qquad 3\text{-}47$$

where "super minus" denotes the predicted value of estimate or the covariance matrix, and "super plus" is a reminder of the updated value for estimate or the covariance matrix.

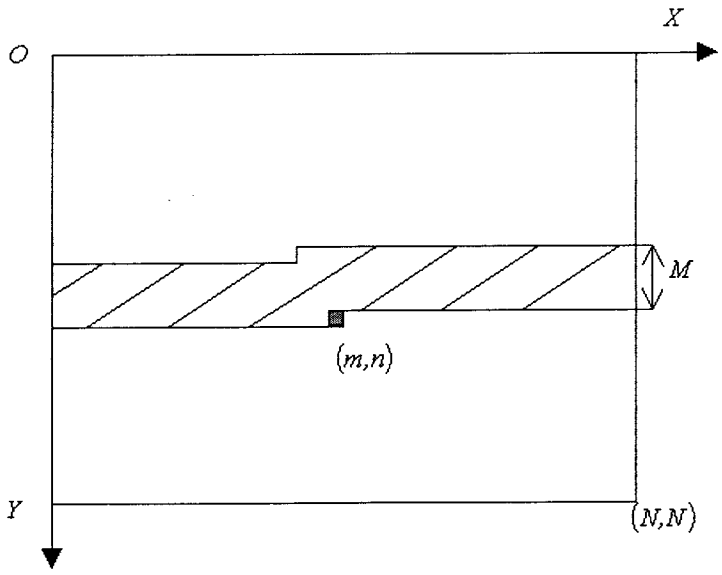

Figure 3-5 Defining a 2-D state vector

Now try to extend the Kalman filter from one dimension into two dimensions. Woods (1981) indicated a way of using generalized 2-D Markov image models to establish differential relationships over an image, and therefore establish recursive Kalman models in two dimensions. In order to do so, the state vector should be defined as follows (see Figure 3-5):

$$\mathbf{s}(m,n) = [s(m,n), s(m-1,n), \ \Lambda\ , \ s(1,n); \Lambda\ ; \\ s(N,n-M), \ \Lambda\ , \ s(m-M+1,n-M)]^T \qquad 3\text{-}48$$

Since the scanning operation transforms the 2-D problem into an equivalent 1-D problem, with this transformation the following equations will be obtained:

$$\mathbf{s}(m,n) = \mathbf{C}\mathbf{s}(m-1,n) + \mathbf{w}(m,n) \qquad 3\text{-}49$$

$$\mathbf{r}(m,n) = \mathbf{H}\mathbf{s}(m,n) + \mathbf{v}(m,n) \qquad 3\text{-}50$$

Thus, the Kalman equations, i.e. a 2-D Kalman scalar filter, could be immediately written down, which would be Eq. 3-43 through to Eq. 3-47, with the above interpretation of the $\mathbf{s}$ vector.

The difficulty of this 2-D Kalman filter is the amount of computation and memory requirements associated with it. For example, consider an observation region consisting of an $N \times N$ square with $N >> M$. The dimension of the matrix equations in Eq. 3-43 through to Eq. 3-47 is approximately $M \times N$. This means that in general the order of the computation is approximately $M^3 \times N^3$. However, taking advantage of spatial invariant structure of the signal model this is reduced to $M^2 \times N^2$. For $M = 4$ and $N = 100$, the order of 160,000 multiplies and adds per output point are required. The overall total computation for the 10,000 element image would be about 10^9. In addition, the data storage problems are immense. To store $\mathbf{P}^-$ and $\mathbf{P}^+$ at each stage needs $M^2 \times N^2$ storage locations. These numbers indicated that the exact 2-D Kalman scalar filter is computational unmanageable (Woods 1981).

Woods and Radewan (1977) attempted to minimise the width of the above 2-D state vector, and developed the 2-D Kalman Strip Filter, which was further extended into the Reduced Update Kalman Filter (RUKF) by further approximation of the update estimate yielded by the strip model. These two Kalman processors overcome the computational problems mentioned above. Both vector and scalar scanning methods were considered in their work, but emphasis was placed on the scalar scan because it leads to processors which are recursive in both dimensions, i.e. a 2-D recursive processor. The results have applications to a range of problems involving estimation on both space and space-time data fields, including image processing problems where most emphasis has been placed. The Kalman algorithms allow the use of space-variant models which provide a better match to local source statistics leading to a greater noise reduction. The two processors developed in Woods and Radewan (1977) subsequently have been widely adopted and improved by other researchers (Woods and Ingle 1981, Azimi-Sadjadi and Wong 1987, Tekalp *et al* 1989, Wu and Kundu1992).

3.5.2 Limitations

Most existing 2-D Kalman processors, including the Reduced Update Kalman Filter, have been developed for image processing, especially for image restoration. They do not fully suit applications for terrain modelling using grid DEMs. Kalman filtering is a model-based filter (Brown and Hwang 1992). This means that it is assumed that the *a priori* model parameters are known, and the derived results are the second-order statistics of the processes of an application at hand. The developed 2-D Kalman filters were established based on the characteristics of the relevant image processing, such as image restoration. They would not suit the applications of terrain surface modelling using grid DEMs, which have different characteristics. For example, compared with a image, DEMs are special 2-D data in which each DEM point represents terrain elevation. Elevation is not the only terrain variable of interest for terrain modelling. Estimates of other terrain variables, such as gradient, are also required to be derived from a noisy DEM for terrain modelling purposes, etc.

For these reasons the existing 2-D Kalman filtering techniques have not been adopted in this thesis but an entirely new 2-D Kalman filtering algorithm for terrain modelling application has been developed.

CHAPTER 4

THE 2-D KALMAN FILTER

4.1 Stochastic Digital Terrain Models for Grid DEMs

In defining the terrain characteristics as accurately as possible from a discrete DEM, it is necessary to establish a suitable terrain model. According to Wang *et al* (1998a, 1999), a stochastic terrain model was developed based on the following assumptions. First, terrain surfaces, which DEMs represent, are assumed as continuous surfaces, and their terrain attributes, which can be directly derived from DEMs, are generally correlated within the mapping area. The topographic characteristics of urban areas are not included in this study. Secondly, other research has shown that the correlation of the terrain variables depends on the distance between the DEM neighbouring points (Evans 1980, Zevenbergen and Thorne 1987). DEM points are a large distance away from a target point contribute weakly to the modelling of the terrain topographic attributes at that point, while DEM points close to the point will contribute more significantly to the modelling of terrain attributes. Thirdly, according to the terrain geometry, the mathematical relationships between the adjacent DEM points, in terms of elevation, and the first partial derivatives of elevation along the X and Y-axes, could be approximated as being linear with random model errors if the DEM sampling interval is small enough.

In order to develop the strict mathematical formulae based on the above assumptions, the raster scanning described in Section 3.5, and Figure 3-4, is adopted for processing a DEM with $N \times M$ grid points. From a Kalman filtering point of view, the DEM data would be separated into "past", "present", and "future" groups. The words have their conventional meaning with respect to the order in which the DEM points are processed.

According to the assumptions made about the terrain geometry, the terrain variables of point (i, j) may be approximately modelled by its neighbouring point $(i-1, j)$ along the X direction (see Figure 4-1). The first order model, in terms of the first order partial derivative of elevation, along the X direction can be easily assumed as:

$$H(i,j) = H(i-1,j) + H_x(i-1,j)dx + v_{H_b}(i,j) \quad 4\text{-}1$$

$$H_x(i,j) = H_x(i-1,j) + v_{H_{x_b}}(i,j) \quad 4\text{-}2$$

$$H_y(i,j) = H_y(i-1,j) + v_{H_{y_b}}(i,j) \quad 4\text{-}3$$

Where $H(i,j)$, $H_x(i,j)$, and $H_y(i,j)$ are the elevation, the first partial derivatives of elevation along the X and Y directions of point (i,j) respectively. $H(i-1,j)$, $H_x(i-1,j)$, and $H_y(i-1,j)$ are the elevation, the first partial derivatives of elevation along the X and Y direction of point $(i-1,j)$ respectively. dx is the sampling intervals of the DEM in X direction. v_{H_b}, $v_{H_{x_b}}$, and $v_{H_{y_b}}$ are assumed as white noise sequences, which are to be filtered.

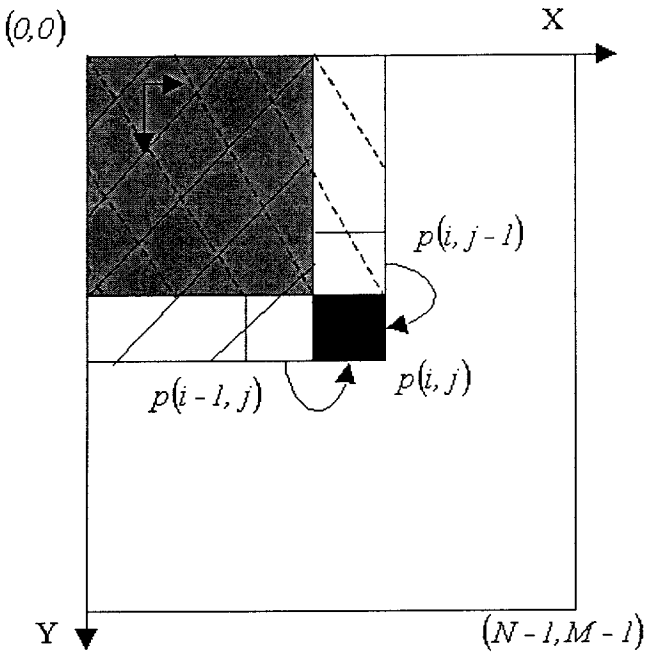

Figure 4-1 Modelling terrain topographic attributes in a grid DEM

The terrain variables of point (i,j) may also be approximately modelled by its adjacent point $(i,j-1)$ in the Y direction (see Figure 4-1). The first order model, in terms of order of partial derivative of elevation, along the Y direction can be similarly assumed as:

$$H(i,j)=H(i,j-1)+H_y(i,j-1)dy+v_{H_c}(i,j) \quad 4\text{-}4$$

$$H_x(i,j)=H_x(i,j-1)+v_{H_{x_c}}(i,j) \quad 4\text{-}5$$

$$H_y(i,j)=H_y(i,j-1)+v_{H_{y_c}}(i,j) \quad 4\text{-}6$$

Where $H(i,j\text{-}1)$, $H_x(i,j\text{-}1)$, and $H_y(i,j\text{-}1)$ are the elevation, the first partial derivatives of elevation along the X and Y directions of point $(i,j\text{-}1)$ respectively. dy is the sampling intervals of the DEM in Y direction. v_{H_c}, $v_{H_{x_c}}$, and $v_{H_{y_c}}$ are assumed as white noise sequences.

4.2 Developing a 2-D Kalman Filter for Terrain Surface Modelling

4.2.1 Derivation of 2-D Kalman equations for terrain surface modelling

Based on the established stochastic terrain models, a 2-D Kalman filter will be developed. Three elements are chosen, i.e. elevation and its two first partial derivatives of elevation, to form the state vector as:

$$\mathbf{S}(i,j)=\begin{bmatrix} H(i,j) \\ H_x(i,j) \\ H_y(i,j) \end{bmatrix} \quad 4\text{-}7$$

Rewriting the stochastic terrain model Eq. 4-1 to Eq. 4-3 into vector and matrix forms leads to the following equation:

$$\mathbf{S}_x(i,j)=\mathbf{\Phi}_x(i,j)\mathbf{S}(i-1,j)+\mathbf{V}_{\mathbf{S}_x}(i,j) \quad 4\text{-}8$$

where, $\mathbf{\Phi}_x(i,j)=\begin{bmatrix} 1 & dx & 0 \\ 0 & 1 & 0 \\ 0 & 0 & 1 \end{bmatrix}$ is the system matrix, and $\mathbf{V}_{\mathbf{S}_x}(i,j)=\begin{bmatrix} v_{H_b} \\ v_{H_{xb}} \\ v_{H_{yb}} \end{bmatrix}$ is the random process. The subscript x indicates that the state vector is derived by its adjacent DEM point in the X direction. The relevant covariance matrix $\mathbf{Q}_x(i,j)$ of Eq. 4-8 are:

$$E\left[\mathbf{V}_{\mathbf{S}_x}(i,j)\mathbf{V}_{\mathbf{S}_x}(i',j')^T\right]=\begin{cases}\mathbf{Q}_x(i,j) & i=i' \quad and \quad j=j' \\ 0 & otherwise\end{cases} \qquad 4\text{-}9$$

Similarly, re-writing Eq. 4-4 to 4-6 into vector and matrix forms, the following equations can also be obtained:

$$\mathbf{S}_y(i,j)=\mathbf{\Phi}_y(i,j)\mathbf{S}(i,j-1)+\mathbf{V}_{\mathbf{S}_y}(i,j) \qquad 4\text{-}10$$

where, $\mathbf{\Phi}_y(i,j)=\begin{bmatrix}1 & 0 & dy\\ 0 & 1 & 0\\ 0 & 0 & 1\end{bmatrix}$, and $\mathbf{V}_{\mathbf{S}_y}(i,j)=\begin{bmatrix}v_{H_c}\\ v_{H_{xc}}\\ v_{H_{yc}}\end{bmatrix}$. The subscript y indicates that the state vector is derived by its neighbouring point in the Y direction. The covariance matrix associated $\mathbf{Q}_y(i,j)$ with Eq. 4-10 is:

$$E\left[\mathbf{V}_{\mathbf{S}_y}(i,j)\mathbf{V}_{\mathbf{S}_y}(i',j')^T\right]=\begin{cases}\mathbf{Q}_y(i,j) & i=i' \quad and \quad j=j' \\ 0 & otherwise\end{cases} \qquad 4\text{-}11$$

Now the terrain topographic relationships between the adjacent DEM points have been established, and Eq. 4-8 and Eq. 4-10 are the dynamic models of the 2-D Kalman filter. Using these relationships to process a DEM, according to the theory of Kalman filtering, the relevant predicted estimate of state vector and the associated variance-covariance matrix can be derived from either two orthogonal directions as:

$$\mathbf{S}_x^-(i,j)=\mathbf{\Phi}_x(i,j)\mathbf{S}^+(i-1,j) \qquad 4\text{-}12$$

$$\mathbf{P}_x^-(i,j)=\mathbf{\Phi}_x(i,j)\mathbf{P}^+(i-1,j)\mathbf{\Phi}_x^T(i,j)+\mathbf{Q}_x(i,j) \qquad 4\text{-}13$$

or

$$\mathbf{S}_y^-(i,j)=\mathbf{\Phi}_y(i,j)\mathbf{S}^+(i,j-1) \qquad 4\text{-}14$$

$$\mathbf{P}_y^-(i,j) = \Phi_y(i,j)\mathbf{P}^+(i-1,j)\Phi_y^T(i,j) + \mathbf{Q}_y(i,j) \qquad 4\text{-}15$$

where $\mathbf{S}^+(i,j)$ and $\mathbf{P}^+(i,j)$ are the relevant updated estimates of the state vector and the associated variance-covariance matrix of DEM point (i,j).

The correlation between the predicted estimates of state vectors $\mathbf{S}_x^-(i,j)$ and $\mathbf{S}_y^-(i,j)$ is considered weak, since they are derived from data along the orthogonal directions and different terrain models. $\mathbf{S}_x^-(i,j)$ and $\mathbf{S}_y^-(i,j)$ are assumed to be independent. Therefore, the optimal predictions of point (i,j) may be considered as a linear combination of $\mathbf{S}_x^-(i,j)$ and $\mathbf{S}_y^-(i,j)$:

$$\mathbf{S}^-(i,j) = \mathbf{P}^-(i,j)\left[\left(\mathbf{P}_x^-(i,j)\right)^{-1}\mathbf{S}_x^-(i,j) + \left(\mathbf{P}_y^-(i,j)\right)^{-1}\mathbf{S}_y^-(i,j)\right] \qquad 4\text{-}16$$

$$\mathbf{P}^-(i,j) = \left[\left(\mathbf{P}_x^-(i,j)\right)^{-1} + \left(\mathbf{P}_y^-(i,j)\right)^{-1}\right]^{-1} \qquad 4\text{-}17$$

On the other hand, the observation of elevation is assumed to have a linear relationship with the state vector $\mathbf{S}(i,j)$ at the relevant position. The functional model obtained is:

$$Z(i,j) = \mathbf{D}\mathbf{S}(i,j) + v_Z(i,j) \qquad 4\text{-}18$$

where $\mathbf{D} = [1 \quad 0 \quad 0]$ is the observation vector, and $v_Z(i,j)$ is the observation noise, assumed as a white noise sequence having zero cross-correlation with the $\mathbf{V}_{S_x}(i,j)$ and $\mathbf{V}_{S_y}(i,j)$ sequences. In other words:

$$E\left[v_Z(i,j)v_Z(i',j')^T\right] = \begin{cases} R(i,j) & i = i' \quad and \quad j = j' \\ 0 & otherwise \end{cases} \qquad 4\text{-}19$$

$$E\left[\mathbf{V}_{S_x}(i,j)v_Z(i',j')^T\right]=0 \quad for \quad any \quad i,\ i',\ j \quad and\ j' \tag{4-20}$$

$$E\left[\mathbf{V}_{S_y}(i,j)v_Z(i',j')^T\right]=0 \quad for \quad any \quad i,\ i',\ j \quad and\ j' \tag{4-21}$$

where $R(i,j)$ is DEM observation variance.

Following the 1-D Kalman five recursive equations, i.e. Eq. 3-8, Eq.3-17, Eq. 3-21, Eq. 3-22, and Eq. 3-24, the covariance matrix $\mathbf{P}^-(i,j)$ may be substituted into Eq.3-17 to obtain the Kalman gain $\mathbf{K}(i,j)$. The optimal prediction $\mathbf{S}^-(i,j)$ and its covariance matrix $\mathbf{P}^-(i,j)$ are substituted into Eq. 3-8 and Eq. 3-21, to derive the optimal updated estimate $\mathbf{S}^+(i,j)$ and its covariance matrix $\mathbf{P}^+(i,j)$, by using the observation $Z(i,j)$, to improve the prediction:

$$\mathbf{K}(i,j)=\mathbf{P}^-(i,j)\boldsymbol{D}^T(\mathbf{D}\mathbf{P}^-(i,j)\mathbf{D}^T+R(i,j))^{-1} \tag{4-22}$$

$$\mathbf{S}^+(i,j)=\mathbf{S}^-(i,j)+\mathbf{K}(i,j)(Z(i,j)-\mathbf{D}\mathbf{S}^-(i,j)) \tag{4-23}$$

$$\mathbf{P}^+(i,j)=(\mathbf{I}-\mathbf{K}(i,j)\mathbf{D})\mathbf{P}^-(i,j) \tag{4-24}$$

In this way, the 2-D Kalman recursive equations used for terrain surface modelling are derived, consisting of nine equations Eq. 4-12, Eq. 4-13, Eq. 4-14, Eq. 4-15, Eq. 4-16, Eq. 4-17, Eq. 4-22, Eq. 4-23 and Eq. 4-24.

Compared with 1-D Kalman recursive equations Eq. 3-8, Eq.3-17, Eq. 3-21, Eq. 3-22, and Eq. 3-24, four more equations Eq. 4-12 through to Eq. 4-17 are included in the 2-D Kalman filter to derive the predicted estimate and its covariance matrix. This is due to the complexity of two-dimensional applications.

4.2.2 2-D Kalman recursive procedure

The recursive process of the 2-D Kalman filter over a DEM is similar to the process of the 1-D Kalman filtering discussed in Section 3.2.3, but with more complexity to enable it to handle the initial values and the predictions at each DEM point.

When applying the 2-D Kalman filter to a DEM shown in Figure 4-1, the filter starts from the first row of the DEM data, and point $(0,0)$ will be the first DEM point to be processed. At this point, the *a priori* estimate $\mathbf{S}^-(0,0)$ and its covariance matrix $\mathbf{P}^-(0,0)$ are given by the boundary conditions of the filtering. Kalman gain at DEM point $(0,0)$, ie. $\mathbf{K}(0,0)$, will be determined first using Eq.4-22. Then, the elevation measurement $Z(0,0)$ is used to update the initial value $\mathbf{S}^-(0,0)$ through Eq.4-23, resulting in the updated estimate of $\mathbf{S}^+(0,0)$. Next, the associated variance-covariance matrix of $\mathbf{S}^+(0,0)$, ie. $\mathbf{P}^+(0,0)$, is computed using Eq. 4-24. In the following step, the filter needs to generate the project ahead estimate for the next DEM point in the row, i. e. $\mathbf{S}^-(1,0)$ and its covariance matrix $\mathbf{P}^-(1,0)$, to complete the processing loop of point $(0,0)$. At this time, along the X direction, $\mathbf{S}^+(0,0)$ and $\mathbf{P}^+(0,0)$ are now available, and therefore the predicted estimate $\mathbf{S}_x^-(1,0)$ and its covariance matrix $\mathbf{P}_x^-(1,0)$ could be determined using Eq. 4-12 and Eq. 4-13. However, along the Y direction, $\mathbf{S}_y^-(1,0)$ and its covariance matrix $\mathbf{P}_y^-(1,0)$ will still be the *a priori* values, since no DEM point has been processed along this direction and no more computation is needed. The predicted estimate $\mathbf{S}^-(1,0)$ and its covariance matrix $\mathbf{P}^-(1,0)$ are obtained from the newly computed $\mathbf{S}_x^-(1,0)$ and $\mathbf{P}_x^-(1,0)$, and the initial value of $\mathbf{S}_y^-(1,0)$ and $\mathbf{P}_y^-(0,1)$ using Eq. 4-16 and Eq. 4-17. Once the project ahead estimate $\mathbf{S}^-(0,1)$ and its covariance matrix $\mathbf{P}^-(1,0)$ are computed, they will be used as input to enter the Kalman loop again for processing the DEM point $(1,0)$. Following this procedure, the filter processes each point in succession by point until the end of the first row.

As soon as the first row of the DEM is processed, the filter starts to process the second row of the DEM. In this case, the first DEM point $(1,0)$ of the row is the boundary of the filtering. When the filter needs to determine the predicted estimate $\mathbf{S}^-(1,1)$ and its covariance matrix $\mathbf{P}^-(1,1)$, the predicted estimate from the X direction, i. e. $\mathbf{S}_x^-(1,1)$

and $\mathbf{P}_x^-(1,1)$ will still be the *a priori* values. The predicted estimate from the Y direction, i. e. $\mathbf{S}_y^-(1,1)$ and its covariance matrix $\mathbf{P}_y^-(1,1)$ should be derived by Eq. 4-14 and Eq. 4-15 based on the updated $\mathbf{S}^+(0,0)$ and $\mathbf{P}^+(0,0)$, and so on.

Following this recursive procedure, the best estimates of terrain variables $\mathbf{S}^+(i,j)$ of any arbitrary DEM point (i,j) will be derived by using all DEM measurements of the solid and dashed line shaded area illustrated in Figure 4-1.

4.3 A Discussion of Boundary Conditions of the 2-D Kalman filter

This section focuses on the 2-D boundary condition problem for the 2-D spatial Kalman filter, beginning with a review of the role of boundary conditions in 1-D recursive estimation.

The initial condition problem for 1-D Kalman filtering is to select an optimal initial estimate of the state, along with its associated error covariance. According to Woods (1981), often this estimate is simply the mean of the signal process as would be appropriate, for example, when no *a priori* information is available. When the data set is finite, a boundary value problem consisting of both initial and final conditions must in general be considered. If one has a finite length section of a data set of infinite length, the causal filtering problem ignores any final conditions, thus enabling one to reduce the general boundary condition problem to an initial value problem. A causal filter is a system for which the output at any time does not depend on future values of the input (Minkler and Minkler 1993). Hence the two-point boundary nature of a finite length data set can be ignored in the 1-D case by the expedient of causal filtering.

Unlike its one dimension counterpart, the boundary condition problem in two dimensions does not degenerate to an initial value condition problem for causal filtering. This is because the data scan processing causes the boundaries to be encountered repetitively in the course of the filtering, at the beginning and end of each scan line. Thus, in addition to initial conditions at the top and final conditions on the

bottom, the majority of the boundary consists of points that cannot be so categorised and therefore have no 1-D counterpart.

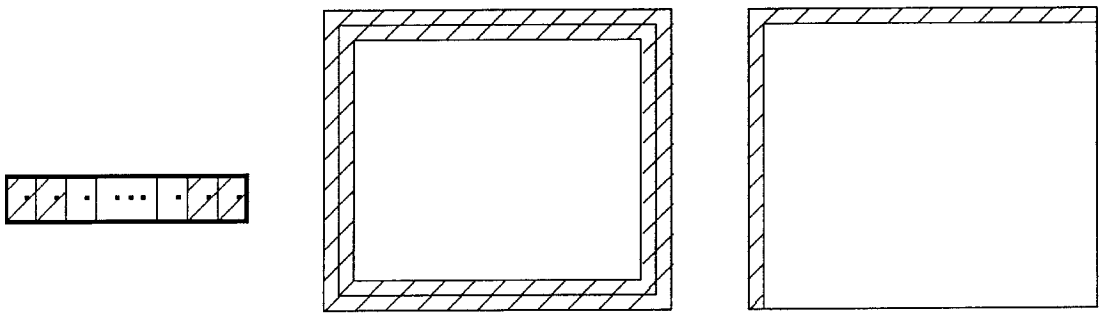

Figure 4-2 Boundary value problems

In performing the developed 2-D Kalman recursive estimation, the boundary conditions are the top and left (see Figure 4-2(c)) lines of a DEM, since they are the initial values for the filtering along the x and y-axes of a DEM, respectively.

The boundary values of the 2-D Kalman filter are assumed to be deterministic. All three elements of the state vector are taken to be zero, and correspondingly, the associated **P** matrix comprises large variances:

$$\mathbf{S}^{-}(i,j) = \begin{bmatrix} 0 \\ 0 \\ 0 \end{bmatrix} for \quad all \quad i=0 \quad or \quad j=0 \tag{4-25}$$

$$\mathbf{P}^{-}(i,j) = \begin{bmatrix} \infty & 0 & 0 \\ 0 & \infty & 0 \\ 0 & 0 & \infty \end{bmatrix} for \quad all \quad i=0 \quad or \quad j=0 \tag{4-26}$$

This assumption simplifies the determination of the filtering initials, and experiments (Wang 1998, Wang *et al* 1998a, 1998b) have shown that such an approximation does not significantly affect the filtering results, compared with when using the true values of the terrain variables at the relevant DEM positions. In this case, the boundary conditions are simply inserted in the Kalman equations when needed, making it completely

analogous to the 1-D Kalman filter with deterministic input, and in fact through the raster scanning, is equivalent to it.

4.4 Considerations of the Determination of Stochastic Models

4.4.1 Dynamic model error

The variance-covariance matrices $\mathbf{Q}_x(i,j)$ and $\mathbf{Q}_y(i,j)$ represented in the dynamic model Eq. 4-9 and Eq. 4-11 are assumed to be known in the developed 2-D Kalman filter for computing the variance-covariance matrix of the predicted estimate $\mathbf{P}^-(i,j)$. They are the model variance-covariance matrices used in the two orthogonal modelling directions, respectively, representing the possible errors that the dynamic models of Eq. 4-8 and Eq. 4-10 may introduce into the estimates of the three terrain attributes.

The dynamic model error reflects the differences between the 'true' terrain topographic attributes of a DEM point and the relevant predicted values derived from the DEM adjacent points. For example, using the dynamic model of Eq. 4-8 to derive the elevation of point $k+1$ from its adjacent DEM point k is illustrated in Figure 4-3. The vertical axis of Figure 4-3 represents the elevation, and the horizontal axis represents points of the DEM. Based on the elevation and the first partial derivative along the X direction of point k, the elevation of point $k+1$ can be predicted using the dynamic model Eq. 4-8, presented as $\mathbf{DS}(k+1)$. The difference between the true elevation $H(k+1)$ and $\mathbf{DS}(k+1)$ is defined as the model error, and in this case, the model error for elevation element presented as $v_{H_b}(k+1)$.

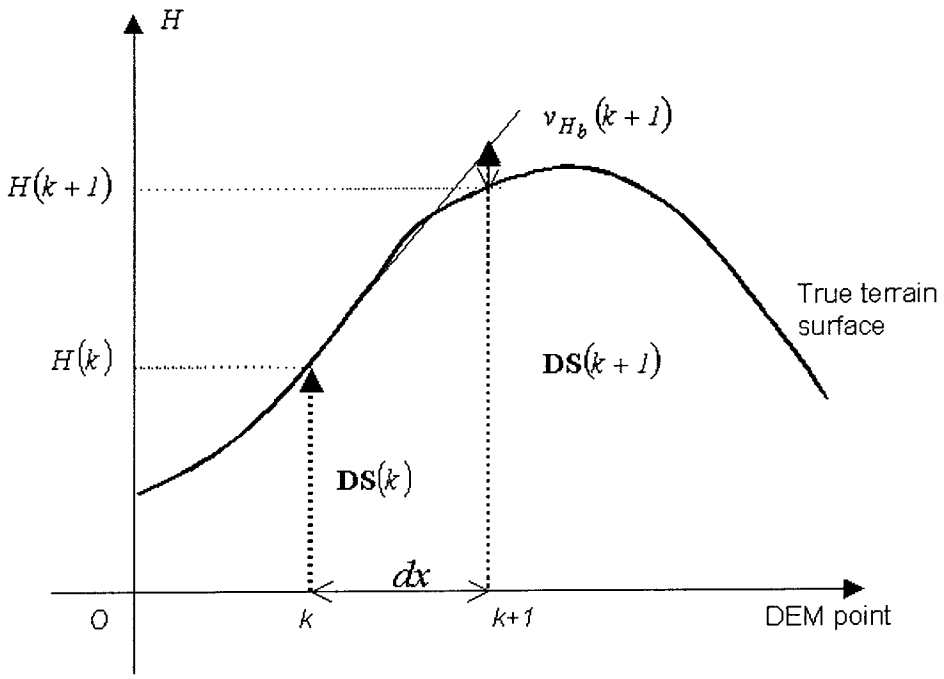

Figure 4-3 The physical meaning of dynamic model error

Determination of model errors

If the terrain surface is homogeneous and smooth, the associated model error would be mainly affected by the level of the second order partial derivatives of elevation of the terrain surface. Suppose that the terrain models of Eq. 4-1 to Eq. 4-3 are extended to include the second order partial derivatives of elevation. According to the relevant assumptions in Section 4.1, the following equations may be derived:

$$H(i,j)=H(i-1,j)+H_x(i-1,j)dx+\frac{1}{2}H_{xx}(i-1,j)(dx)^2+v_{H_{bb}}(i,j) \quad 4\text{-}27$$

$$H_x(i,j)=H_x(i-1,j)+H_{xx}(i-1,j)dx+v_{H_{xbb}}(i,j) \quad 4\text{-}28$$

$$H_y(i,j)=H_y(i-1,j)+H_{yx}(i-1,j)dx+v_{H_{ybb}}(i,j) \quad 4\text{-}29$$

where $H_{xx}(i,j)$ and $H_{yx}(i,j)$ are the second order partial derivatives of elevation along the x and y axes, and $v_{H_{bb}}(i,j)$, $v_{x_{bb}}(i,j)$ and $v_{y_{bb}}(i,j)$ are the relevant model errors.

Then the relevant model errors for the elevation, X and Y derivatives using the terrain model defined in Eq. 4-1 to Eq. 4-3 can be determined as:

$$v_{H_b}(i,j) = \frac{1}{2} H_{xx}(i-1,j)(dx)^2 + v_{H_{bb}}(i,j) \quad 4\text{-}30$$

$$v_{H_{xb}}(i,j) = H_{xx}(i-1,j)dx + v_{H_{xbb}}(i,j) \quad 4\text{-}31$$

$$v_{H_{yb}}(i,j) = H_{yx}(i-1,j)dx + v_{H_{ybb}}(i,j) \quad 4\text{-}32$$

If the model error in the second order terrain models, defined by Eq. 4-26 to Eq. 4-28, are ignored in Eq. 4-30 to Eq. 4-32, the model errors in Eq. 4-1 to Eq. 4-3 can be further approximated as:

$$v_{Hb}(i,j) \approx \frac{1}{2} H_{xx}(i-1,j)(dx)^2 \quad 4\text{-}33$$

$$v_{H_{xb}}(i,j) \approx H_{xx}(i-1,j)dx \quad 4\text{-}34$$

$$v_{H_{yb}}(i,j) \approx H_{yx}(i-1,j)dx \quad 4\text{-}35$$

Similar relationships between the second order partial derivatives of elevation and the model errors used in Eq. 4-4 to Eq. 4-6 can be derived as:

$$v_{H_c}(i,j) \approx \frac{1}{2} H_{yy}(i,j-1)(dy)^2 \quad 4\text{-}36$$

$$v_{H_{xc}}(i,j) \approx H_{xx}(i,j-1)dy \quad 4\text{-}37$$

$$v_{H_{yc}}(i,j) \approx H_{xy}(i,j-1)dy \quad 4\text{-}38$$

The estimation of suitable model errors over smoothing terrain surfaces is now simplified to that of determining the level of the second partial derivatives of elevation over the specific mapping area. It is obvious that if the terrain surface is smooth the second order partial derivative of elevation would be set small, and the relevant model error will be small. On the other hand, if the terrain surface is rough, the value should be set larger. This is consistent with the analysis in terms of accuracy of the predictions. If the terrain is smooth, the prediction accuracy would be high and therefore the model errors should be small, whereas in modelling a rough terrain surface, the accuracy of predictions is reduced and the relevant model errors should be large. In such

circumstances, the 2-D Kalman filter requires high density of DEM sampling over a rough terrain surface to obtain accurate modelling results.

Effect of DEM resolutions

The change rate of the first partial derivatives of elevation for a specific mapping area determines the magnitude of the second order partial derivatives of elevation for that area. The 'true' second order partial derivatives of elevation of a mapping area will not change when the terrain is sampled with different resolutions. So it will be the same in the estimation of the relevant model errors used to process the DEMs with different resolutions, if the mapping area is the same.

Therefore, the impact of DEM resolution on estimating model errors is also modelled in Eq. 4-33 to Eq. 4-38. For example, if the second order partial derivatives of elevation of a terrain surface are assumed to be 0.08, using Eq. 4-33 to Eq. 4-35, or Eq. 4-36 to Eq. 4-38, the model errors suitable for processing of a 5m DEM will be 1m for elevation, 0.4 for X and Y derivatives. The model errors for a 10m DEM of the same terrain will be 4m for elevation, 0.8 for the X and Y derivatives.

Effect of terrain roughness and breaklines

However, the real terrain surfaces are often rough and contain breaklines. If terrain surfaces are rough, the accuracy of predictions of the 2-D Kalman filter can be improved by increasing DEM resolution. However, if breaklines occur in a DEM data, increasing the DEM sampling interval would not solve the problem. Suppose a cliff exists in the DEM mapping area (see Figure 4-4) where terrain topographic characteristics change abruptly, and this is not caused by outliers in the DEM, then, DEM points (k) and $(k+1)$ belong to different kinds of landscapes, and the elevation of point $(k+1)$ is actually unpredictable from the point (k), or the model error should be set large to handle this big discrepancy. However, this will conflict with the remaining DEM points in smoothing terrain where there are no such discrepancies. In order to apply the 2-D Kalman filter to this kind of terrain surface, an adaptive (self-learning) Kalman filter needs to be developed that is capable of adapting itself to different landscapes that occur in the data.

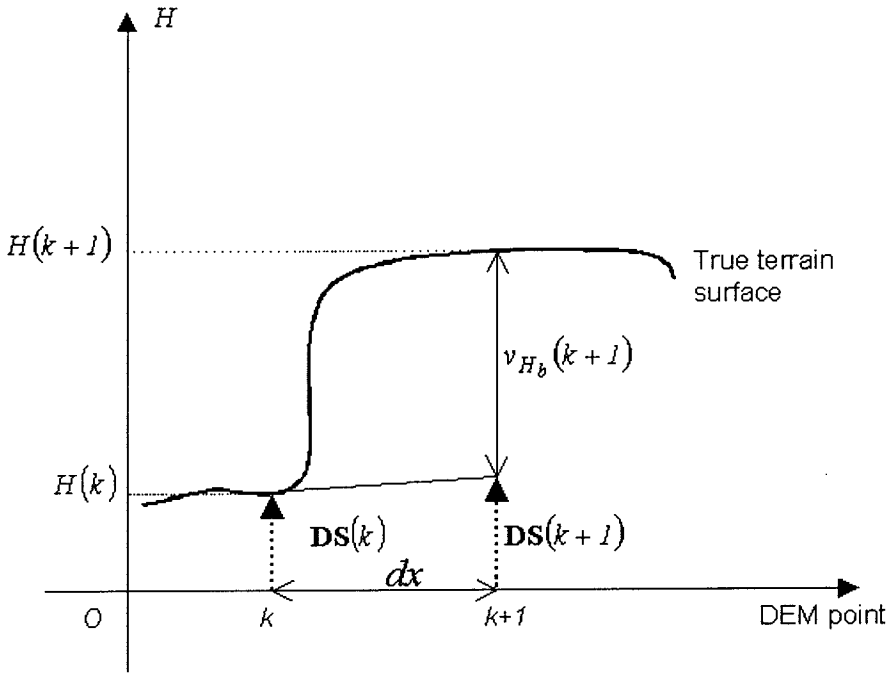

Figure 4-4 Effect of breakline to the determination of model error

4.4.2 Observation error

The DEM observation error, the variance of which is represented by $R(i,j)$, significantly affects the derivation of terrain variables, and therefore is the target of the filtering. The estimation of $R(i,j)$ should be based on the analysis of DEM data. The methods of estimating DEM random noise from DEM data that was introduced in Section 2.2.1 could be used as the guide for the approximation of $R(i,j)$ in the 2-D Kalman filter.

4.5 Testing the 2-D Kalman filter for Terrain Surface Modelling

A mathematical surface was simulated to test the efficiency of the 2-D Kalman filter in terms of reducing DEM random noise and its effect on the derivation of terrain variables. Due to the difficulty of obtaining the ground truth elevations, and the relevant first partial derivatives of a real terrain surface, an artificial terrain surface was generated and used in the testing.

4.5.1 Testing data

A 150 × 150 sized curved surface was simulated using Eq. 4-39, sampled with 1m interval in both X and Y directions as shown in Figure 4-5. The range in elevation was from –18.32 m to 18.56 m, with 0.03 m as the average height:

$$H(i,j) = (i \times dx - 75) \times (50 - j \times dy)/400 \qquad 4\text{-}39$$

where i and j are the coordinates of the DEM point, dx and dy are the sampling intervals.

The two first partial derivative surfaces of the simulated data were also computed from the differential equations of Eq. 4-39, as shown in Figure 4-5(b) and Figure 4-5(c). Based on these two first partial derivatives of elevation, the slope and aspect surfaces of the simulated DEM were also created using the slope and aspect formulae Eq. 2-5 and Eq. 2-6, shown in Figure 4-8 and Figure 4-9. The slope value of the artificial surface varies from 0° to 18°. The aspect values range from –90° to 90° with –100° assigned for the flat DEM points, when the value of the first partial derivative along the X axis of the point is zero. The data included 150 points assigned –100°. The aspect values were not converted into compass degrees to make it simple for the relevant comparison. The simulated DEM, associated with the first partial derivatives, slope and aspect surfaces, are the ground truth data for algorithm testing and relevant comparison.

The random noise with standard deviation of 0.5m was added to the simulated DEM creating a noisy DEM shown in Figure 4-6 for processing using the 2-D Kalman filter and other terrain models.

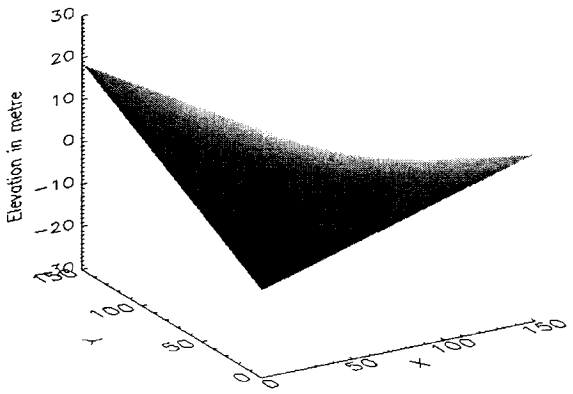

Figure 4-5(a) Elevation

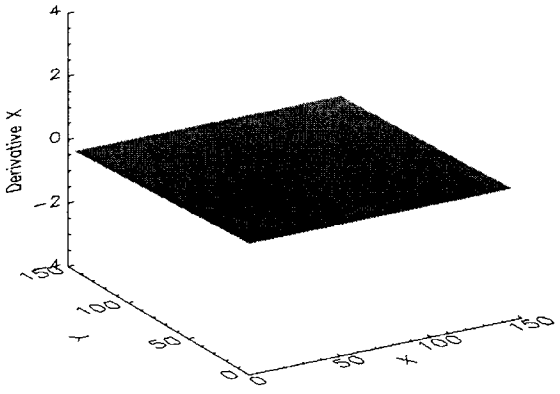

Figure 4-5(b) X derivative

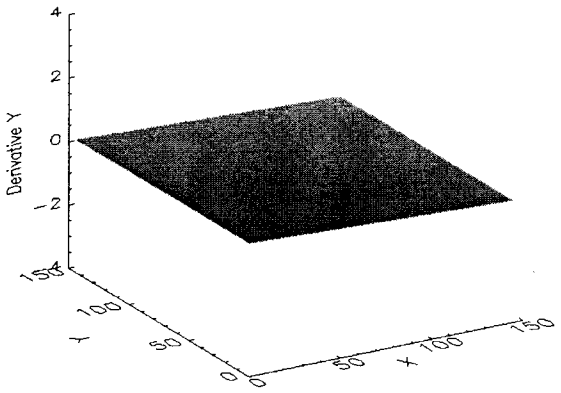

Figure 4-5(c) Y derivative

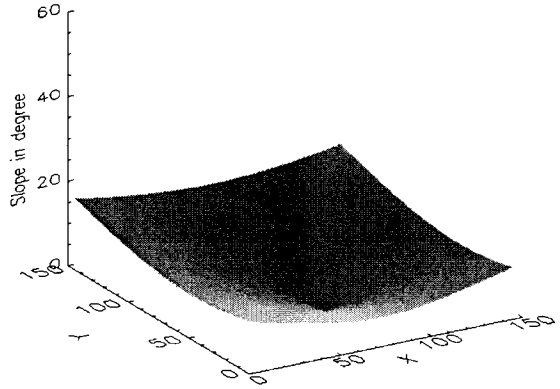

Figure 4-5(d) Slope

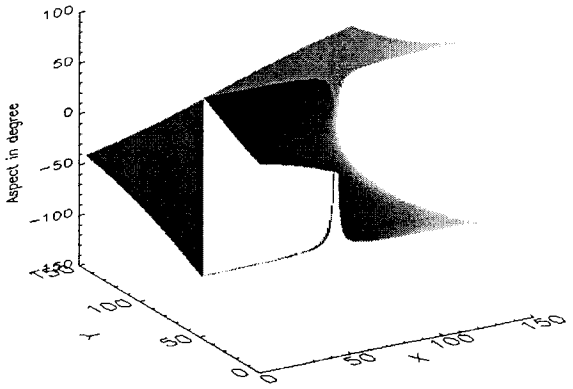

Figure 4-5(e) Aspect

Figure 4-5 The simulated data

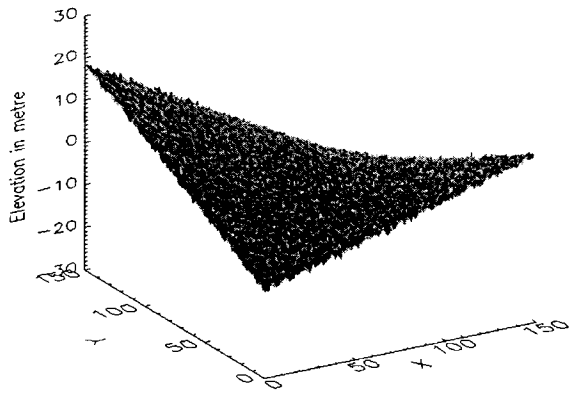

Figure 4-6 The simulated noisy DEM

4.5.2 Results of the 2-D Kalman filter

The 2-D Kalman filter was applied over the simulated noisy DEM, producing simultaneously the estimate of surface elevation and two first partial derivatives shown in Figure 4-7(a), (b) and (c). The slope and aspect surfaces of the noisy DEM were also calculated, using the estimates of derivatives, slope and aspect equations, as shown in Figure 4-7(d) and (e).

The boundary of the 2-D Kalman filter was the first row and first column of the noisy DEM, for which the *a priori* estimates of the state vectors were set to zero and the corresponding variance-covariance factors to about 100 times the relevant model errors. The observation error of this data was known to be 0.5m, equals to the random noise applied in the DEM. Because this is a mathematical surface, the true value of the second order the partial derivatives of elevation is zero. In this experiment, a very small value of the second partial derivative was used to estimate the relevant model errors.

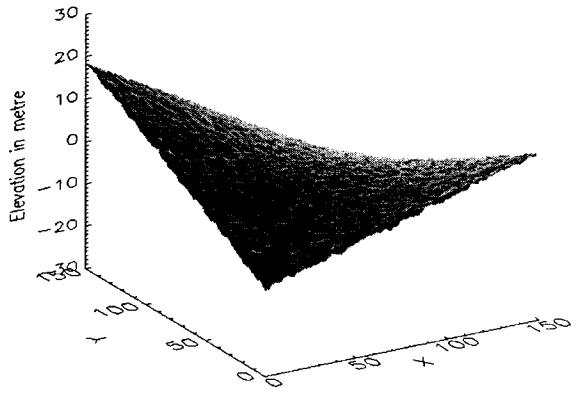

Figure 4-7(a) Elevation

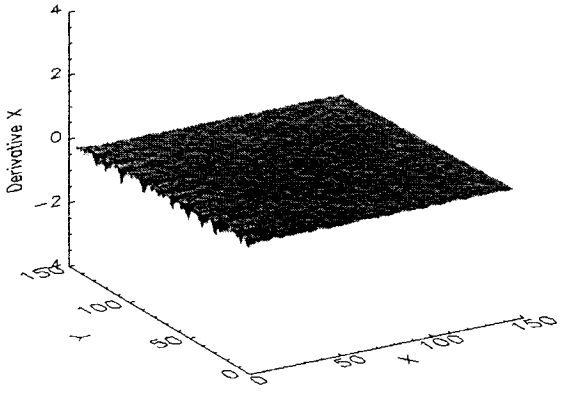

Figure 4-7(b) Derivative X

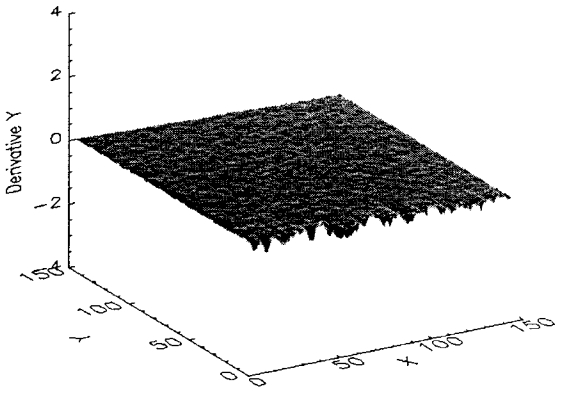

Figure 4-7(c) Derivative Y

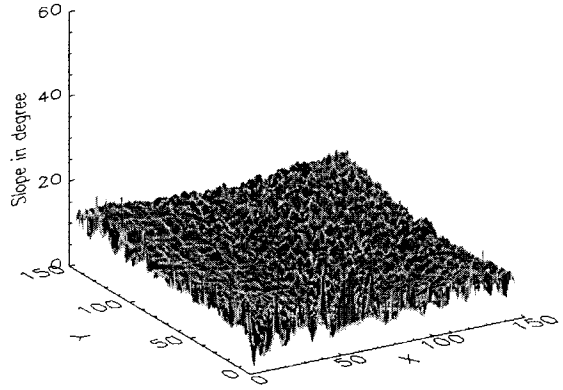

Figure 4-7 (d) Slope

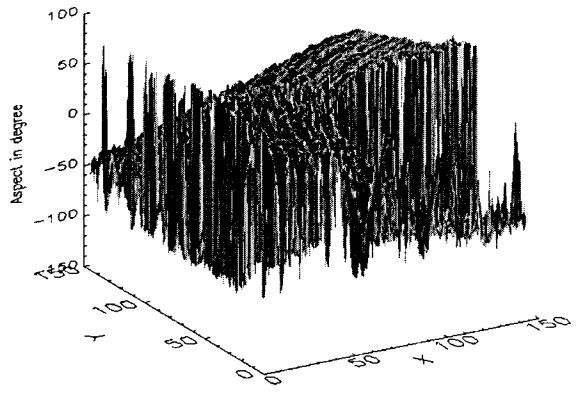

Figure 4-7(e) Aspect

Figure 4-7 The results of the 2-D Kalman filter

Examining the results of the Kalman filtering, the initial estimates of elevation and the derivatives were poor at the boundaries. However, the estimates improved significantly as the number of the processed points increased. Compared with the noisy DEM illustrated in Figure 4-6, the elevation surface for the 2-D Kalman filter is much smoother. The estimates of X and Y derivatives are also considerably smoother and follow the trends of their ground truth. The derived estimates of slope are somewhat irregular, especially for the top row and left column, but it still produced correct slopes for the most of the data. The estimated aspect surface is poor at the boundary and the points where the surface is actually flat, but they improved for the rest of the data, and delineated the basic pattern of the aspect.

4.5.3 Results of the Evans method

The noisy DEM was also processed by the Evans method, which is currently quoted as the most accurate terrain modelling algorithm (Florinsky 1998), resulting in derivatives in terms of X and Y, slope and aspect surfaces as shown in Figure 4-8.

The derivatives of the X and Y surfaces of the Evans method are much noisier and more irregular than the results of the 2-D Kalman filter, when compared with the ground truth. The effects of DEM random noise are even greater in the derived slope and aspect surfaces, which failed to produce correct surfaces.

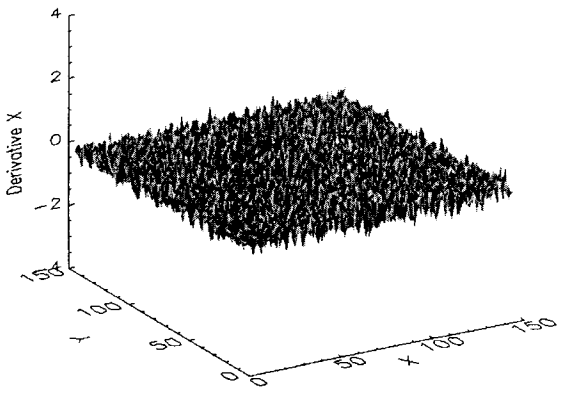

Figure 4-8(a) X derivative

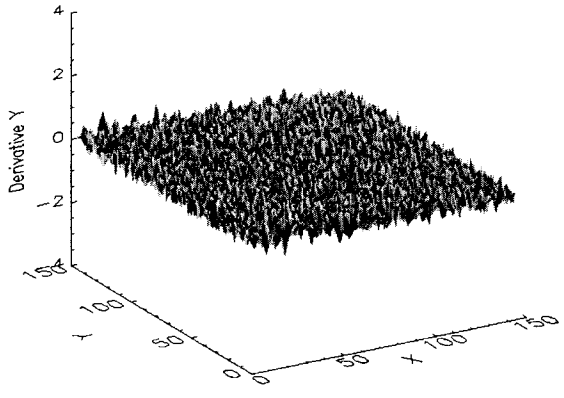

Figure 4-8(b) Y derivative

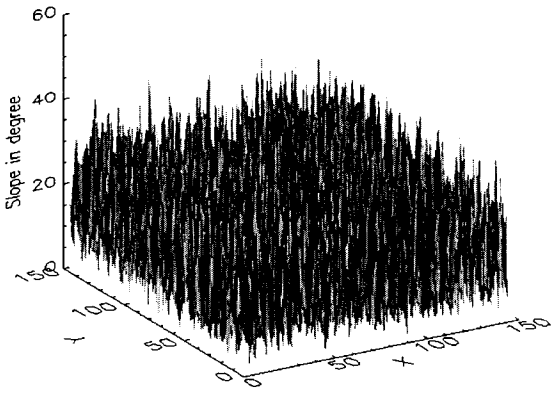

Figure 4-8(c) Slope

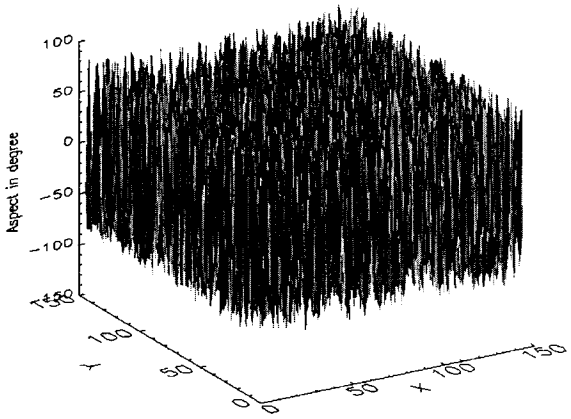

Figure 4-8(d) Aspect

Figure 4-8 The results of the Evans method

4.5.4 Comparison of the test results

The terrain variables derived from the 2D Kalman filter and the Evans method were further quantitatively compared with the ground truth values to evaluate the accuracy of the terrain models and the efficiency of reducing the effects of DEM random noise.

Only the 2-D Kalman filter successfully produced estimates of elevation, as well as other estimates of the terrain variables, from the noisy DEM data. Therefore, the errors in the estimates of elevation derived by the 2-D Kalman filter were compared with the initial random noise in the DEM data. Subtracting the noisy DEM from the ground truth produced the errors in the noisy DEM, which are plotted in Figure 4-9(a) and summarized in Table 4-1. Similarly, errors in the estimates of elevation from the 2-D Kalman filter are also plotted in Figure 4-9(b) and given in Table 4-1. The efficiency of the 2-D Kalman filter is significant in reducing the influence of DEM random noise. The standard deviation of the estimates of elevation has been reduced by 72%, using the developed 2-D Kalman filter.

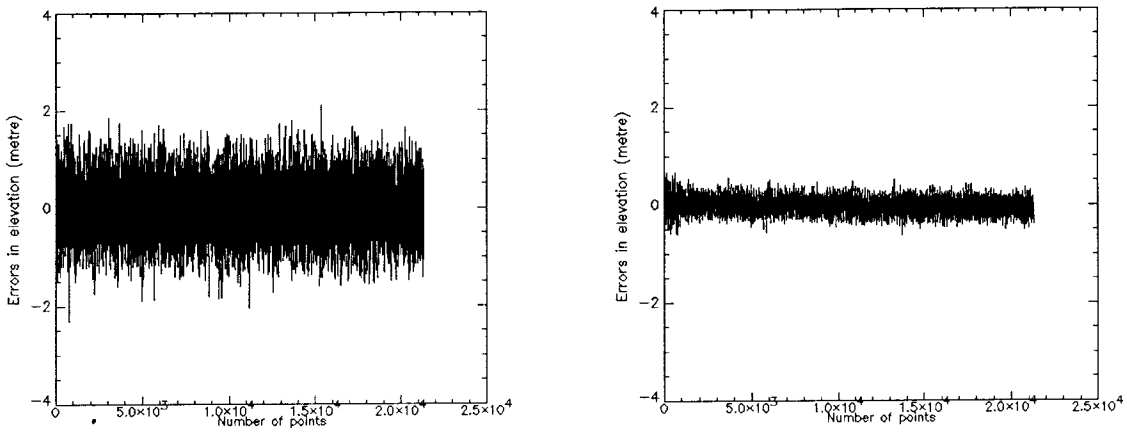

(a) Random noise added in the noisy DEM **(b) Errors in the estimates**

Figure 4-9 Comparison of elevation derived from the 2-D Kalman filter

Table 4-1 Comparing errors in the noisy DEM and the estimates of elevation using the 2-D Kalman filter

	Minimum	Maximum	Mean	Standard deviation	Improvement*
The noisy DEM	-2.30	2.10	0.00	0.50	---
2-D Kalman filter	-0.61	0.67	-0.01	0.14	**72%**

*The improvement is in terms of the standard deviation, and was derived by comparing the Kalman filter result with that of the noisy DEM. The unit is in meters.

A statistical analysis of the estimates of the X and Y derivatives, slope and aspect from the 2-D Kalman filter and the Evans method was also undertaken. Following the same procedures used for comparing the elevations, the errors in the relevant Kalman filtering results and the Evans method were obtained and plotted in Figure 4-10. In the Figures, the horizontal axis represents the number of the DEM points, and the vertical axis represents the errors in the derived terrain variables, using the 2-D Kalman filter and the Evans method, at each DEM position. The details of the statistical comparisons are summarised in Table 4-2.

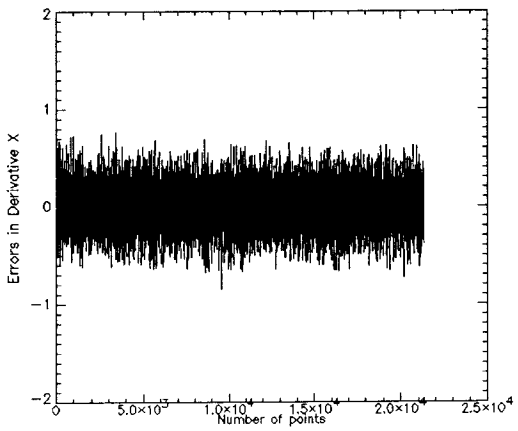

Figure 4-10(a) the Evans method

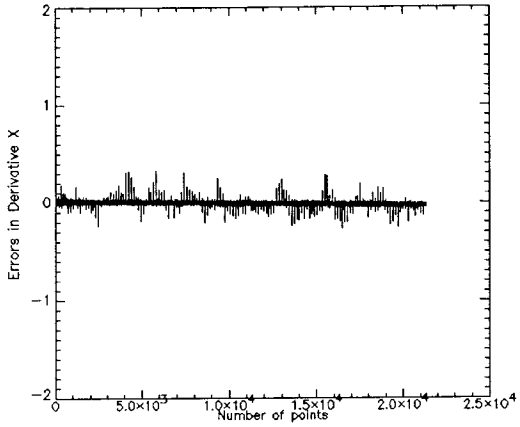

Figure 4-10(b) Kalman filter

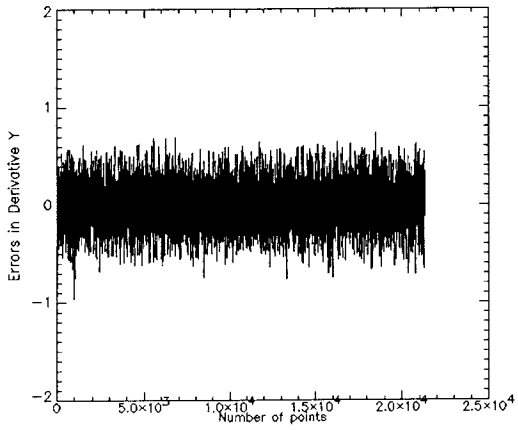

Figure 4-10(c) the Evans method

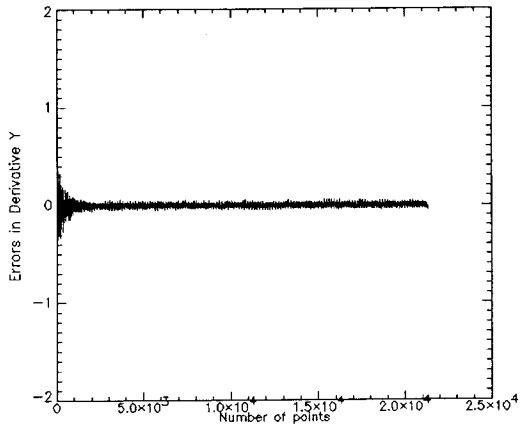

Figure 4-10(d) Kalman filter

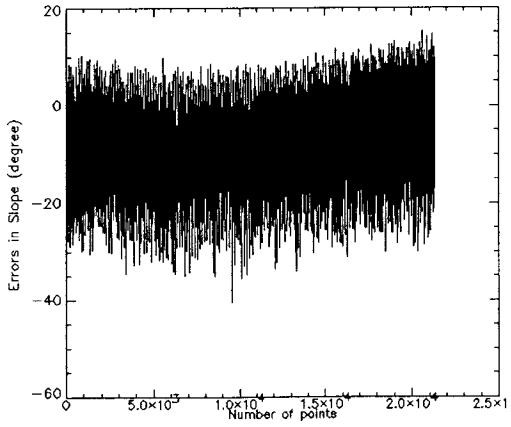

Figure 4-10(e) the Evans method

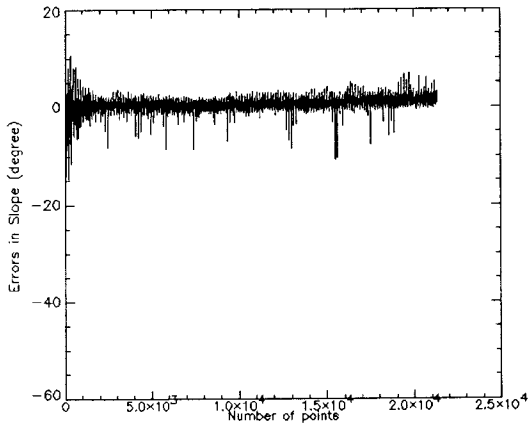

Figure 4-10(f) Kalman filter

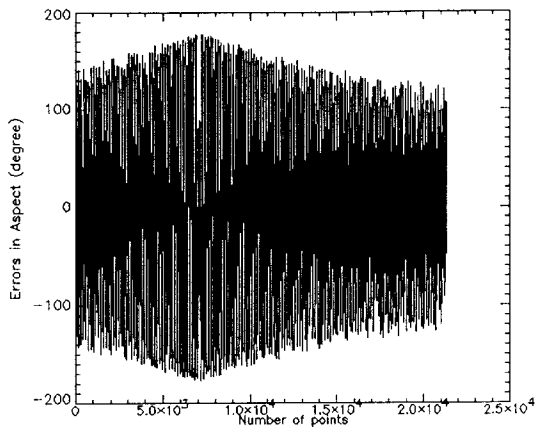

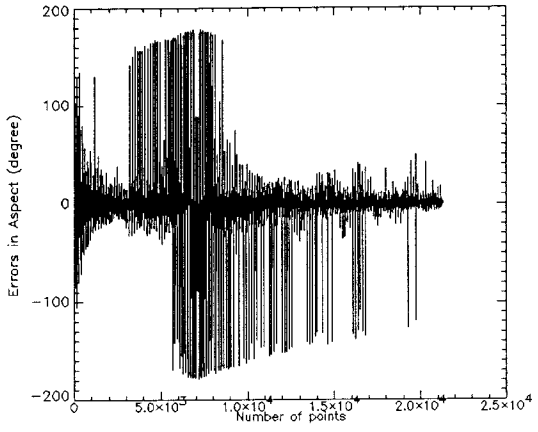

Figure 4-10(g) the Evans method **Figure 4-10 (h) Kalman filter**

Figure 4-10 Comparison of the errors in the results of the 2-D Kalman filter and the Evans method

Table 4-2 Comparing errors in the results of the 2-D Kalman filter and the Evans method

	Minimum	Maximum	Mean	Standard deviation	Improvement
X derivative					
Evans method	-0.84	0.76	0.00	0.20	---
2-D Kalman filter	-0.26	0.33	0.00	0.02	**90%**
Y derivative					
Evans method	-0.96	0.74	0.00	0.20	---
2-D Kalman filter	-0.35	0.38	0.00	0.03	**85%**
Slope (degree)					
Evans method	-40.33°	15.33°	-7.55°	7.85°	---
2-D Kalman filter	-14.55°	10.73°	0.83°	1.07°	**86%**
Aspect (degree)					
Evans method	-177.27°	177.69°	-0.42°	68.52°	---
2-D Kalman filter	-178.68°	178.60°	0.63°	30.18°	**56%**

The comparison indicates that the improvement using 2-D Kalman filter algorithm compared to the Evans method is very significant. Using the 2-D Kalman filter over the same noisy DEM, the standard deviation is reduced by 85-90% for the first partial derivatives, 86% for the slope surface, and 56% for the aspect in comparison with the results of the Evans method. More experimental results are presented in Chapter 7.

4.6 Conclusions

In this Chapter, the development of the 2-D Kalman filter for terrain surface modelling is presented. The Chapter commenced with the assumptions of terrain topography with the emphasis on the establishment of a linear differential equation monitoring the terrain attributes between the adjacent DEM points. The relevant terrain models were generated in a stochastic rather than deterministic manner by introducing dynamic model errors in the model, whose 'physical' meaning was further explained and analysed in Section 4.4.

The developed 2-D Kalman filter is a truly recursive two-dimensional filter suitable for applications to terrain surface modelling using grid DEMs. The particular strategies applied to enable it to successfully handle the 2-D DEM are the use of two dynamic models over the orthogonal directions of the 2-D data, and more importantly, the technique of combining two estimates from the orthogonal directions to produce $\mathbf{S}^-$ and the associated variance-covariance matrix $\mathbf{P}^-$.

Some important computational considerations have been also addressed in this Chapter, including the boundary problems of the filter, and the determination of the filtering parameters, such as the model error and the observation error. The influence of terrain roughness, DEM resolution and breaklines on the 2-D Kalman filter also have been discussed.

The developed 2-D Kalman filter was tested over a simulated surface, and the results were compared with those from what is generally agreed to be the currently most accurate terrain modelling algorithm, i. e. the Evans method. The test results indicated that the 2-D Kalman filter is efficient in reducing the effect of DEM random noise in the derivation of terrain topographic variables, such as elevation, the first partial derivatives of elevation, slope and aspect. The 2-D Kalman filter significantly improves the quality of terrain surface modelling when tested with noisy data, compared with the Evans method.

CHAPER 5

DEM OUTLIER DETECTION AND REMOVAL

This Chapter will focus on detecting and removing DEM outliers for terrain surface modelling using the 2-D Kalman filter. As mentioned in Chapter 2, outliers in a DEM may significantly affect the quality of derived terrain attributes, but methods for detecting and removing outliers have not been developed. This is largely due to the inability of algorithms to separate outliers from valid elevation data.

The Kalman filtering technique provides a technical base to solve this problem. The technique developed in this study for DEM outlier detection and removal is an application of the theory of statistical hypothesis testing, or detection theory, which is the term used in engineering. In the following sections, the theory of hypothesis testing will be introduced.

5.1 Introduction of Statistical Hypothesis Testing

5.1.1 Binary hypothesis testing

The solution of statistical hypothesis testing deals with the following situation. Suppose a data set is corrupted by different kinds of noise and the situation is not deterministically predictable. In order to determine which of these affects the data at hand, the possible situations are specified into m probabilistic models, i.e. hypotheses $\boldsymbol{H}_i$, $i = 0, \Lambda, m-1$. Among them, a decision $\boldsymbol{D}_j$ may be made to determine hypothesis $\boldsymbol{H}_j$ that best describes the state of affairs at the time.

If only two hypotheses are involved, usually numbered $\boldsymbol{H}_0$ and $\boldsymbol{H}_1$, it is a binary hypothesis testing problem. Traditionally, hypothesis $\boldsymbol{H}_0$ is called the null hypothesis, and $\boldsymbol{H}_1$ is the alternative hypothesis. Then the data space is divided into two regions

$\boldsymbol{R}_0$, called the acceptance region ($\boldsymbol{H}_0$ is accepted and $\boldsymbol{H}_1$ is rejected) and $\boldsymbol{R}_1$ the critical region, or the rejection region ($\boldsymbol{H}_0$ is rejected and $\boldsymbol{H}_1$ is accepted).

The relevant decision is evaluated in terms of relevant errors associated with it. There are two Types of errors. If hypothesis $\boldsymbol{H}_0$ is actually true in the data, but decision $\boldsymbol{D}_1$ is made, i.e. $\boldsymbol{H}_1$ was wrongly believed to be in effect, a so-called Type I error will be made. The probability of Type I error α, also called the risk of the test, would be expressed as:

$$\alpha = \boldsymbol{P}(\boldsymbol{D}_1 \mid \boldsymbol{H}_0) \qquad 5\text{-}1$$

On the other hand, if $\boldsymbol{H}_1$ is actually true in the data, but the decision $\boldsymbol{D}_0$ is wrongly made, i. e. $\boldsymbol{H}_0$ is chosen, then a Type II error is committed. The probability of Type II error β is represented as:

$$\beta = \boldsymbol{P}(\boldsymbol{D}_0 \mid \boldsymbol{H}_1) \qquad 5\text{-}2$$

where $1-\beta$ is also called the power of the test.

The binary hypothesis testing is illustrated in Figure 5-1, in which $p_i(y)$ is the probability density function, while $p_0(y)$ and $p_1(y)$ are the probability density functions for the null hypothesis $\boldsymbol{H}_0$ and the alternative hypothesis $\boldsymbol{H}_1$ respectively. The space of the data y is split into the acceptance region R_0 and the critical region R_1 by ξ. Associated with this ξ, the probability of the Type I error is the shaded area marked with symbol ①, while the probability of the relevant Type II error is marked with symbol ②.

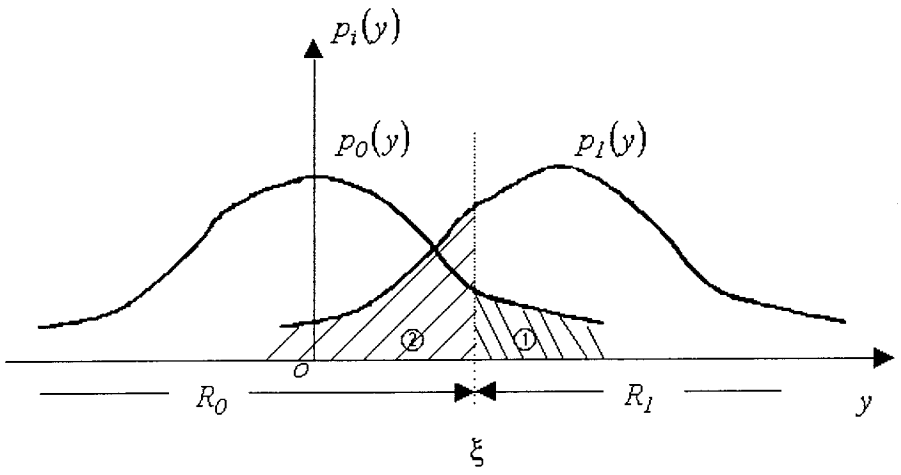

Figure 5-1 Binary hypothesis testing

5.1.2 Neyman-Pearson strategy

There are a number of strategies for making the "best" decision. Among them, the Neyman-Pearson criterion is applied in the case where both hypotheses are simple, and the decision is made in such way that the probability of Type I error is chosen as large as it can be tolerated, and the minimum probability of Type II error is sought under this limitation. That is, the probability of Type I error is made larger than some specified upper bound $\boldsymbol{P_f}$ and within that constraint, while the power of testing is maximised (McDonough and Whalen 1995, pp151-155, p159):

$$\min \boldsymbol{P}(\boldsymbol{D}_0 \mid \boldsymbol{H}_1), \quad \boldsymbol{P}(\boldsymbol{D}_1 \mid \boldsymbol{H}_0) \leq \boldsymbol{P}_f \qquad 5\text{-}3$$

In another words, the approach maximises the power of the test while maintaining the risk of the test not more than the specified level $\boldsymbol{P_f}$:

$$\max(1-\beta), \quad \alpha \leq \boldsymbol{P}_f \qquad 5\text{-}4$$

The Neyman-Pearson criterion described in Eq. 5-4 will be later used in the reliability study of DEM outlier detection and removal in this Chapter.

5.2 Outlier Detection

5.2.1 Innovation series

To detect the outliers from the valid observations of a DEM, an innovation series $l(i,j)$ is formed to represent the bias between the predicted estimate of elevation $\mathbf{DS}^{-}(i,j)$ and its observation $Z(i,j)$ at any arbitrary DEM position (i,j) :

$$l(i,j) = Z(i,j) - \mathbf{DS}^{-}(i,j) \qquad 5\text{-}5$$

According to the assumptions of the dynamic and functional models established in the 2-D Kalman filter in Chapter 4, $Z(i,j)$ and $\mathbf{DS}^{-}(i,j)$ are independent random variables, since one is the DEM observation and the other one is a variable derived by the dynamic models. The standard deviation of $l(i,j)$ can be derived as:

$$\sigma_{l(i,j)} = \sqrt{\mathbf{D}\mathbf{P}^{-}(i,j)\mathbf{D}^{T} + R(i,j)} \qquad 5\text{-}6$$

5.2.2 Hypotheses for outlier detection

In order to simplify the descriptions in the following description, the test statistic for outlier detection is defined as:

$$L(i,j) = l(i,j)/\sigma_{l(i,j)} \qquad 5\text{-}7$$

Assuming the distribution of $L(i,j)$ is normal, represented as $N(m,1)$, or:

$$p(L(i,j)) = (2\pi)^{-1/2} \exp\left[-(L(i,j)-m)^{2}/2\right] \qquad 5\text{-}8$$

where $p(L(i,j))$ is the probability density of $L(i,j)$, and m is the mean.

Two hypotheses assumed for outlier detection are:

$$\boldsymbol{H}_0: \quad m = m_0 = 0 \quad with \quad p_{m_0}(L(i,j)) \sim N(0,\ 1) \tag{5-9}$$

$$\boldsymbol{H}_1: \quad m = m_1 \neq 0 \quad with \quad p_{m1}(L(i,j)) \sim N(m_1,\ 1) \tag{5-10}$$

where $\boldsymbol{H}_0$ is the null hypothesis, and $\boldsymbol{H}_1$ is the alternative hypothesis.

Assume that the predicted estimate of elevation is accurate. Then if $\boldsymbol{H}_0$ is in effect, which means that there is no significant dispersion between the predicted estimate of elevation $\mathbf{DS}^-(i,j)$ and the elevation measurement of DEM point (i,j). In other words, the predicted estimate of elevation agrees with the relevant observation. In this case, it is unlikely that $Z(i,j)$ would be an outlier. An example is illustrated in Figure 5-2, in which the horizontal axis represents the DEM point and the vertical axis represents the elevation value. $\mathbf{DS}^-(k+1)$ is the predicted estimate of elevation of DEM point $(k+1)$, which is derived from the updated estimate of elevation $\mathbf{DS}^+(k)$ of the neighbouring point (k) through the 2-D Kalman dynamic model, and $Z(k+1)$ is the observation. The dispersion between $\mathbf{DS}^-(k+1)$ and $Z(k+1)$ is represented as $l(k+1)$, which is not significant, and therefore it is unlikely that $Z(k+1)$ is an outlier.

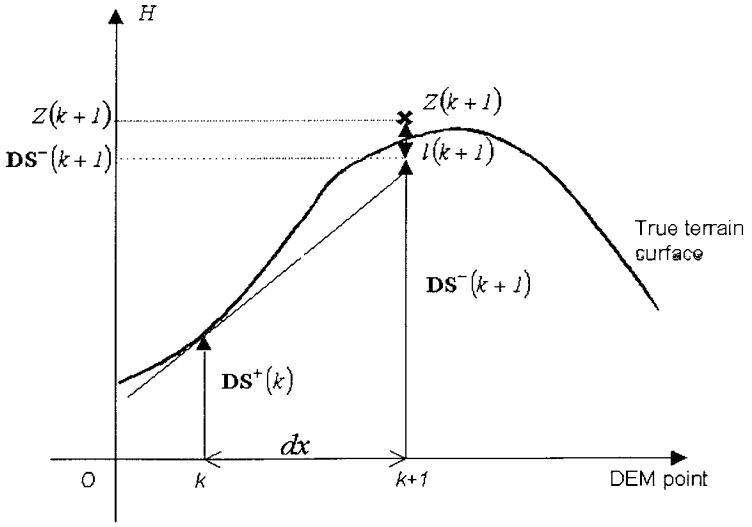

Figure 5-2 Small dispersion represented as $l(k+1)$ between the predicted estimate of elevation and the DEM observation

If $\boldsymbol{H}_1$ is the case, there will be a large dispersion between the predicted estimate of elevation $\mathbf{DS}^-(i,j)$ and the measurement (i,j) as shown in Figure 5-3. In this situation, the bias is caused from the observation $Z(k+1)$, and therefore $Z(k+1)$ will be considered as an outlier, since the predicted estimate of elevation had been assumed correct.

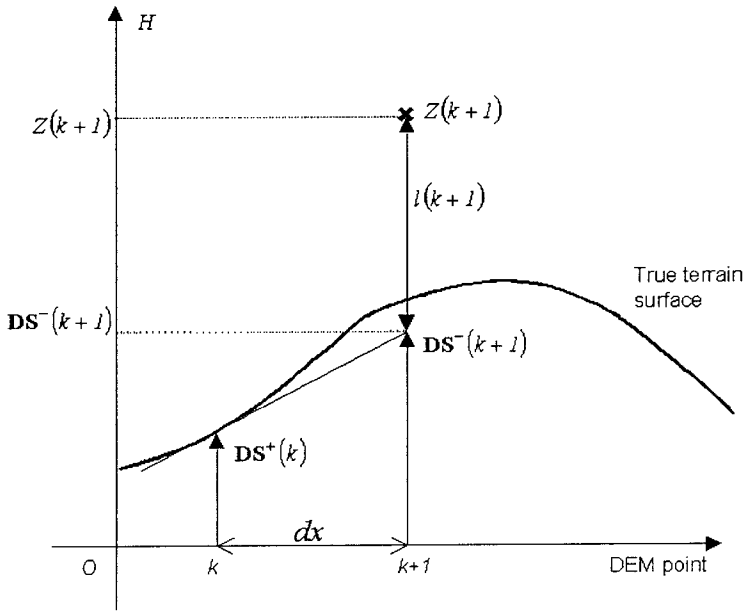

Figure 5-3 Large dispersion represented as $l(k+1)$ between the predicted estimate of elevation and the DEM observation

The Neyman-Pearson strategy is adopted for outlier detection and the relevant analysis. Suppose the risk of test is set as not larger than the specified, that is, the limit set for the risk of the outlier detection is α, then:

$$\boldsymbol{P}(\boldsymbol{D}_1 \mid \boldsymbol{H}_0) \leq \alpha \qquad 5\text{-}11$$

The probability α could be derived by (see Figure 5-1):

$$\alpha = 2\int_{\xi_\alpha}^{\infty} p_{\boldsymbol{m}_0}(y)dy \qquad 5\text{-}12$$

where y is used to simplify the representation of $L(i,j)$, $p_{m_0}(y)$ is the probability density of defined $L(i,j)$ in Eq. 5-12, and ξ_α is the critical value associated with the risk α. Using Eq. 5-12, if α is selected as 5%, 1% or 0.1%, then the subsequent critical values will be $\xi_{0.05} = 1.96$, $\xi_{0.01} = 2.58$, or $\xi_{0.001} = 3.29$, respectively.

The outlier is detected by:

$$| L(i,j) | \rhd \xi_\alpha \qquad 5\text{-}13$$

In other words, given a constraint ξ_α, the entire $L(i,j)$-space will be split into the acceptable region R_0 and the remainder R_1 (the critical region, in which H_0 is rejected) (see Figure 5-1). If the test statistic $L(i,j)$ falls in the region R_0, the corresponding observation $Z(i,j)$ is considered as a good observation, since $L(i,j)$ stays within the specified limits. On the other hand, if $L(i,j)$ falls into the region R_1, the relevant observation $Z(i,j)$ deviates too much from the predicted estimate and is considered as outlier.

It is necessary to mention that the condition of using Eq. 5-13 to detect an outlier in a DEM is that the predicted estimate of elevation $\mathbf{DS}^-(i,j)$ is assumed correct. In other words, the dynamic models are assumed correct. However, a bias in the test statistic $L(i,j)$ could be introduced either by the Kalman filtering model through the calculation of $\mathbf{DS}^-(i,j)$, i.e. the Kalman filter's dynamic model, or by an outlier in the DEM measurements. To distinguish whether the detected bias is an outlier in the observation or a model error of the 2-D Kalman filter, is complicated in some situations. This is related to the terrain roughness, DEM resolution, and breaklines. Appropriate selection of the dynamic noise level (or $\mathbf{Q}_x(i,j)$ and $\mathbf{Q}_y(i,j)$ matrix), discussed in Chapter 4, could avoid outliers in the Kalman dynamic model (Wang 1998, Wang et al 1998b). However, over a rough terrain surface where abrupt changes of terrain surface occur, or the assigned dynamic noise level is inadequate, the situation becomes ambiguous, and further investigations are required.

5.3 Reliability of Outlier Detection

The reliability of estimated parameters can be described by the sensitivity of detected errors in the mathematical model and by the influence of undetectable model errors on the parameters (Förstner 1981). The reliability of detecting outliers from DEM measurements is investigated in the sense of internal and external reliability.

5.3.1 Minimum detectable bias (internal reliability)

The concept of internal reliability is closely related to the probability of outlier detection. The greater the probability of locating erroneous observations, the higher is the degree of internal reliability of the model.

Now the two hypotheses of Eq. 5-13 and Eq. 5-14 are modified into more general form:

$$\boldsymbol{H}_0 : \quad m = 0 \quad with \quad p_0(L(i,j)) \sim N(0, \quad 1) \tag{5-14}$$

$$\boldsymbol{H}_1 : \quad m = \delta \neq 0 \quad with \quad p_\delta(L(i.j)) \sim N(\delta, \quad 1) \tag{5-15}$$

where δ is a variable.

Following the outlier detection criterion in Eq. 5-13, a decision $\boldsymbol{D}_\delta$ is on the critical value ξ_α of $L(i,j)$ with a risk level α. The associated Type II error of decision $\boldsymbol{D}_\delta$ is β, then the power of the outlier detection will be:

$$1-\beta = \boldsymbol{P}(\boldsymbol{D}_\delta \mid \boldsymbol{H}_1) \tag{5-16}$$

Now examine how the "best" decision $\boldsymbol{D}_\delta$ is made, since many different decisions can be made with different powers of the test for a given value of ξ_α. An example is illustrated in Figure 5-4, in which the critical value ξ_α is given and two possible alternative hypotheses $\boldsymbol{H}_1$ and $\boldsymbol{H}_1'$ are chosen. In the case of alternative hypothesis $\boldsymbol{H}_1$, the corresponding power of the test is the solid-line shaded area, which is less than 50%, in terms of probability. Increasing the value of δ to δ' obtains another alternative

hypothesis H_1'. The relevant power of test of H_1' is the dotted-line shaded area, which is greater than 50%. Therefore, the distribution of the composite alternative hypothesis H_1 can be varied, according to the different choice of δ while keeping the same critical value ξ_α.

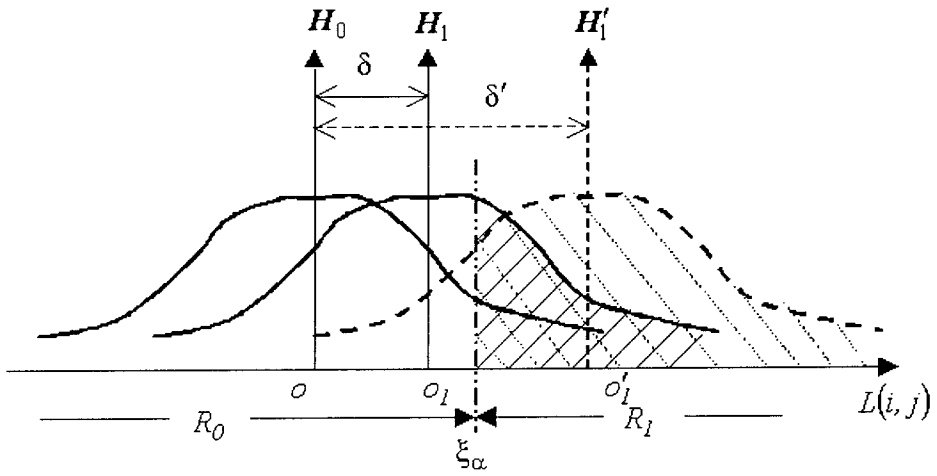

Figure 5-4 The power of testing increases choosing large δ with a given ξ_α

If the Neyman-Pearson strategy, Eq. 5-3 or Eq. 5-4, is used as the criterion to determine the "best" decision D_δ, the optimal decision D_δ should be the decision of which the power of test is maximised while the Type I error is at most at the specified level α in the rejection region R_1:

$$\max(1-\beta) = \max\left(\int_{R_1} p_\delta(y)dy\right) \quad while \quad P(D_\delta \mid H_0) = \int_{R_1} p_0(y)dy \le \alpha \qquad 5\text{-}17$$

Under this criterion, if the minimum acceptable power of test is chosen as 50%, the corresponding critical value ξ_δ should be:

$$\xi_\delta = \delta \qquad 5\text{-}18$$

Substituting Eq. 5-17 into Eq. 5-12, the detectable bias is derived as:

$$|L(i,j)| \geq \delta \qquad 5\text{-}19$$

Then the minimum detectable bias is:

$$\min|L(i,j)| = \delta \qquad 5\text{-}20$$

5.3.2 Maximum effect of the undetectable bias (external reliability)

In spite of all the sophisticated testing procedures, there will never be certainty about having detected all gross errors in the DEM. Furthermore, some small errors must be expected in the data that are just below the established boundary values. Therefore, one of the crucial points of model analysis is to gain an understanding of the effect of these model errors on the parameter estimation.

A mathematical model is said to have external reliability if it responds insignificantly to undetected errors (Caspary 1988, p91). Now, the maximum effect of the undetectable bias to the DEM outlier detection will be investigated.

Recall that the updated estimate of state vector $\mathbf{S}^+(i,j)$ is derived by the following equation using the elevation observation $Z(i,j)$ of the DEM point (i,j):

$$\begin{aligned}\mathbf{S}^+(i,j) &= \mathrm{f}(Z(i,j)) \\ &= \mathbf{S}^-(i,j) + \mathbf{K}(i,j)(Z(i,j) - \mathbf{D}\mathbf{S}^-(i,j))\end{aligned} \qquad 5\text{-}21$$

Suppose that there is a bias δh in $Z(i,j)$, which cannot be detected by using Eq. 5-13. The effect of the undetected bias δh on the derivation of the updated estimate $\mathbf{S}^+(i,j)$ is:

$$\begin{aligned}\Delta\mathbf{S}_L &= \mathrm{f}(Z(i,j)+\delta h) - \mathrm{f}(Z(i,j)) \\ &= \left[\mathbf{S}^-(i,j) + \mathbf{K}(i,j)\left((Z(i,j)+\delta h) - \mathbf{D}\mathbf{S}^-(i,j)\right)\right] - \left[\mathbf{S}^-(i,j) + \mathbf{K}(i,j)\left(Z(i,j) - \mathbf{D}\mathbf{S}^-(i,j)\right)\right] \\ &= \mathbf{K}(i,j)\cdot\delta h\end{aligned} \qquad 5\text{-}22$$

where vector $\Delta \mathbf{S}_L$ is the bias of the state vector $\mathbf{S}^+(i,j)$ caused by the undetectable error δh in the observation $Z(i,j)$ of any arbitrary DEM point.

5.4 Outlier Removal

Once an outlier is detected using the method described in Section 5.2, it needs to be removed to eliminate its effect on the modelling of the proceeding DEM point.

This can be achieved by reducing the weight of the current observation $Z(i,j)$, which has been detected as an outlier, while computing the Kalman gain. If a DEM measurement $Z(i,j)$ is identified as an outlier, the relevant $\mathbf{K}(i,j)$ is computed by keeping the same variance covariance $\mathbf{P}^-(i,j)$, but amplifying the observation error $R(i,j)$ into a large value, using Eq. 4-22:

$$R(i,j) \to \infty \qquad 5\text{-}23$$

In this way, the derivation of the updated estimate of state vector $\mathbf{S}^+(i,j)$ will entirely depend on the predicted estimate $\mathbf{S}^-(i,j)$, since its weight is increased, and the effect of DEM outlier is eliminated.

5.5 Experiments

5.5.1 Testing data

The tests were aimed at examining the efficiency of DEM outlier detection and removal in the 2-D Kalman filtering algorithm. The tests used the same artificial surface as that in Chapter 4, with five outliers and 0.5m random noise added to the elevation surface. The outlier affected DEM is shown in Figure 5-5, and details of the five outliers are listed in Table 5-1. The ground truth of the elevation, X and Y derivatives, slope and aspect surfaces of the outlier affected DEM are the same as those simulated in Chapter 4.

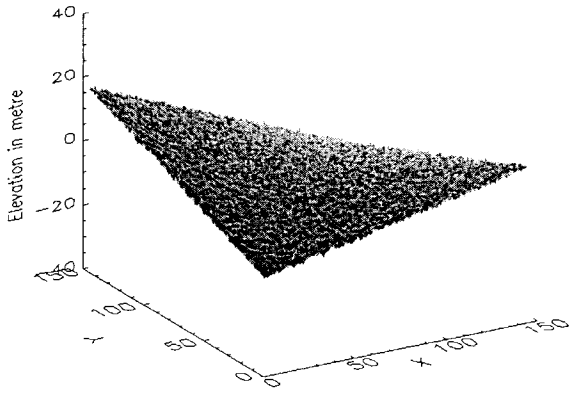

Figure 5-5 The noisy DEM

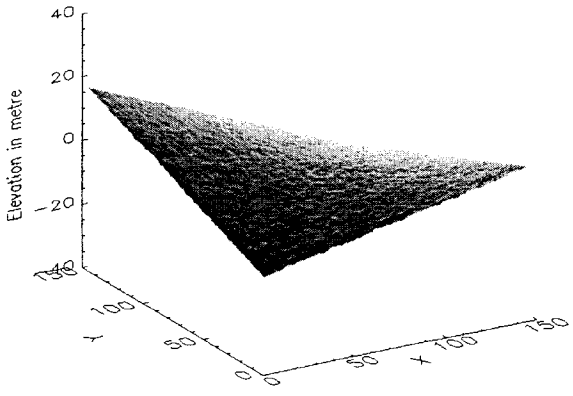

Figure 5-6(a) Elevation

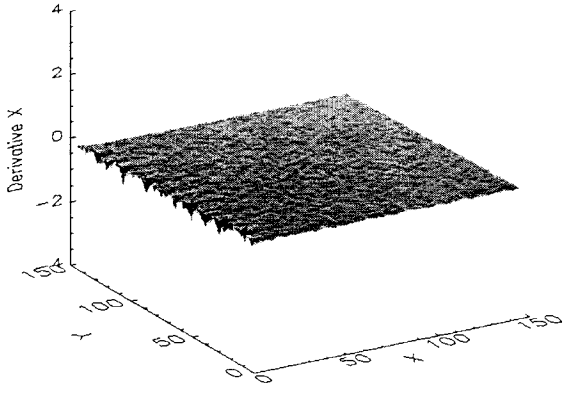

Figure 5-6(b) X derivative

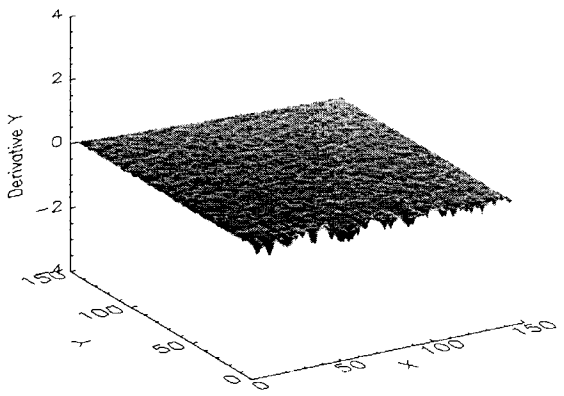

Figure 5-6(c) Y derivative

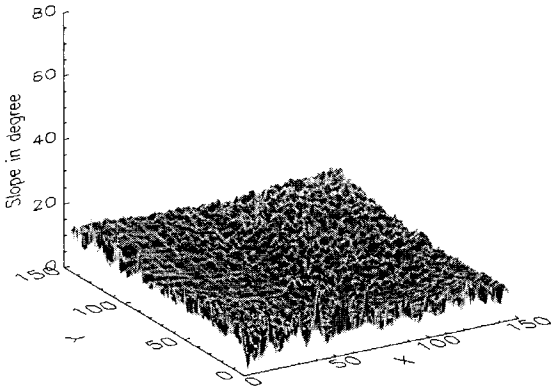

Figure 5-6(d) Slope

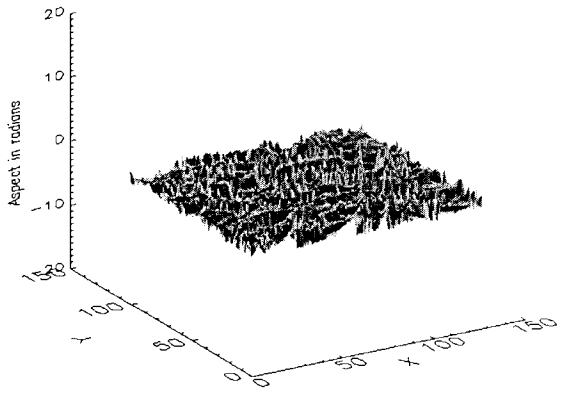

Figure 5-6(e) Aspect

Figure 5-6 2-D Kalman filtering results

Table 5-1 Outliers in the simulated DEM

(unit: metres)

	Outlier#1	Outlier#2	Outlier#3	Outlier#4	Outlier#5
Outlier	7.5	5.9	-10.6	-8.8	-6.5

5.5.2 Results of the 2-D Kalman filtering algorithm

The extended 2-D Kalman filtering algorithm with outlier detection and removal was applied to the DEM illustrated in Figure 5-6. The critical value ξ_α was chosen as 2.58, that is, it was assumed that the Type I error in the test is not larger than 1%. All other

filtering parameters used were the same as those used in the testing discussed in Chapter 4.

The estimated surface of elevation and the first partial derivatives of the test data were generated simultaneously, and plotted in Figure 5-6(a), (b) and (c). The slope and aspect surfaces of the data were also computed using the Kalman filtering results and the relevant slope and aspect equations, and are also displayed in Figure 5-6(d) and (e).

The results of the tests indicate that all five outliers were detected and completely removed from the elevation surface, and therefore a smoothing elevation surface has been generated. The effect of the outliers on the X and Y derivatives, slope and aspect were also fully removed. The algorithm produced accurate estimated surfaces of all these four terrain attributes, compared with the ground truth.

5.5.3 Results of the Evans method

Applying the Evans method over the outlier-affected DEM also produced the terrain variables for the same test data, including X and Y derivatives, slope and aspect, which are shown in Figure 5-7.

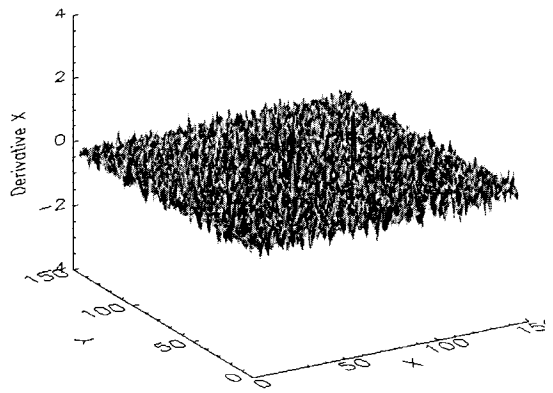

Figure 5-7(a) Derivative X

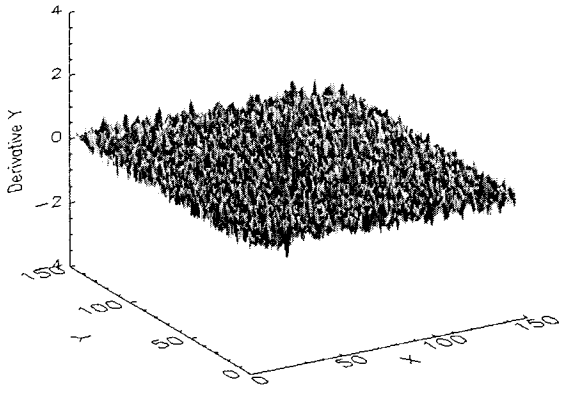

Figure 5-7(b) Derivative Y

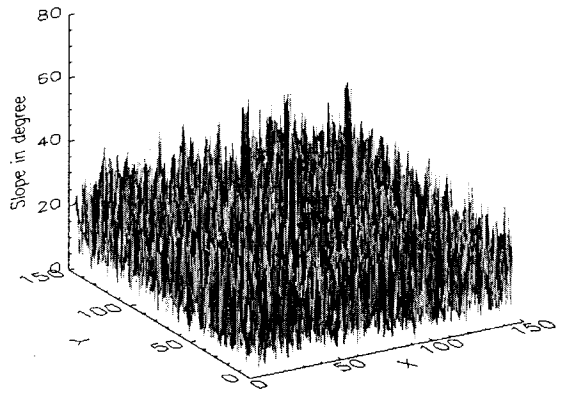

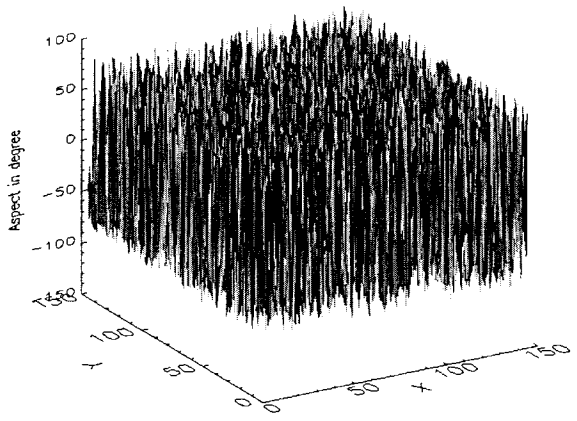

Figure 5-7(c) Slope **Figure 5-7(d) Aspect**

Figure 5-7 The Evans method results

The results of the Evans method indicate the considerable influence of DEM outliers on the derivation of all terrain variables. Small peaks occurred in the surfaces of X and Y derivatives, and slope in the places where the outliers exist. Further, it is inevitable that a single outlier can affect more than one DEM point, since no process was included in the Evans method for DEM outlier treatment. Since the Evans method could not completely smooth the random noise, the resultant aspect surface is too noisy to directly observe the impact of the outliers.

5.5.4 Comparison of the results of the 2-D Kalman filtering algorithm and the Evans method

The results of the 2-D Kalman filtering and the Evans method were compared with the ground truth in order to further examine the significance of the outlier detection and removal by the 2-D Kalman filtering.

In the comparison of the estimates of elevation derived by 2-D Kalman filter with the ground truth, outliers added to the test data are plotted in Figure 5-8(a), while the errors remaining after the Kalman filtering are plotted in Figure 5-8(b). The differences between the elevation estimates of the 2-D Kalman filtering, which is extended with the function of outlier detection and removal, and the ground truth elevations were in the range of -0.05m to 0.05m, as shown in Figure 5-8(b). This result indicates that the

outliers in the test data were completely detected and efficiently removed by the process of outlier detection and removal of the 2-D Kalman filtering algorithm.

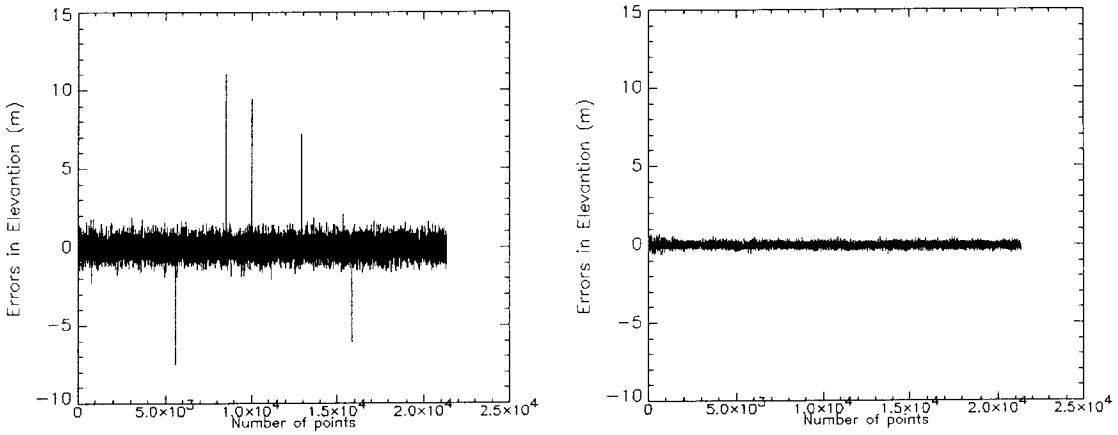

(a) Test data **(b) Result of Kalman filtering**

Figure 5-8 Errors in the elevation of the noisy DEM and the 2-D Kalman filtering

The estimates of the X and Y derivatives, slope and aspect of the Kalman filtering were compared with those derived by the Evans method. The errors in the estimates of the X and Y derivatives, slope and aspect by the 2-D Kalman filtering and the Evans method were derived by subtracting the ground truth from the relevant data. The comparison of results are plotted in Figure 5-9, in which the horizontal axes represent of the number of the DEM points and the vertical axes represent the magnitudes of the errors remained in the estimates of terrain variables derived by the Evans method and the 2-D Kalman filtering algorithm.

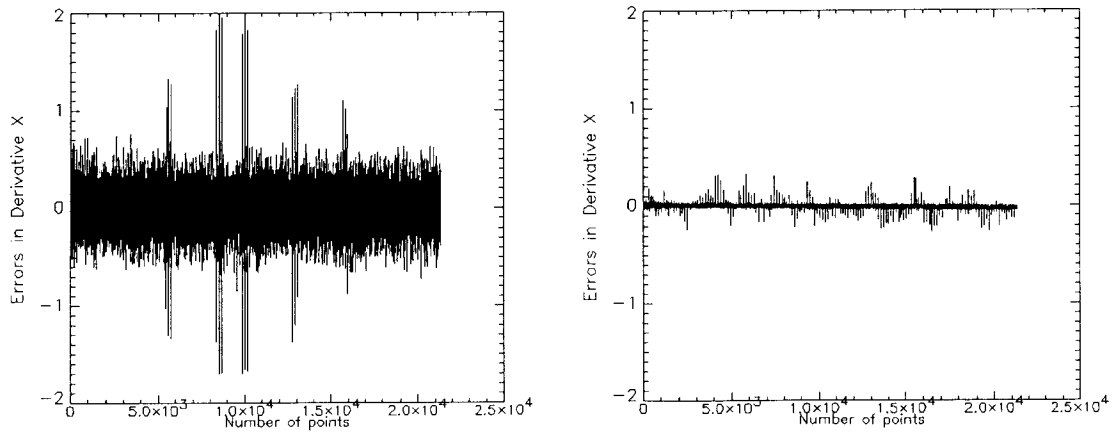

Figure 5-9(a) The Evans method **Figure 5-9(b) Kalman filtering**

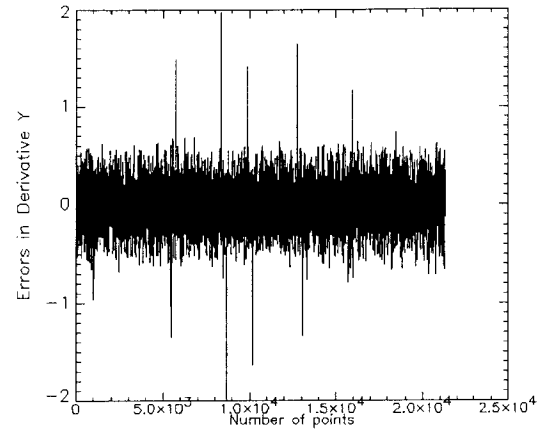

Figure 5-9(c) The Evans method

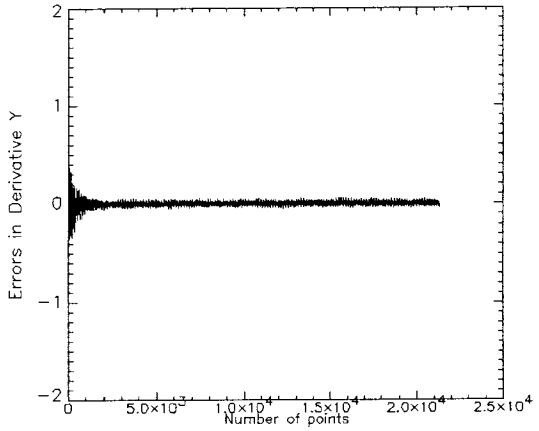

Figure 5-9(d) Kalman filtering

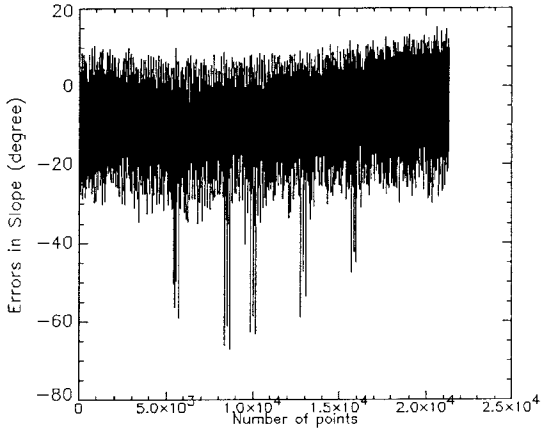

Figure 5-9(e) The Evans method

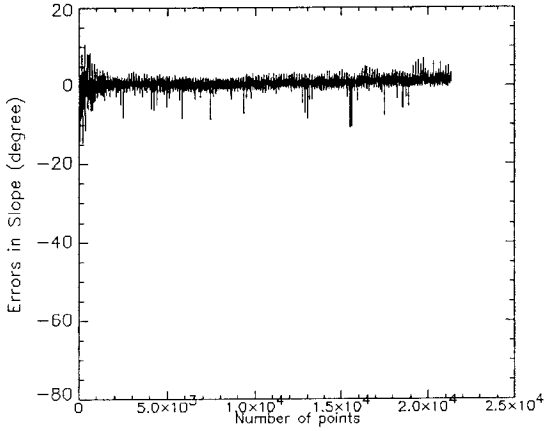

Figure 5-9(f) Kalman filtering

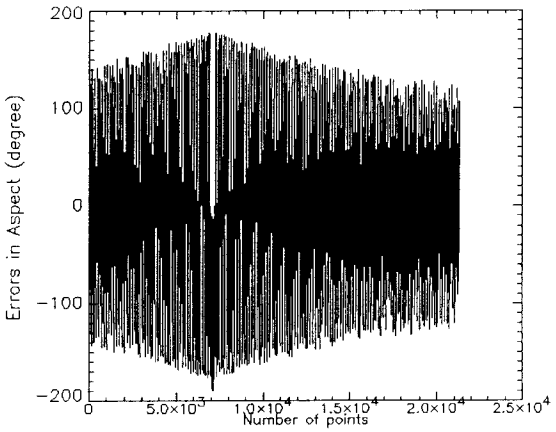

Figure 5-9(g) The Evans method

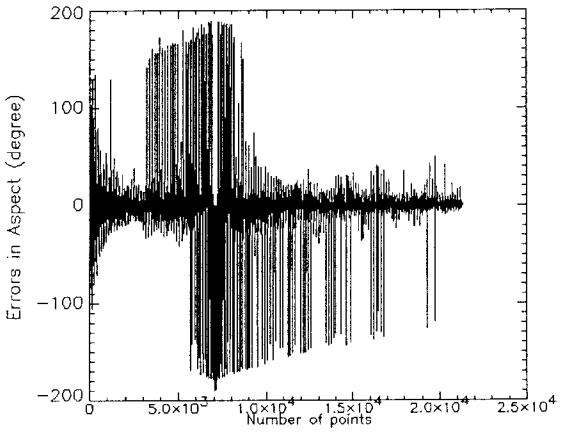

Figure 5-9(h) Kalman filtering

Figure 5-9 Comparison of errors in the estimates of terrain variables by the Evans method and the 2-D Kalman filtering algorithm

The comparison clearly indicates that the effects of DEM outliers on the X and Y derivatives were almost fully removed using the 2-D Kalman filtering algorithm. Errors remaining in the estimates of X and Y derivatives derived by the 2-D Kalman filtering algorithm are minor, between -0.34 to 0.38. However, the effect of the outliers on the results of the Evans method is strong. Five outliers had affected thirty DEM points to produce incorrect estimates of the X and Y derivatives respectively. The magnitudes of the error ranges from -2 to 2, which is significantly larger than the 2-D Kalman filtering algorithm.

Since the effects of outliers were completely removed in the estimates of the X and Y derivatives, the slope and aspect surface by the 2-D Kalman filtering algorithm were more accurate than those derived by the Evans method at the DEM points where the outliers occurred. Compared with the ground truth, the errors in the results of the 2-D Kalman filtering ranged from –14.54° to 10.73° for the slope surface. However, due to the five added outliers, the error in the estimates of slope derived by the Evans method is more than 67°. The errors remaining in the aspect surfaces derived by the Evans method and the 2-D Kalman filtering algorithm follow similar patterns as shown in Figure 4-9(g) and Figure 4-9(h). The influence of DEM random noise is strong in the aspect of the Evans method, so the impact of outliers on the Evans method may only worsen the situation.

It is concluded that the method of DEM outlier detection and removal developed in this Chapter for the 2-D Kalman filtering algorithm is efficient in detecting and removing DEM outliers, and therefore, it is able to produce more accurate results than the Evans method.

5.6 Conclusions

In this Chapter, the method of DEM outlier detection and removal has been presented. This method is based on the application of the 2-D Kalman filter, developed in Chapter 4, and the theory of statistical hypothesis testing.

The test statistic developed for DEM outlier detection is based on an innovation series, which represents the dispersions between the predicted estimate of elevation, derived by the 2-D Kalman filter, and the elevation measurement at each DEM point. DEM outliers are detected at the DEM locations where large discrepancies occurred.

The internal and external reliabilities of outlier detection were further investigated in this Chapter. The internal reliability is examined in the sense of the minimum detectable bias, in which two hypotheses for outlier detection were established and the Neyman-Pearson strategy was applied as the relevant criterion. The external reliability of the outlier detection was discussed in terms of the maximum effect of the undetectable bias on the DEM outlier detection.

The method of outlier removal developed in this Chapter is also based on the application of the 2-D Kalman filter. If a DEM observation is detected as an outlier, it will be removed through the derivation of Kalman gain at the point by amplifying the relevant observation error to a large value. In this way, an updated estimate of the point is derived entirely depending on the predicted value, and the effect of the outlier is removed.

The experiments indicate that the method developed in this Chapter is significant in detecting and removing DEM outliers from a DEM data set. The extended 2-D Kalman filter with outlier detection and removal may produce more accurate terrain variables than the Evans method for the same outlier-affected test data.

CHAPTER 6

THE 2-D KALMAN SMOOTHER

6.1 Introduction

The 2-D Kalman filter for terrain surface modelling developed in Chapter 4 is a causal filter, in which DEM measurements and the predicted information of the random process are used. Before introducing the 2-D Kalman smoother, it is necessary to explain how such information is used in the 2-D Kalman filtering process. An example illustrated in Figure 6-1 and Figure 6-2 indicates how the updated estimate of point $(1,1)$ is derived. Suppose the 2-D Kalman filter processes a grid DEM, starting from its top left corner and moving towards the bottom right corner of the DEM. The neighbouring points used for generating $\mathbf{S}^{+}(1,1)$ are shown in Figure 6-1. A flow chart of how the associated information of the neighbouring points is applied in the relevant recursive process is shown in Figure 6-2.

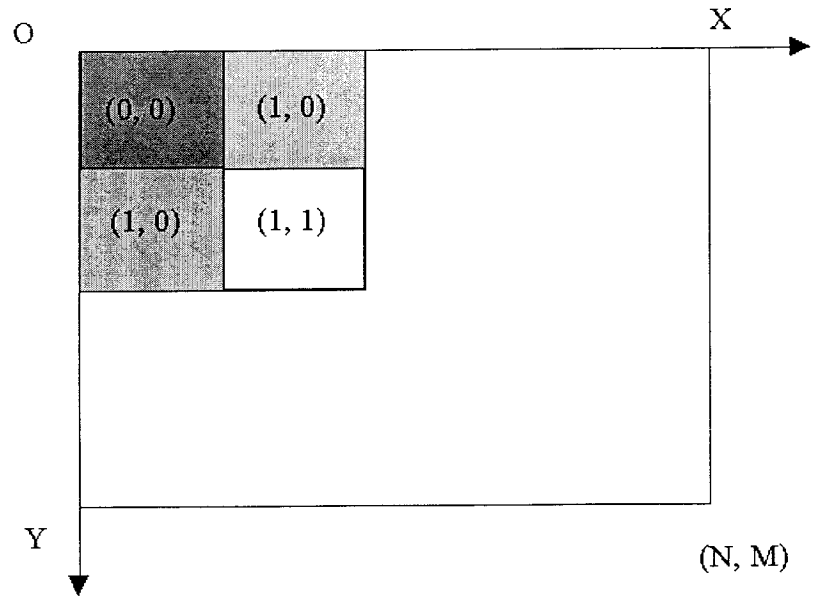

Figure 6-1 Using the 2-D Kalman filter to process a DEM

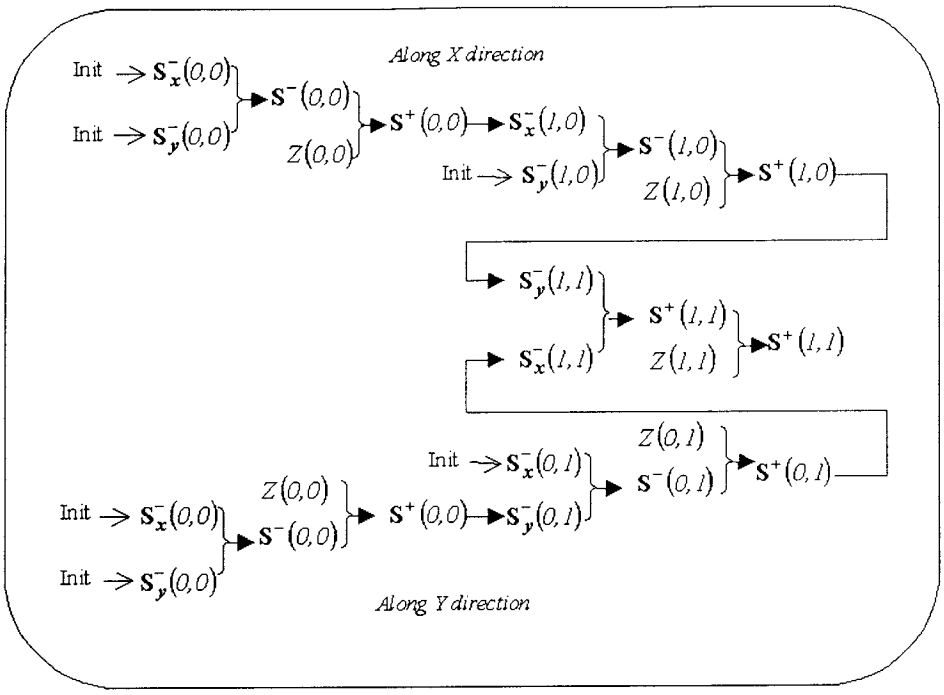

Figure 6-2 Information used in the determination of $S^+(1,1)$

Suppose the recursive Kalman process starts from the point $(0,0)$. The predicted estimates along the X and Y directions represented as $S_x^-(0,0)$ and $S_y^-(0,0)$ should use the relevant initial values, since point $(0,0)$ is located on the boundary. The predicted estimate $S^-(0,0)$ is a linear combination of $S_x^-(0,0)$ and $S_y^-(0,0)$, which is used together with the observation of the point $Z(0,0)$, in producing the updated estimate $S^+(0,0)$. The next processing point is point $(1,0)$. The predicted estimate along the X direction $S_x^-(1,0)$ is generated using the updated estimate $S^+(0,0)$ and the relevant dynamic model. The predicted estimate along the Y direction $S_y^-(1,0)$ still uses the initial value, since there is no point has been processed along the Y direction. The updated estimate $S^+(1,0)$ is derived using $S_x^-(1,0)$ and $S_y^-(1,0)$, through $S^-(1,0)$, and the observation of the point $Z(1,0)$.

Following this procedure to process the rest of the row, the following information has been used to produce the predicted estimate $S^-(i,0)$ or the updated estimate $S^+(i,0)$,

including all the predicted estimates and the observations along the X direction up to the processing point $(i,0)$:

$$\left.\begin{array}{llllll} Z(0,0), & Z(1,0), & \ldots, & Z(k,0), & k=0, & \ldots, \; i-1 \\ \mathbf{S}_x^-(0,0), & \mathbf{S}_x^-(1,0), & \ldots, & \mathbf{S}_x^-(k,0), & k=0, & \ldots, \; i \\ \mathbf{S}_y^-(0,0), & \mathbf{S}_y^-(k,0), & \ldots, & \mathbf{S}_y^-(k,0), & k=0, & \ldots, \; i \end{array}\right\} \Rightarrow \mathbf{S}^-(i,0) \qquad 6\text{-}1$$

$$\left.\begin{array}{llllll} Z(0,0), & Z(1,0), & \ldots, & Z(k,0), & k=0, & \ldots, \; i \\ \mathbf{S}_x^-(0,0), & \mathbf{S}_x^-(1,0), & \ldots, & \mathbf{S}_x^-(k,0), & k=0, & \ldots, \; i \\ \mathbf{S}_y^-(0,0), & \mathbf{S}_y^-(k,0), & \ldots, & \mathbf{S}_y^-(k,0), & k=0, & \ldots, \; i \end{array}\right\} \Rightarrow \mathbf{S}^+(i,0) \qquad 6\text{-}2$$

The only difference between Eq. 6-1 and Eq. 6-2 is whether the observation $Z(i,0)$ is used or not. The derivation of the predicted estimate does not use the observation of the processing point, while the updated estimate should involve the observation of the processing point.

Coming back to the determination of the predicted estimate $\mathbf{S}_y^-(1,1)$, which is used for the calculation of the updated estimate $\mathbf{S}^+(1,1)$, in this case the observation $Z(0,0)$ and $Z(1,0)$, the predicted estimate $\mathbf{S}_x^-(0,0)$, $\mathbf{S}_y^-(0,0)$, $\mathbf{S}_x^-(1,0)$ and $\mathbf{S}_y^-(1,0)$, and the updated estimate $\mathbf{S}^+(1,0)$ are used.

Now consider the determination of the predicted estimate $\mathbf{S}_x^-(1,1)$. The information used, shown in Figure 6-2, includes the observation $Z(0,0)$ and $Z(0,1)$, the predicted estimate $\mathbf{S}_x^-(0,0)$, $\mathbf{S}_y^-(0,0)$, $\mathbf{S}_x^-(0,1)$ and $\mathbf{S}_y^-(0,1)$, and the updated estimate $\mathbf{S}^+(0,1)$.

The DEM point $(0,0)$ is the overlapping area, and the information associated with this point has been used twice in the derivation of $\mathbf{S}_x^-(1,1)$ and $\mathbf{S}_y^-(1,1)$. However, the information associated with the adjacent point $(1,0)$ and point $(0,1)$, including the observations and the predicted estimates, has only been used once to produce the updated estimate $\mathbf{S}^+(1,1)$. The situation is similar for the calculation of the predicted or

updated estimate of any arbitrary DEM point (i,j) illustrated in Figure 6-3. The grey colour shaded area covers the DEM points for which information has been used twice, while the dashed and solid line filled row and column indicate the DEM points which are only used once in the generation of $\mathbf{S}^{-}(i,j)$ or $\mathbf{S}^{+}(i,j)$. The observation $Z(i,j)$ should be included if the updated estimate $\mathbf{S}^{+}(i,j)$ is considered. Otherwise, for the computation of the updated estimate $\mathbf{S}^{-}(i,j)$, the observation $Z(i,j)$ should be excluded.

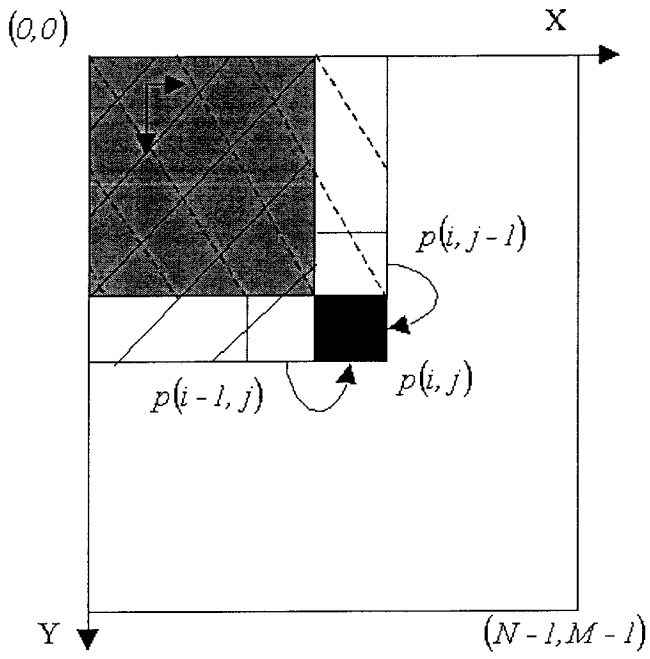

Figure 6-3 Information used in the derivation of $\mathbf{S}^{-}(i,j)$ or $\mathbf{S}^{+}(i,j)$

In this case, the advantage of the 2-D Kalman filter is that it can be used for real-time processing. However, the disadvantage is that a better result could not be derived at the commencement of the process, since only part of the measurements are used. Furthermore some measurements are used only once and other are used twice. Modelling the terrain surface using DEMs is mostly an off-line data process. It is of practical interest to incorporate all elevation measurements of a DEM to yield the best estimate of the state vector of each DEM grid point. This issue refers to the Kalman smoothing problem.

To achieve this aim, a 2-D Kalman smoother was developed based on the extended 2-D Kalman filter, which includes the outlier detection and removal process. The smoother is intended to use the whole DEM data equally to produce the best optimal estimates of three terrain variables for each single DEM point, therefore, further improving the accuracy.

6.2 An Alternative Way of Computing the Mean Value – A Case Study

Firstly, an example is used to derive a relevant fact, which will be used in the development of the 2-D Kalman smoother.

Suppose to measure the length of a road, three independent length measurements were obtained as l_1, l_2 and l_3, and the associated variance is represented as σ_1^2, σ_2^2 and σ_3^2. Now it is required to derive the mean value for the length of the road.

In order to simplify the following expression, the weight of the observation l_1, l_2 and l_3 represented as w_1, w_2 and w_3 will be used in the following discussion:

$$w_1 = \frac{1}{\sigma_1^2} \qquad 6\text{-}3$$

$$w_2 = \frac{1}{\sigma_2^2} \qquad 6\text{-}4$$

$$w_3 = \frac{1}{\sigma_3^2} \qquad 6\text{-}5$$

The mean could be derived as the sum of the three observations weighted by their weight factors:

$$\bar{L}_{123} = \frac{w_1 l_1 + w_2 l_2 + w_3 l_3}{w_1 + w_2 + w_3} \qquad 6\text{-}6$$

$$\sigma^2_{\bar{L}_{123}} = \frac{1}{w_1 + w_2 + w_3} \qquad 6\text{-}7$$

where $\sigma^2_{\bar{L}_{123}}$ is the associated variance with the derived mean.

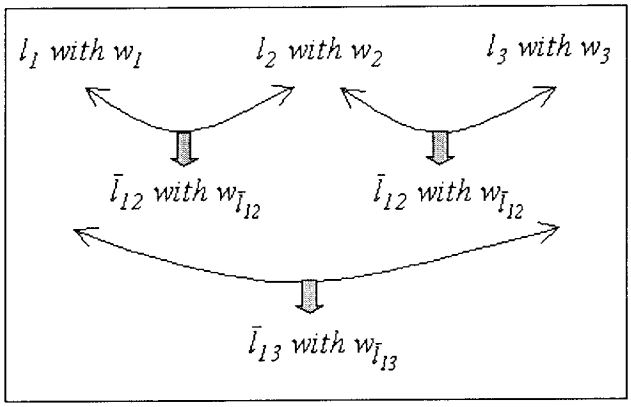

Step 1

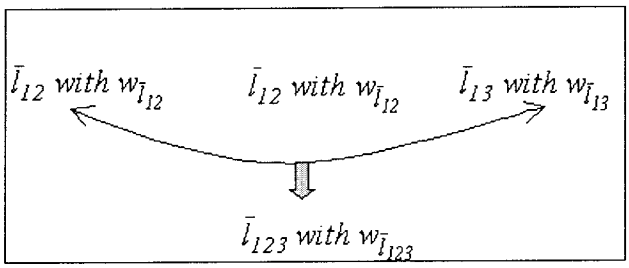

Step 2

Figure 6-4 Derivation of the mean value by double using the observations

The mean could also be derived in the way illustrated in Figure 6-4, which uses two steps of calculation and applies the observation twice to compute the mean value. In Step 1, the mean values of any two observations are calculated as:

$$\bar{l}_{12} = \frac{w_1 l_1 + w_2 l_2}{w_1 + w_2} \quad with \quad \sigma^2_{\bar{l}_{12}} = \frac{1}{w_1 + w_2} \tag{6-8}$$

$$\bar{l}_{23} = \frac{w_2 l_2 + w_3 l_3}{w_2 + w_3} \quad with \quad \sigma^2_{\bar{l}_{23}} = \frac{1}{w_2 + w_3} \tag{6-9}$$

$$\bar{l}_{13} = \frac{w_1 l_1 + w_3 l_3}{w_1 + w_3} \quad with \quad \sigma^2_{\bar{l}_{13}} = \frac{1}{w_1 + w_3} \tag{6-10}$$

The variance - covariances of the three intermediate variables are:

$$\mathbf{D}_{\bar{l}_{123}} = \begin{bmatrix} \frac{1}{w_1 + w_2} & \frac{w_2}{(w_1 + w_2)(w_2 + w_3)} & \frac{w_1}{(w_1 + w_2)(w_1 + w_3)} \\ \frac{w_2}{(w_1 + w_2)(w_2 + w_3)} & \frac{1}{w_2 + w_3} & \frac{w_3}{(w_1 + w_3)(w_2 + w_3)} \\ \frac{w_1}{(w_1 + w_2)(w_1 + w_3)} & \frac{w_3}{(w_1 + w_3)(w_2 + w_3)} & \frac{1}{w_1 + w_3} \end{bmatrix} \qquad 6\text{-}10a$$

If $\bar{l}_{12}$, $\bar{l}_{23}$ and $\bar{l}_{13}$ are used with the consideration of their covariance, the optimal estimation of the expectation can be derived from the following Least Squares model:

$$\begin{bmatrix} v_1 \\ v_2 \\ v_3 \end{bmatrix} = \begin{bmatrix} 1 \\ 1 \\ 1 \end{bmatrix} \bar{l}_{123} - \begin{bmatrix} \bar{l}_{12} \\ \bar{l}_{23} \\ \bar{l}_{13} \end{bmatrix} \quad \text{with weight matrix } \mathbf{D}^{-1}_{\bar{l}_{123}} \qquad 6\text{-}10b$$

$$\begin{aligned} \bar{l}_{123} &= \left(\begin{bmatrix} 1 \\ 1 \\ 1 \end{bmatrix}^T \mathbf{D}^{-1}_{\bar{l}_{123}} \begin{bmatrix} 1 \\ 1 \\ 1 \end{bmatrix} \right)^{-1} \begin{bmatrix} 1 \\ 1 \\ 1 \end{bmatrix}^T \mathbf{D}^{-1}_{\bar{l}_{123}} \begin{bmatrix} \bar{l}_{12} \\ \bar{l}_{23} \\ \bar{l}_{13} \end{bmatrix} \\ &= \frac{w_1 l_1 + w_2 l_2 + w_3 l_3}{w_1 + w_2 + w_3} \end{aligned} \qquad 6\text{-}10c$$

$$\sigma^2_{\bar{l}_{123}} = \left(\begin{bmatrix} 1 \\ 1 \\ 1 \end{bmatrix}^T \mathbf{D}^{-1}_{\bar{l}_{123}} \begin{bmatrix} 1 \\ 1 \\ 1 \end{bmatrix} \right)^{-1} = \frac{1}{w_1 + w_2 + w_3} \qquad 6\text{-}10d$$

where v_1, v_2 and v_3 are residuals, and

$$\mathbf{D}^{-1}_{\bar{l}_{123}} = \frac{1}{4} \begin{bmatrix} (w_1 + w_2)^2 \left(\frac{1}{w_1} + \frac{1}{w_2} + \frac{1}{w_3} \right) & (w_1 + w_2)(w_2 + w_3) \left(-\frac{1}{w_1} + \frac{1}{w_2} - \frac{1}{w_3} \right) & (w_1 + w_2)(w_1 + w_3) \left(\frac{1}{w_1} - \frac{1}{w_2} - \frac{1}{w_3} \right) \\ & (w_2 + w_3)^2 \left(\frac{1}{w_1} + \frac{1}{w_2} + \frac{1}{w_3} \right) & (w_2 + w_3)(w_1 + w_3) \left(-\frac{1}{w_1} - \frac{1}{w_2} + \frac{1}{w_3} \right) \\ \textit{symmetric} & & (w_1 + w_3)^2 \left(\frac{1}{w_1} + \frac{1}{w_2} + \frac{1}{w_3} \right) \end{bmatrix} \qquad 6\text{-}10e$$

However, if for some reason that the co-variances are not available, and are further assumed to be zero, the results of the mean value can be derived as Eq: 6-11 and Eq. 6-12, in which the variance of the mean is underestimated.

$$\begin{aligned} \bar{l}_{123} &= \frac{w_1 l_1 + w_2 l_2 + w_2 l_2 + w_3 l_3 + w_1 l_1 + w_3 l_3}{w_1 + w_2 + w_2 + w_3 + w_1 + w_3} \\ &= \frac{w_1 l_1 + w_2 l_2 + w_3 l_3}{w_1 + w_2 + w_3} \end{aligned} \qquad 6\text{-}11$$

$$\begin{aligned} \sigma^2_{pseudo} &= \frac{1}{w_1 + w_2 + w_2 + w_3 + w_1 + w_3} \\ &= \frac{1}{2(w_1 + w_2 + w_2)} \\ &= \frac{1}{2}\sigma^2_{\bar{L}_{123}} \end{aligned} \qquad 6\text{-}12$$

$$\sigma^2_{\bar{l}_{123}} = 2\sigma^2_{pseudo} \qquad 6\text{-}13$$

Comparing these two methods, the observations have been used once in the first method, and twice in the second method. The mean value derived by the method illustrated in Figure 6-4 is equal to the result using Eq. 6-6. Due to the assumption of independence among $\bar{l}_{12}$, $\bar{l}_{23}$, and $\bar{l}_{31}$, the derived variance in the second method is over-optimal, and therefor should be scaled by a factor of 2, represented by Eq. 6-13, in order to give the realistic variance estimate. This is applied in the development of the 2-D Kalman smoother.

6.3 2-D Kalman smoother

The developed 2-D Kalman smoother (Wang *et al* 2000) processes a DEM at four different orientations as shown in Figure 6-5. Orientation 1 is defined as the filtering direction, starting from top left and moving towards the bottom right shown as Figure 6-5(a), and orientation 2 is defined as the filtering direction, starting from top right and proceeding towards bottom left as shown in Figure 6-5(b). Similarly the orientations 3 and 4 are those shown in Figure 6-5(c) and Figure 6-5(d) respectively.

The smoothing algorithm uses the developed 2-D Kalman filter to process the DEM four times at orientation 1, 2, 3 and 4, respectively, and linearly combines the four

filtering results to derive the final estimation. Suppose that 2-D Kalman filter processes the DEM following orientation 1 and derives the updated estimate $\mathbf{S}_1^+(i,j)$ and $\mathbf{P}_1^+(i,j)$ using the observations of elevation of the shaded area in Figure 6-5(a). Similarly, applying the 2-D Kalman filter at the other three orientations shown in Figure 6-5(b), Figure 6-5(c) and Figure 6-5(d), the predicted estimate $\mathbf{S}_2^-(i,j)$ together with $\mathbf{P}_2^-(i,j)$, the updated estimate $\mathbf{S}_3^+(i,j)$ with $\mathbf{P}_3^+(i,j)$, and the updated estimate $\mathbf{S}_4^-(i,j)$ with $\mathbf{P}_4^-(i,j)$ will be derived respectively. The estimates $\mathbf{S}_1^+(i,j)$, $\mathbf{S}_2^-(i,j)$, $\mathbf{S}_3^+(i,j)$, and $\mathbf{S}_4^-(i,j)$ are assumed to be independent. The final estimate $\mathbf{S}_{final}(i,j)$ of $\mathbf{S}(i,j)$ can be formed as a linear combination of $\mathbf{S}_1^+(i,j)$, $\mathbf{S}_2^-(i,j)$, $\mathbf{S}_3^+(i,j)$, and $\mathbf{S}_4^-(i,j)$:

$$\mathbf{S}_{final}(i,j)=\mathbf{P}_{pseudo}(i,j)\begin{bmatrix}\left(\mathbf{P}_1^+(i,j)\right)^{-1}\mathbf{S}_1^+(i,j)+\left(\mathbf{P}_2^-(i,j)\right)^{-1}\mathbf{S}_2^-(i,j)\\+\left(\mathbf{P}_3^+(i,j)\right)^{-1}\mathbf{S}_3^+(i,j)+\left(\mathbf{P}_4^-(i,j)\right)^{-1}\mathbf{S}_4^-(i,j)\end{bmatrix} \quad 6\text{-}14$$

$$\mathbf{P}_{pseudo}(i,j)=\left[\left(\mathbf{P}_1^+(i,j)\right)^{-1}+\left(\mathbf{P}_2^-(i,j)\right)^{-1}+\left(\mathbf{P}_3^+(i,j)\right)^{-1}+\left(\mathbf{P}_4^-(i,j)\right)^{-1}\right]^{-1} \quad 6\text{-}15$$

$$\mathbf{P}_{final}(i,j)=\mathbf{P}_{pseudo}(i,j) \quad 6\text{-}16$$

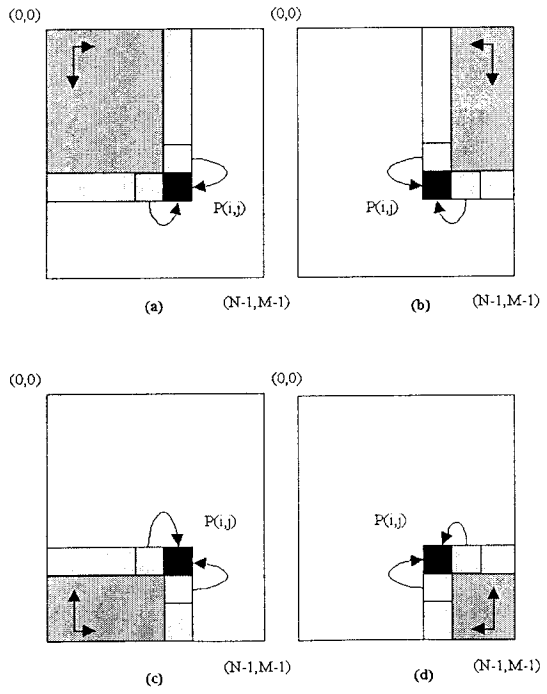

Figure 6-5 The 2-D Kalman smoother

The results of $\mathbf{S}_{final}(i,j)$ and $\mathbf{P}_{pseudo}(i,j)$ are independent of the choice of two predicted estimates and two updated estimates from the four filtering processes. Eq. 6-14 and Eq. 6-15 are only one example of how to choose the estimates and the relevant variance-covariance matrix. The smoother produces the same result using any two predicted $\mathbf{S}^{-}(i,j)$ and $\mathbf{P}^{-}(i,j)$ of four processing orientations, and two updated $\mathbf{S}^{+}(i,j)$ and $\mathbf{P}^{+}(i,j)$ of the other two orientations.

As discussed in the beginning of this Chapter, the 2-D Kalman filter is a casual filter, which unevenly uses the DEM measurements to derive the estimate of terrain variables. The developed 2-D Kalman smoother successfully solves this problem. The observations of the overlapping area of each filtering process are used twice to derive the predicted estimate $\mathbf{S}^{-}(i,j)$ or the updated estimate $\mathbf{S}^{+}(i,j)$. The points of the i th row and j th column have been partly used once in each filtering process while deriving $\mathbf{S}^{-}(i,j)$ or $\mathbf{S}^{+}(i,j)$ as shown in Figure 6-5. So, after four filtering processes, the observations, which have been used twice in the derivation of the relevant estimates of the point (i,j), would cover all DEM points except the point (i,j) itself. The two predicted estimates and two updated estimates in Eq. 6-14 and Eq. 6-15 use the observation $Z(i,j)$ itself, being also applied twice in the generation of the final estimate $\mathbf{S}_{final}(i,j)$ of the modelling point. Therefore, the whole DEM data are evenly used twice to generate the estimates of terrain variables of every DEM point using the 2-D Kalman smoother. For the same reason as described in Section 6.2, $\mathbf{P}_{final}(i,j)$ should be scaled by a factor of 2, as shown in Eq. 6-16.

6.4 Experiments

The 2-D Kalman smoother was tested on the noisy DEM as used in Chapter 5 (Figure 5-5), and the results of the 2-D Kalman smoother were compared with the results of the 2-D Kalman filter to investigate the significance of the smoothing process. The ground truth of the elevation, the partial derivatives of elevation, slope and aspect, for algorithm comparison, are the same as shown in Figure 4-5.

6.4.1 Results of the 2-D Kalman smoother

The same filtering parameters were used in the Kalman smoothing process as those used in Chapter 5. The estimates of elevation, X and Y derivatives, slope and aspect derived by the 2-D Kalman smoother are shown in Figure 6-6, which indicates smoother and better surfaces of the elevation, X and Y derivatives, slope and aspect, compared with the filtering result as shown in Figure 4-7. The significant improvements in the result of the Kalman smoothing appeared at the four boundaries, and this is due to the linear combination of the four filtering results.

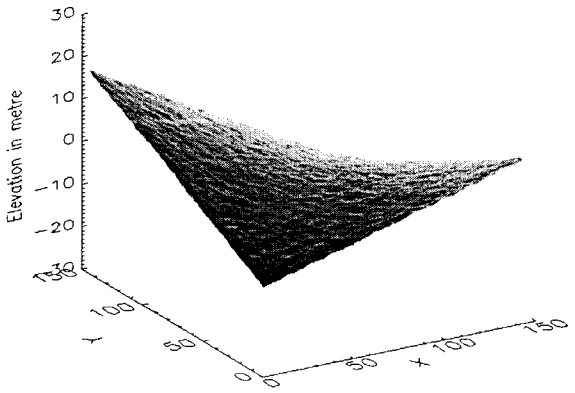

Figure 6-6(a) Elevation

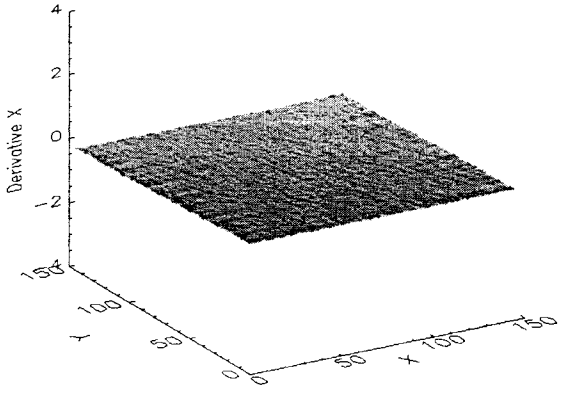

Figure 6-6(b) X Derivative

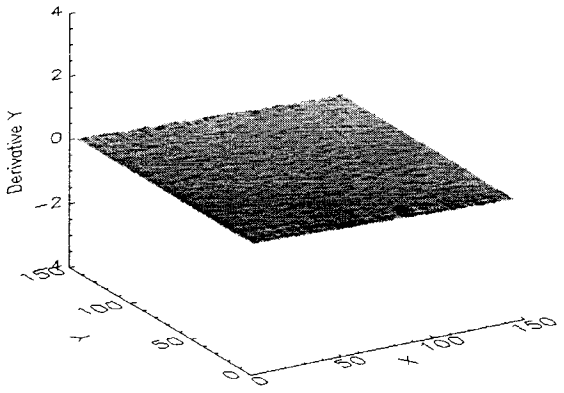

Figure 6-6(c) Y Derivative

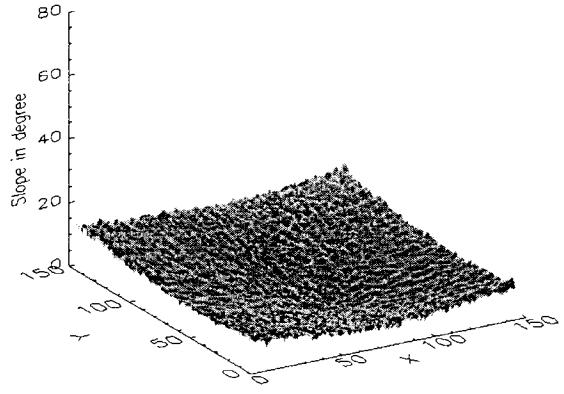

Figure 6-6(d) Slope

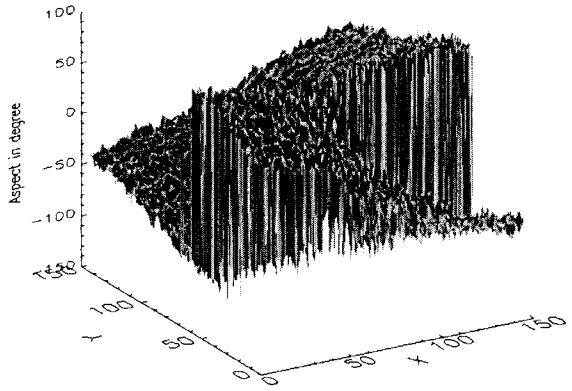

Figure 6-6(e) Aspect

Figure 6-6 Results of the 2-D Kalman smoother

6.4.2 Comparison of the results of the 2-D Kalman smoother with the 2-D Kalman filter

Errors in the estimates of terrain variables derived by the 2-D Kalman filter and smoother were obtained by subtracting the relevant estimates from the corresponding ground truth, which are shown in Figure 6-7. In the Figure, the horizontal axes represent the number of points of the test data, and the vertical axes represents the errors observed in the filtering/smoothing results of elevation, X and Y derivatives, slope or aspect.

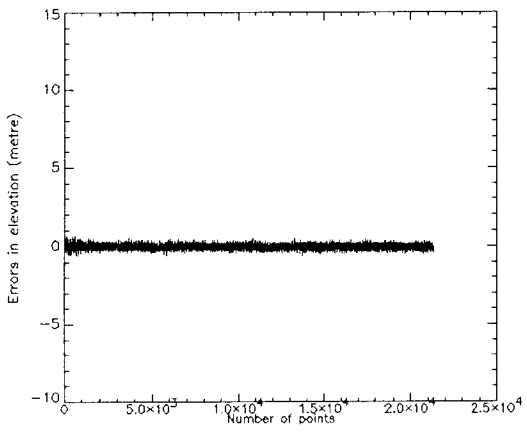

Figure 6-7(a) Kalman filter

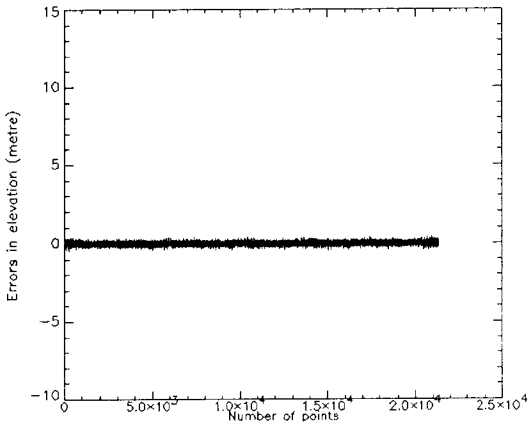

Figure 6-7(b) Kalman smoother

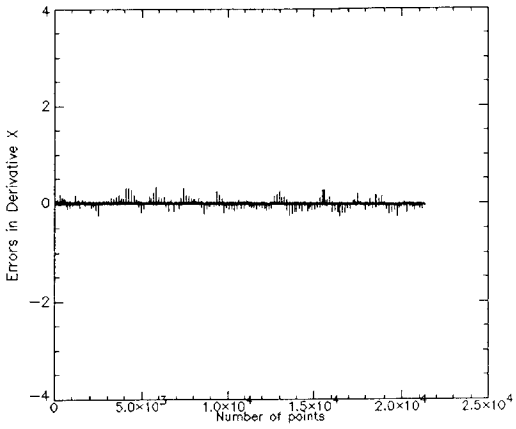

Figure 6-7(c) Kalman filter

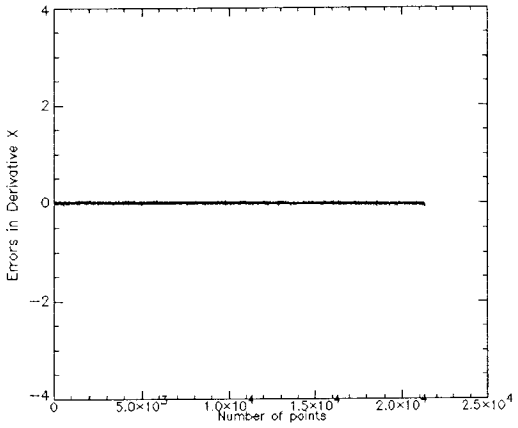

Figure 6-7(d) Kalman smoother

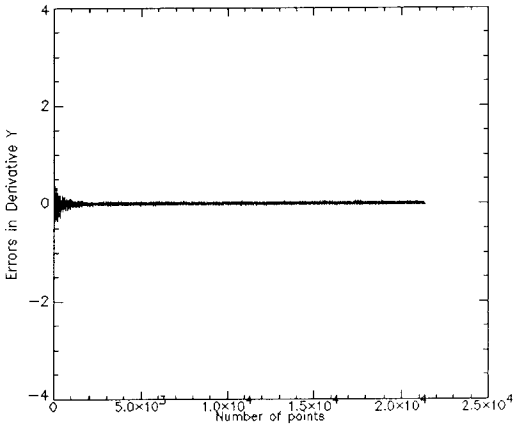

Figure 6-7(e) Kalman filter

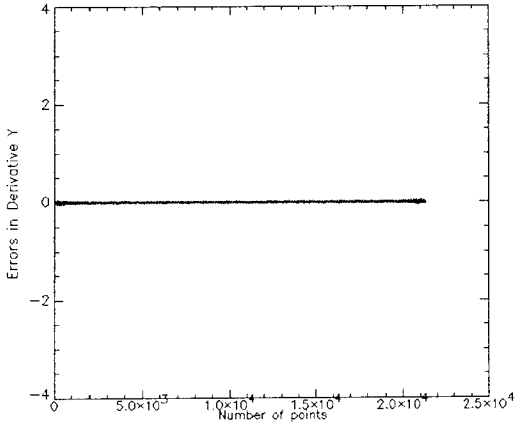

Figure 6-7(f) Kalman smoother

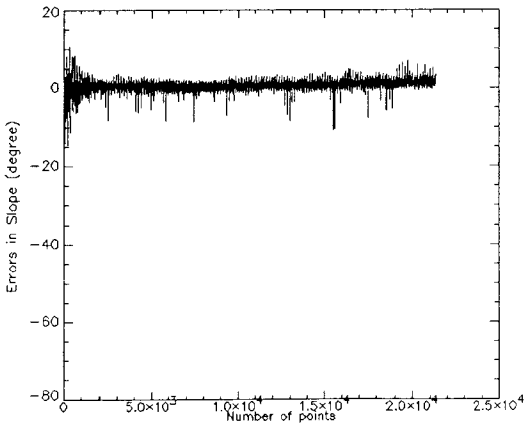

Figure 6-7(g) Kalman filter

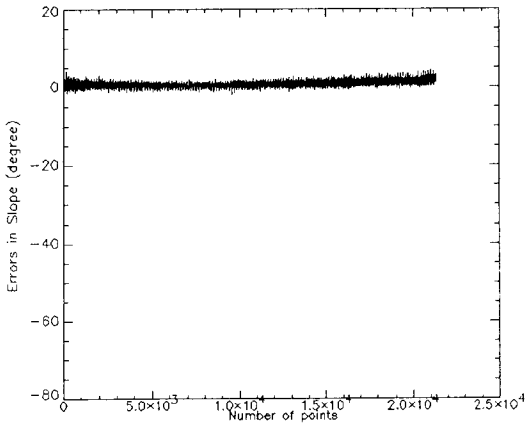

Figure 6-7(h) Kalman smoother

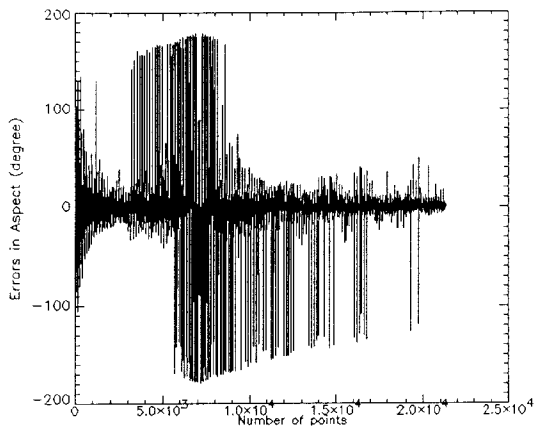

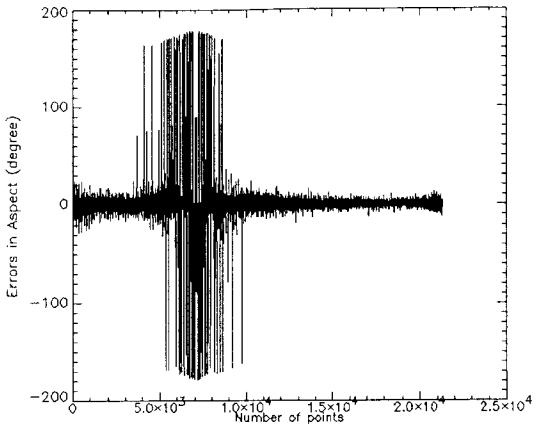

Figure 6-7(i) Kalman filter **Figure 6-7(j) Kalman smoother**

Figure 6-7 Comparing errors remaining in the estimates of terrain variables from the 2-D Kalman filter and smoother

Both the Kalman filtering and smoothing algorithms produced accurate estimates of elevation of the test data, and the remaining errors in the results were small. Outliers were all completely detected and removed in both filtering and smoothing results. The statistical analysis of the estimates of elevation in Table 6-1 indicates that the smoothing result is more accurate than the filtering result. The standard deviation of the elevation estimates derived by the 2-D Kalman smoother has been further improved by 21% over the results of the 2-D Kalman filter.

The differences between the estimates of X and Y derivatives derived using the Kalman smoother and Kalman filter mainly appeared at the boundary of the DEM, where the Kalman smoother produced better results than the Kalman filter. The 2-D Kalman smoother had reduced the standard deviation of the X and Y derivatives by 50% compared with those derived using the 2-D Kalman filter.

Since the 2-D Kalman smoother is more accurate in generating estimates of X and Y derivatives than the 2-D Kalman filter, the quality of the slope computation using the 2-D Kalman smoother is better than the filter. The 2-D Kalman smoother further reduced by 41%, in terms of standard deviation, in slope computation, compared with the 2-D Kalman filter.

The estimates of aspect on the test data is also more accurate using the 2-D Kalman smoother than the 2-D Kalman filter. The improvement of aspect calculation using the 2-D Kalman smoother is 15%, in terms of standard deviation, compared with the result of the 2-D Kalman filter.

Table 6-1 Comparing errors in the results of the 2-D Kalman smoother and the 2-D Kalman filter

	Minimum value	Maximum value	Mean value	Standard deviation	Improvement
Eelvation (m)					
Kalman filtering	-0.62	0.67	-0.01	0.14	---
Kalman smoothing	-0.44	0.45	0.00	0.11	**21%**
X derivatives					
Kalman filtering	-0.26	0.33	-0.01	0.02	---
Kalman smoothing	-0.09	0.06	-0.01	0.01	**50%**
Y derivatives					
Kalman filtering	-0.35	0.38	0.00	0.02	---
Kalman smoothing	-0.06	0.06	0.00	0.01	**50%**
Slope (degrees)					
Kalman filtering	-14.55	10.73	0.83	1.07	---
Kalman smoothing	-1.83	4.26	0.90	0.63	**41%**
Aspect (degrees)					
Kalman filtering	-178.68	178.62	0.63	30.18	---
Kalman smoothing	-178.70	178.62	0.40	25.74	**15%**

6.5 Conclusions

The 2-D Kalman filter for terrain surface modelling developed in Chapter 4 is a causal filter. In the beginning of this Chapter, the method of using observations of a DEM and the relevant estimates to determine the updated estimates of terrain attributes of a DEM point in the 2-D Kalman filtering process was reviewed. A problem existed in the 2-D Kalman filter, mainly associated with the use of information in the filtering, motivating the development of the 2-D Kalman smoother.

The 2-D Kalman smoother presented in this Chapter is a linear combination of four filtering results, which is derived from four different filtering orientations over a DEM. The particular advantage of the Kalman smoothing algorithm over the Kalman filtering algorithm is that it enables the use of all the DEM observations to derive the terrain attributes of each DEM point, and therefore, produces more accurate estimates of the terrain variables.

At this point, the introduction of the developed 2-D Kalman filtering algorithm for terrain surface modelling is complete. It consists of three major parts, including a 2-D Kalman filter, the method of outlier detection and removal, and 2-D Kalman smoother. It could also be considered as a 2-D Kalman smoother with extension of the processes for outlier detection and removal.

The results of the experiments presented in this Chapter indicate that the 2-D Kalman smoother is more accurate in deriving the estimates of X and Y derivatives, slope and aspect, compared with the 2-D Kalman filter, using the simulated data.

CHAPTER 7

EXPERIMENTS RESULTS

7.1 DEM Data

The mapping test site is located in the Katoomba area, New South Wales, and covers 1320m by 1060m. The landscape is considerably rugged with significant breaklines and vegetation coverage, and is a typically undulating terrain suitable for the test purposes. The terrain height varies approximately from 480m to 650m. A Katoomba DEM was produced by digital photogrammetric means from a pair of digitized aerial photos. The scale of original aerial photos is 1:25,000. Following the recommendations of Kubik (1985), the suitable DEM sampling spacing, which may accurately represent such a landscape, is 5m. So the DEM was derived with a sampling interval of 5m by 5m (see Figure 7-1). This 5m DEM was then re-sampled into a 10m DEM (Figure 7-2), which is used in the following Sections to investigate the effect of DEM resolution, and the efficiency of Kalman filter and smoother. According to Section 2.2.1, the accuracy of elevation of the Katoomba DEM is estimated at 0.6m level using the 1:25,000 photos and image matching method.

On viewing the photographs, a number of isolating trees are randomly distributed over the mapping area. By photogrammetric observation, the size of the trees was found to be generally over 3.5m high, with the canopies varying from 20m by 20m to 5m by 5m. The effect of these trees on the produced DEMs could be clearly observed as abrupt small peaks on the elevation surface. If the terrain surface is the main interest of this study, these small peaks could be considered as invalid observations, i.e. outliers, which do not represent the terrain surface and should be removed. A total of 523 outliers was observed in the Katoomba 5m DEM, the magnitudes of which vary from 3.50m to 14.29m, with a mean value of 6.16m. As a result of the change in resolution, only 110 outliers were observed in the 10m Katoomba DEM, which range from 3.50m to 13.26m with a mean of 6.10m. The outliers in the 5m and 10m DEM are plotted in Figure 7-3(a) and (b), in which the vertical axis represents the magnitude of the outliers and the horizontal X and Y axes represent the positions of each outlier in the DEM data.

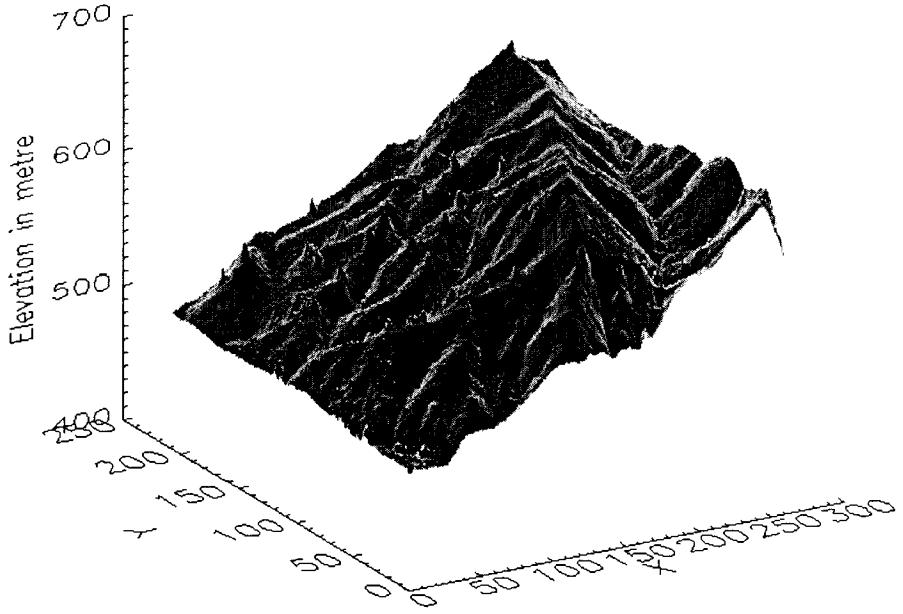

Figure 7-1 Katoomba 5m DEM

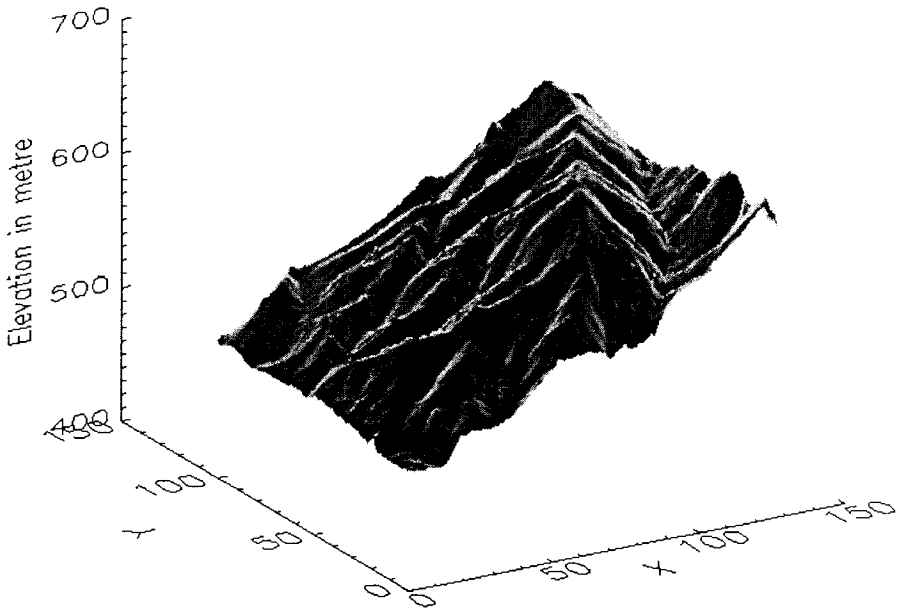

Figure 7-2 Katoomba 10m DEM

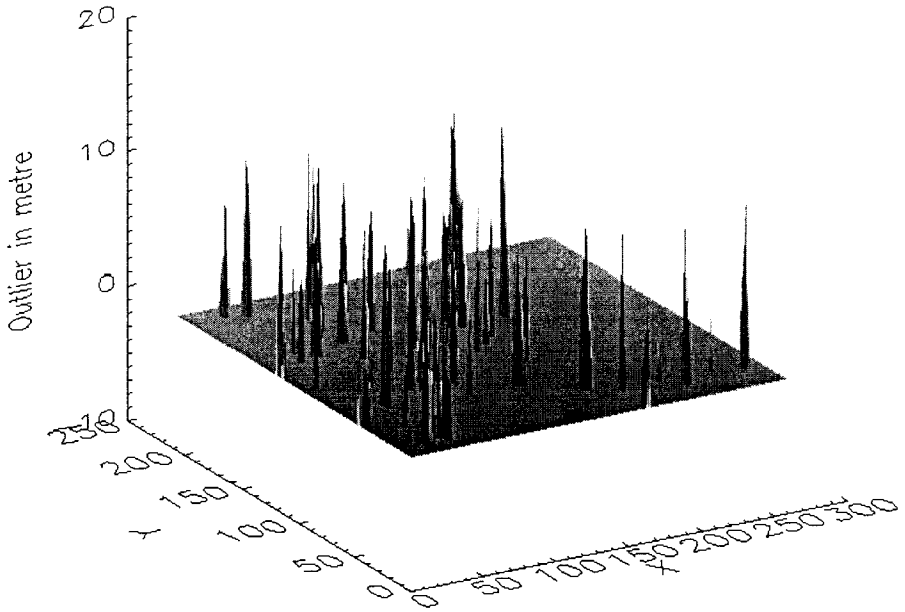

Figure 7-3(a) 5m DEM

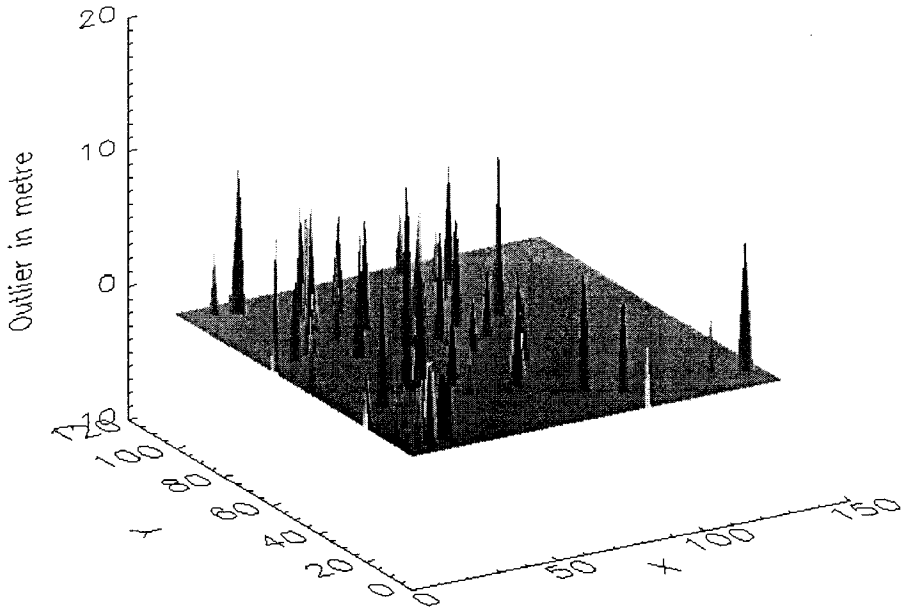

Figure 7-3 (b) 10m DEM

Figure 7-3 Outliers in the 5m and 10m Katoomba DEMs

7.2 Experiments Applying 2-D Kalman Filtering Algorithm on 5m and 10m Katoomba DEMs

The 2-D Kalman filtering algorithm for terrain surface modelling was applied to the two sets of Katoomba DEMs with the four filtering orientations illustrated in Figure 7-4.

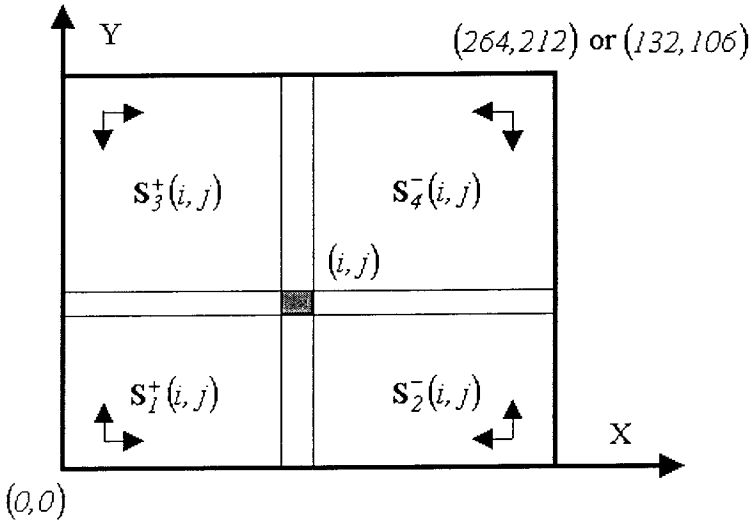

Figure 7-4 The processing orientations applied in the 2-D Kalman filtering algorithm on the 5m and 10m Katoomba DEM

The parameters used for the Kalman filter on the 5m DEM are given in Eq. 7-1 to Eq. 7-3. The same dynamic model errors were used in the four filtering processes, in which the second order partial derivatives of elevations were assumed to be 0.08. The observation variance was used as $0.36m^2$. The critical value ξ_α selected for outlier detection and removal in the 5m Katoomba DEM is 2, which is equivalent to a level of approximation by 95% confidence. It is expected that only 5% of good DEM observations will be rejected in the outlier detection:

$$\mathbf{Q}_x(i,j)=\mathbf{Q}_y(i,j)=\begin{bmatrix}1 & 0 & 0\\ 0 & 0.16 & 0\\ 0 & 0 & 0.16\end{bmatrix} \qquad 7\text{-}1$$

$$R(i,j)=0.36 \qquad 7\text{-}2$$

$$\xi_\alpha = 2 \qquad 7\text{-}3$$

The critical value and the observation variance used on the 10m Katoomba DEM were the same as those used on the 5m Katoomba DEM. The model error used on the 10m Katoomba DEM for the Kalman filter given in Eq. 7-4, was derived from the same value of the relevant second order of derivatives of elevation that was used in the 5m Katoomba DEM. The larger model errors in the 10m DEM, compared with the 5m DEM, are expected since the DEM resolution is enlarged from 5m to 10m and therefore terrain roughness between the adjacent DEM points is increased.

$$\mathbf{Q}_x(i,j)=\mathbf{Q}_y(i,j)=\begin{bmatrix}16 & 0 & 0\\ 0 & 0.64 & 0\\ 0 & 0 & 0.64\end{bmatrix} \qquad 7\text{-}4$$

The results of the 2-D Kalman smoothing on the 5m and 10m Katoomba DEM are displayed in Figure 7-5 and Figure 7-6.

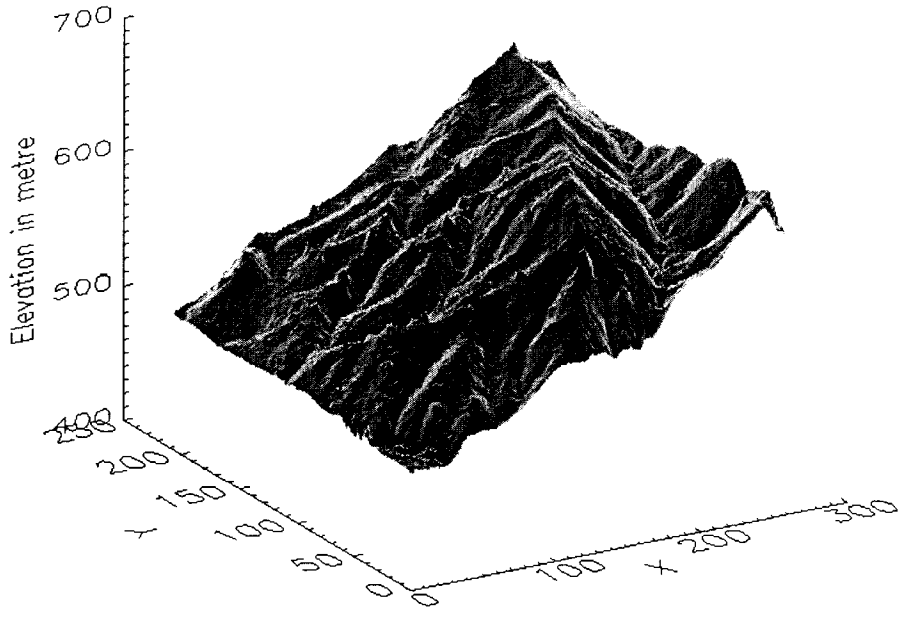

Figure 7-5(a) Estimates of elevation

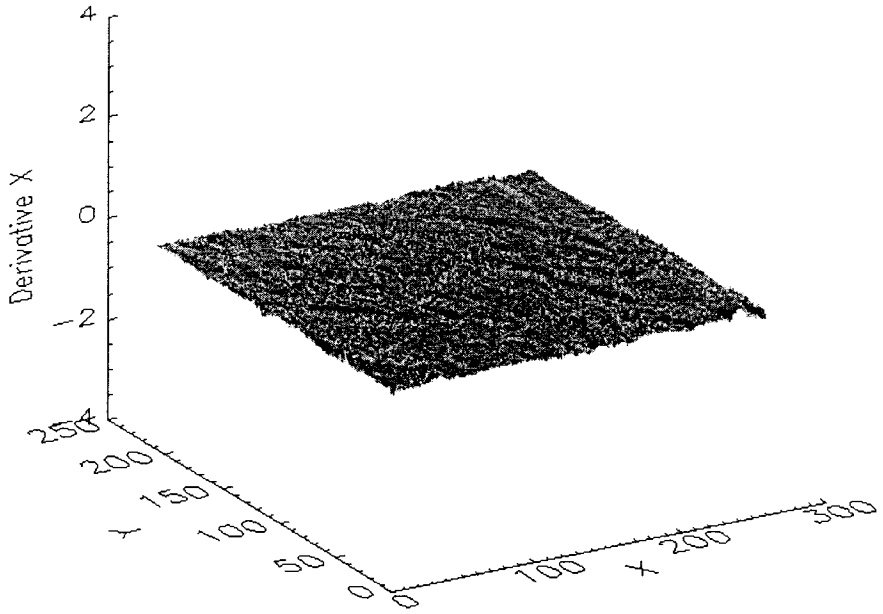

Figure 7-5(b) Estimates of X derivative

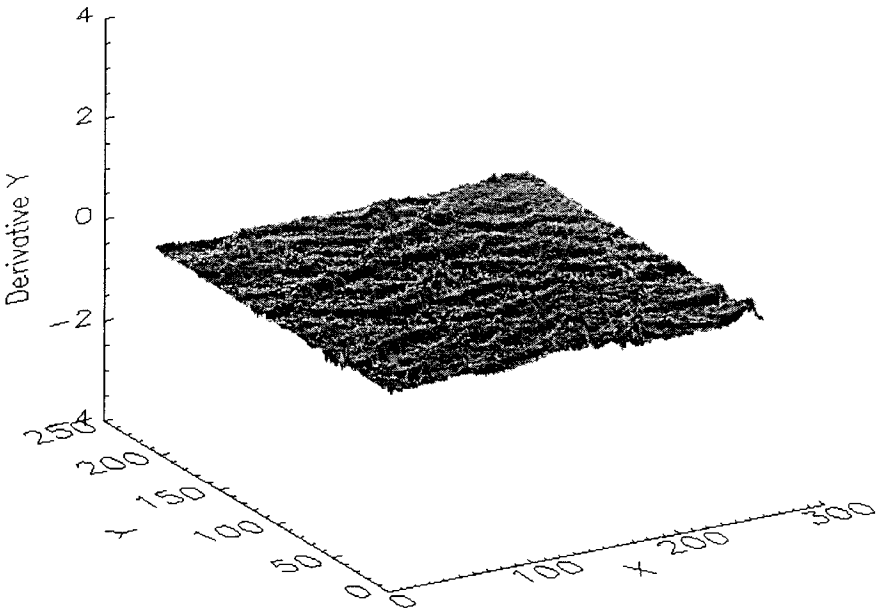

Figure 7-5(c) Estimates of Y derivative

Figure 7-5(d) Estimates of slope

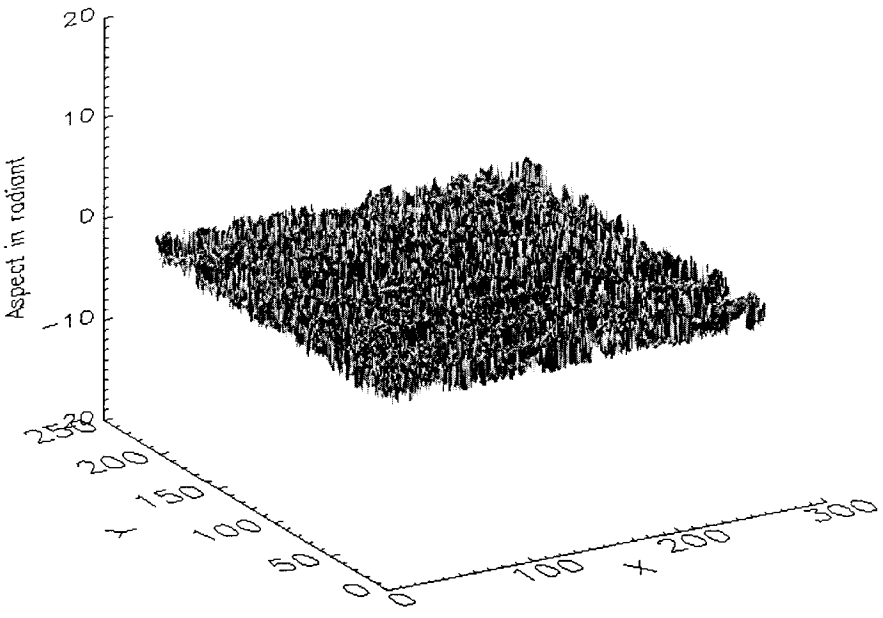

Figure 7-5(e) Estimates of aspect

Figure 7-5 The results of the 2-D Kalman filtering algorithm on the 5m Katoomba DEM

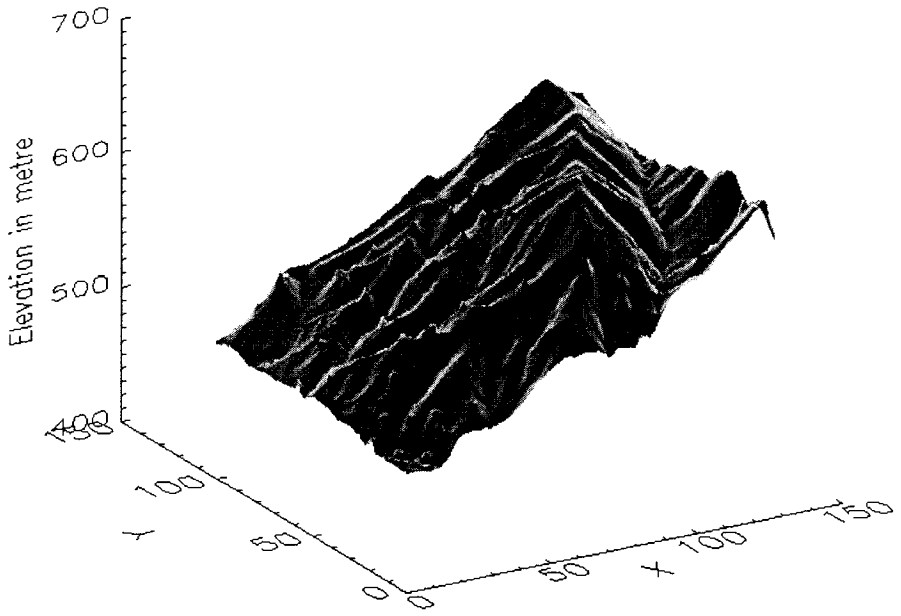

Figure 7-6(a) Estimates of elevation

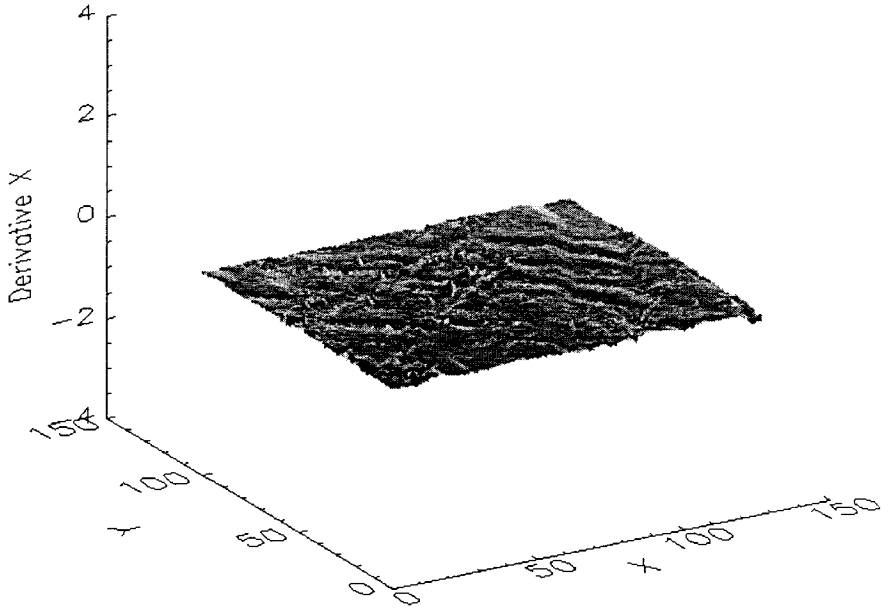

Figure 7-6(b) Estimates of X derivative

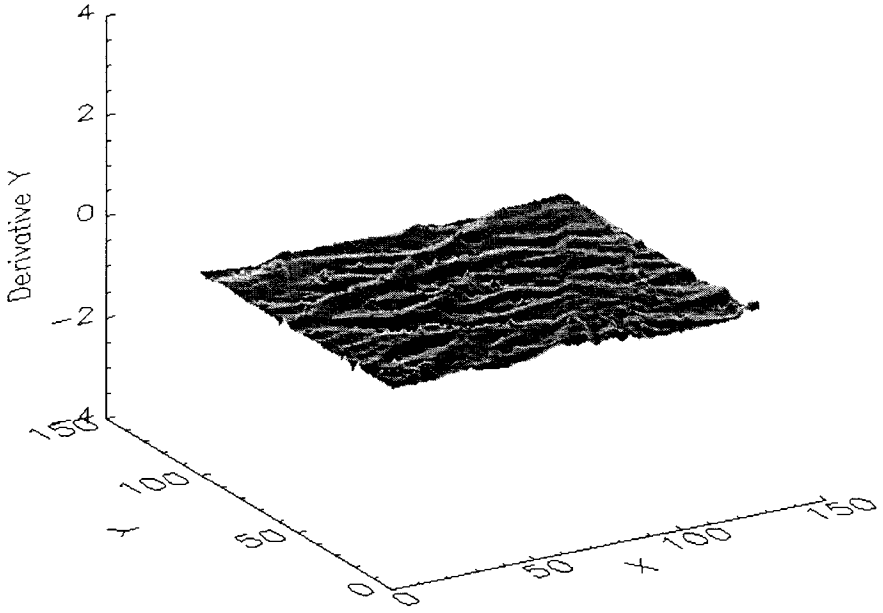

Figure 7-6(c) Estimates of Y derivative

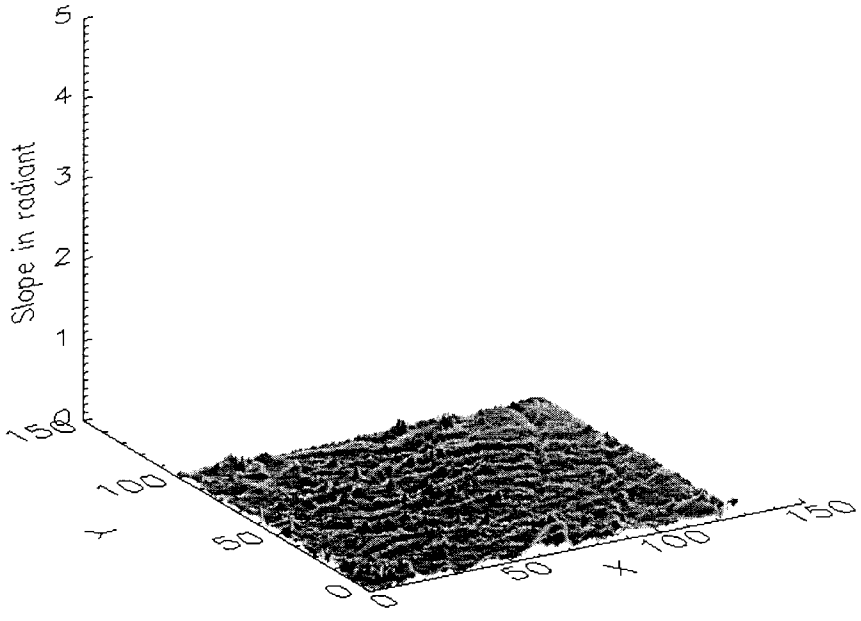

Figure 7-6(d) Estimates of slope

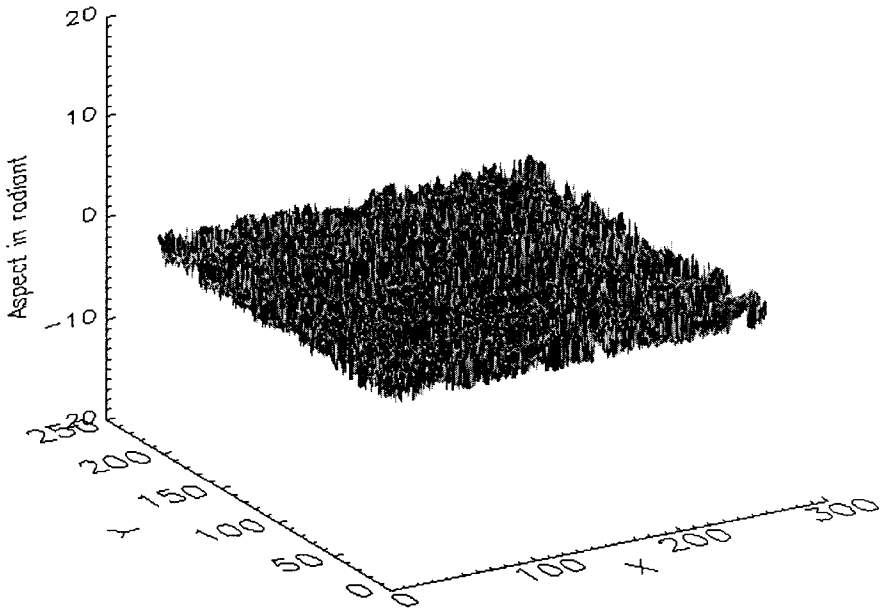

Figure 7-6(e) Estimates of aspect

Figure 7-6 The results of the 2-D Kalman filtering algorithm on the 10m Katoomba DEM

Comparing these two Figures, the results of smoothing of the 5m and 10m Katoomba DEM are all generally effective. The results of the 5m DEM are more accurate than the 10m DEM results in terms of the representation of terrain topographic features, which is due to the use of denser DEM resolutions.

7.3 Results of the 2-D Kalman filter

In this Section, the results of the 2-D Kalman filter of the 5m and 10m Katoomba DEMs will be further examined, and the relevant results will be compared with the Evans method to investigate the efficiency of DEM random noise reduction by the developed 2-D Kalman filter. It is necessary to mention that the results of the 2-D Kalman filter used in this Section over the Katoomba DEMs refer to the results derived by applying the 2-D Kalman filter, not the Kalman smoother.

The derivation of estimates of five terrain variables by the 2-D Kalman filter for the 5m and 10m Katoomba DEMs are plotted in Figures 7-7 and 7-8. The processing followed the orientation of $\mathbf{S}_1^+$ shown in Figure 7-4. The filtering parameters are the same as shown in Eq. 7-1 to Eq. 7-4.

The accuracies of the estimates of the 2-D Kalman filter for the 5m and 10m Katoomba EM are poor at the two boundary areas, but they improve as the filter proceeds from the bottom left direction to the top right.

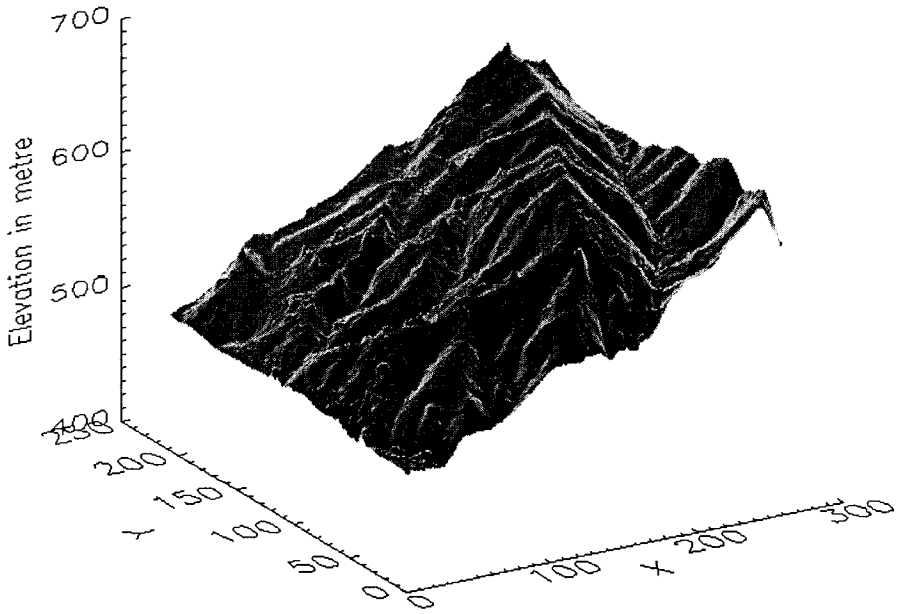

Figure 7-7(a) Estimates of elevation

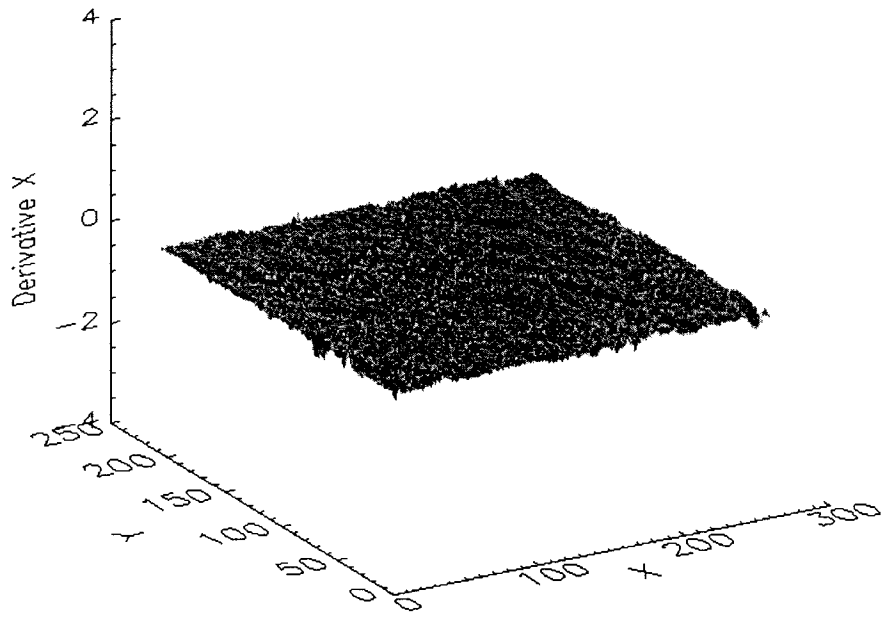

Figure 7-7(b) Estimates of X derivative

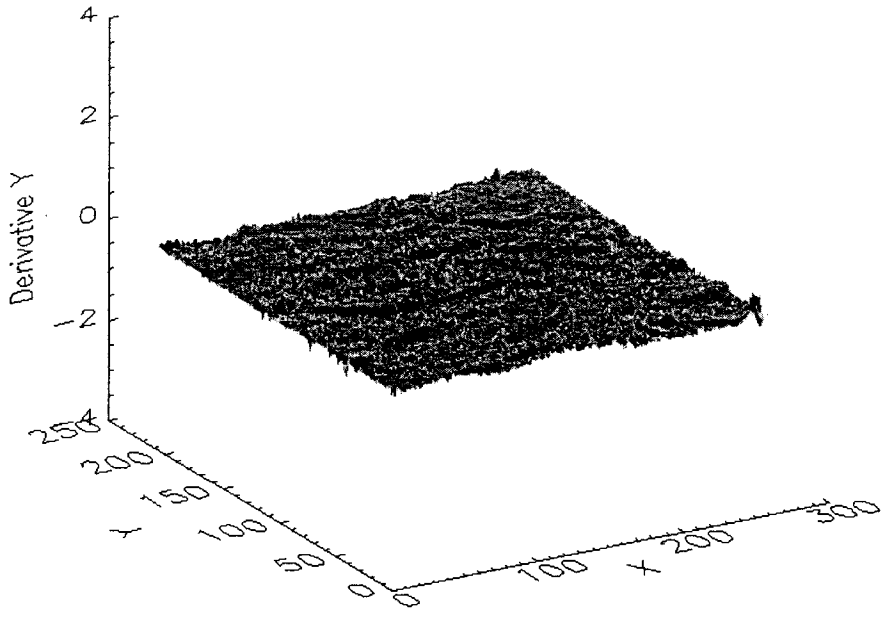

Figure 7-7 (c) Estimates of Y derivative

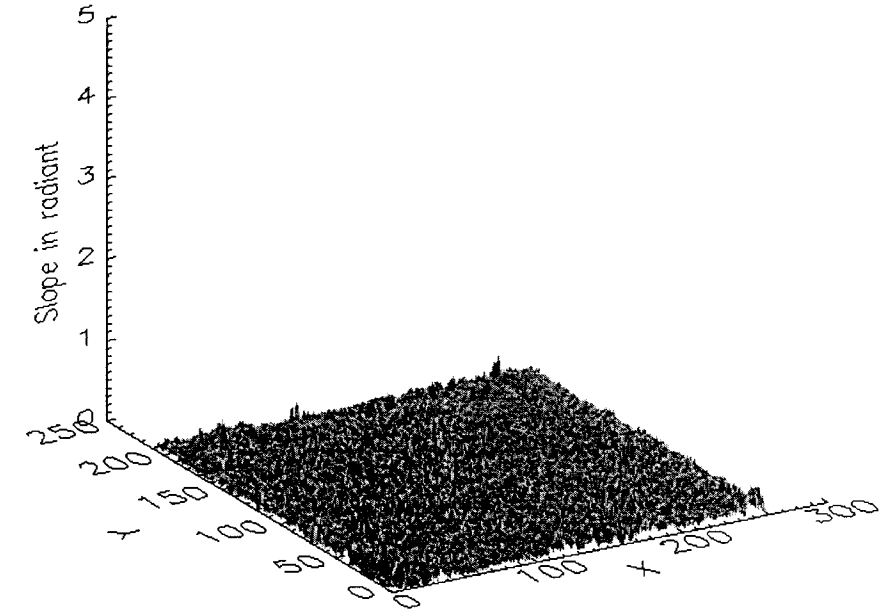

Figure 7-7 (d) Estimates of slope

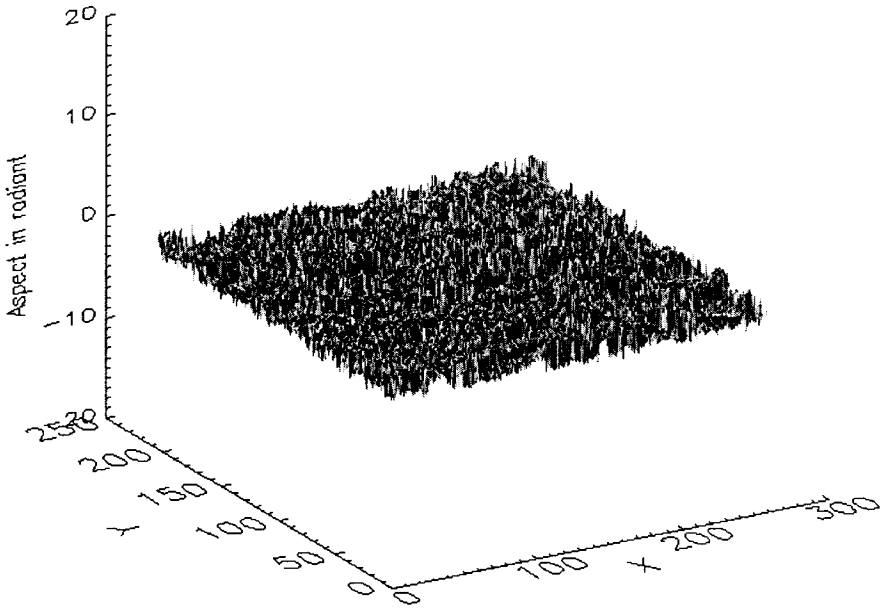

Figure 7-7(e) Estimates of aspect

Figure 7-7 The results of the 2-D Kalman filter using the 5m Katoomba DEM

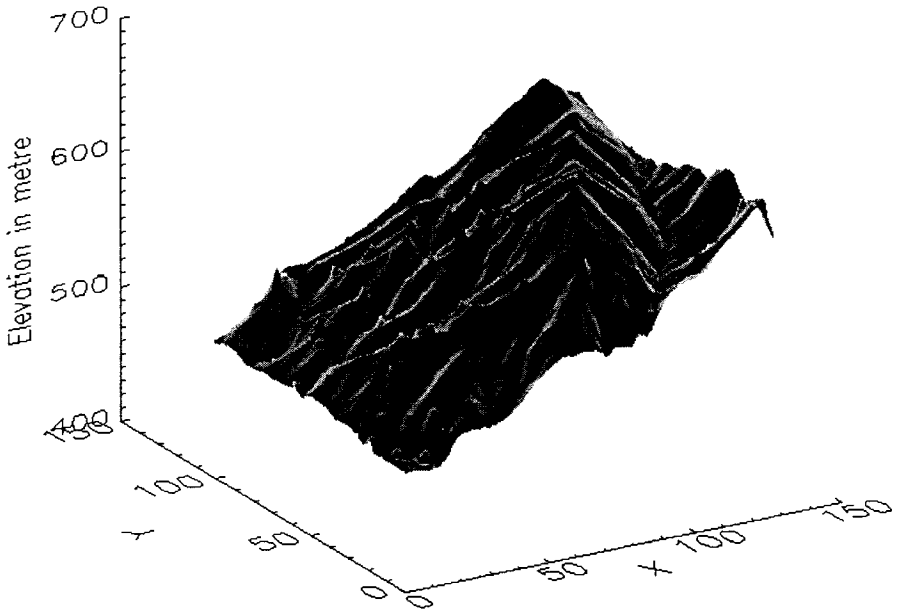

Figure 7-8(a) Estimates of elevation

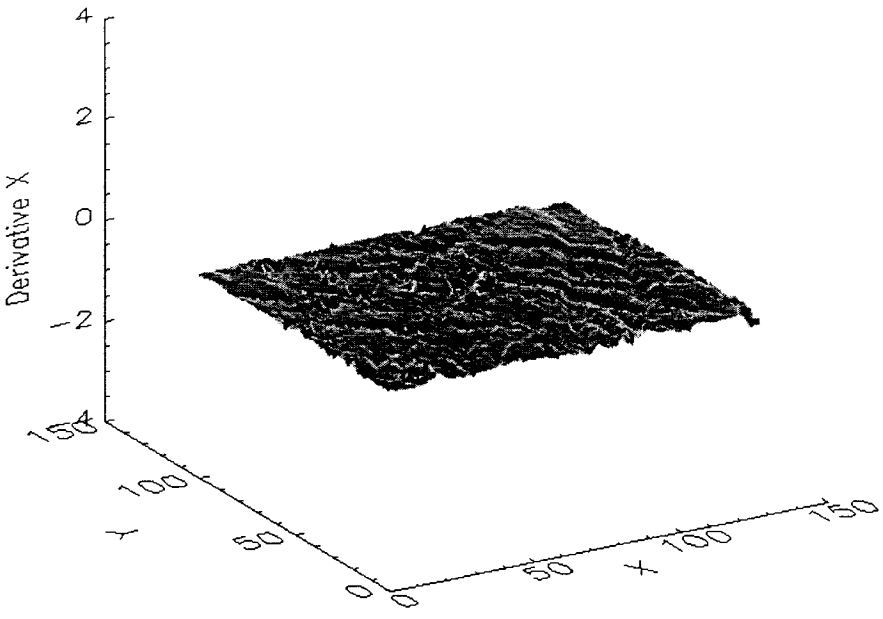

Figure 7-8(b) Estimates of X derivative

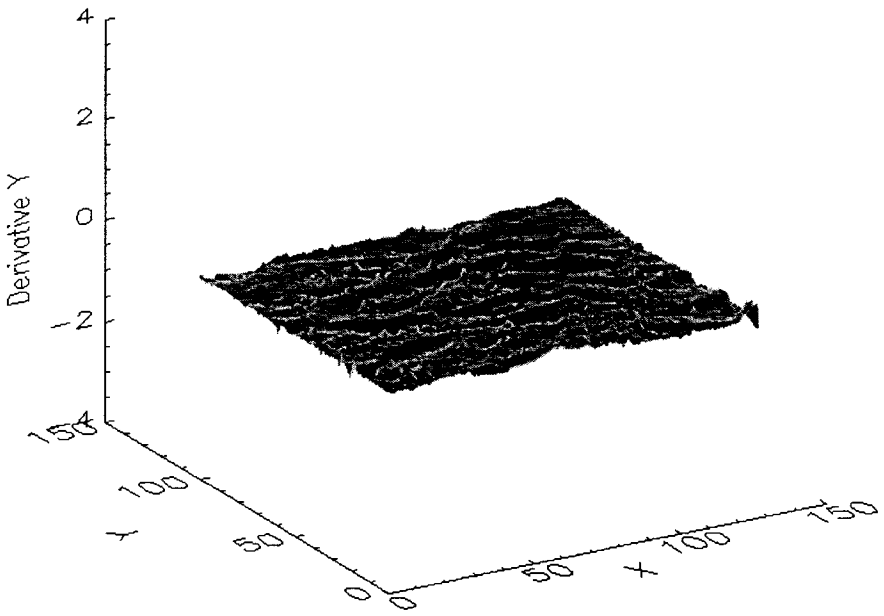

Figure 7-8(c) Estimates of Y derivative

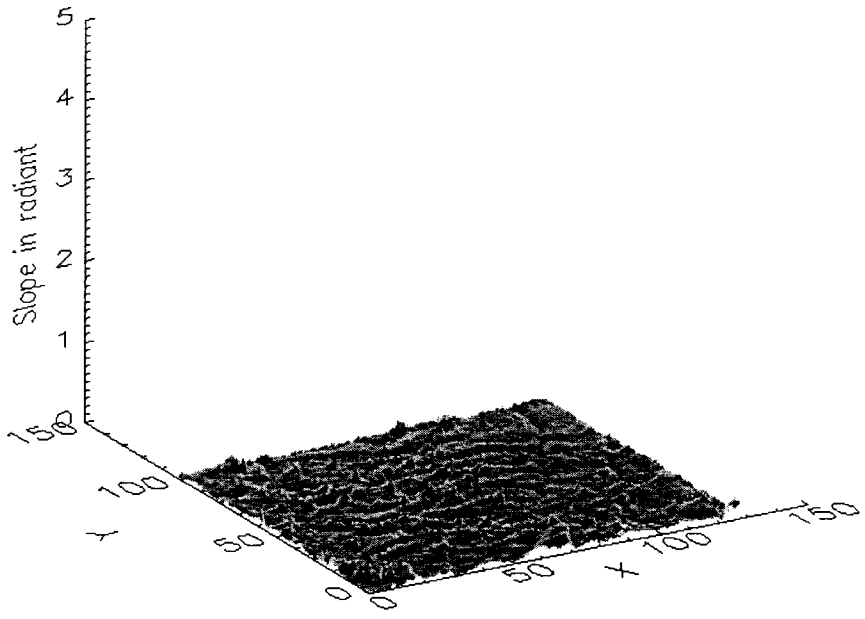

Figure 7-8(d) Estimates of slope

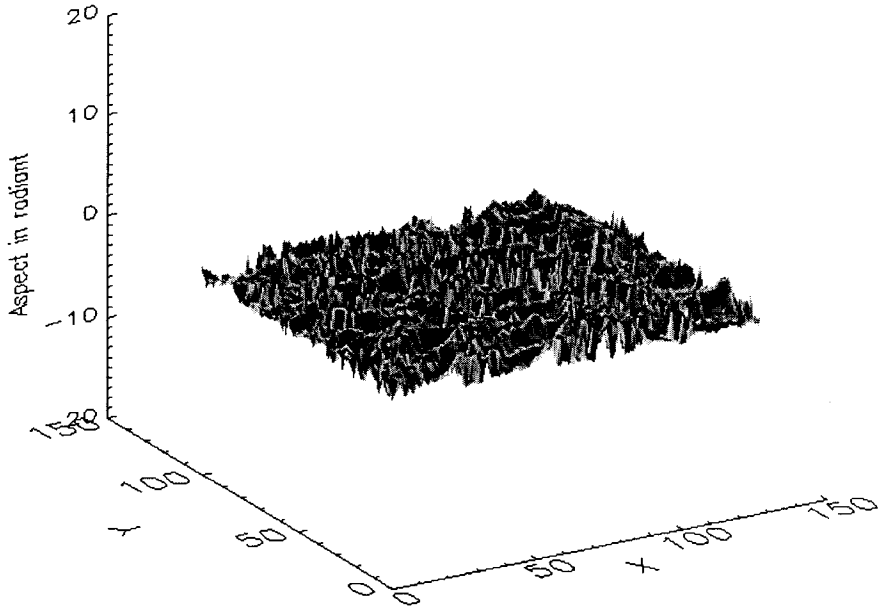

Figure 7-8(e) Estimates of aspect

Figure 7-8 The results of the 2-D Kalman filter using the 10m Katoomba DEM

7.3.1 Effect of DEM resolution on the results of the 2-D Kalman filter

The effect of DEM resolution on the 2-D Kalman filter can be investigated by comparing the results of the 2-D Kalman filtering process using the 5m and 10m Katoomba DEMs. Since the 10m DEM was sampled from the 5m DEM, the differences between the five terrain attributes for the 10m and 5m Katoomba DEM derived by the 2-D Kalman filter are mainly due to changing the resolution from 5m to 10m as summarized in Table 7-1.

So, if the DEM resolution is increased from 5m to 10m over such a terrain surface as the Katoomba mapping area, the effect of DEM resolution on the 2-D Kalman filter are in the range of -6.30m to 8.09m with a mean of –0.01m for the estimates of elevation. In the case of the estimates of the X and Y derivatives, the effect of DEM resolution is about 0.01 on average, which causes about 0.02 radians difference in the slope calculation, and 0.12 radians difference in aspect computation.

Table 7-1 Differences in the results of the 2-D Kalman filter using 5m and 10m Katoomba DEMs

	Minimum value	Maximum value	Mean value	Standard deviation
Elevations (m)	-6.30	8.09	-0.01	0.37
X derivatives	-0.21	0.29	0.01	0.03
Y derivatives	-0.27	0.26	0.01	0.03
Slope (radians)	-0.22	0.28	0.02	0.03
Aspect (radians)	-3.29	3.28	0.12	0.85

7.3.2 Comparing the results of the 2-D Kalman filter with the Evans method

The efficiency of DEM random noise reduction of the 2-D Kalman filter was compared with the Evans method. The results of the Evans method for the 10m Katoomba DEM are plotted in Figure 7-9. Compared with the results of the 2-D Kalman filter (see Figure 7-8), the results of the Evans method are more noisy in the X and Y derivative surfaces, and therefore, less accurate in the estimates of slope and aspect (see Figure 7-9).

It is difficult to obtain the ground truth of elevation, X and Y derivatives, slope and aspect of the Katoomba mapping area. So the 2-D Kalman smoothing results of the 5m Katoomba DEM were used as the bases in this Section to evaluate the accuracy of the 2-D Kalman filter and the Evans method using the 10m Katoomba DEM. Compared with the Kalman smoothing results of the 5m DEM, the errors remaining in the results of the 2-D Kalman filter and the Evans method using the 10m Katoomba DEM were analysed (see Table 7-2). The improvement shown in Table 7-2 represents the improvement of the 2-D Kalman filter, compared with the Evans method, in terms of standard deviation.

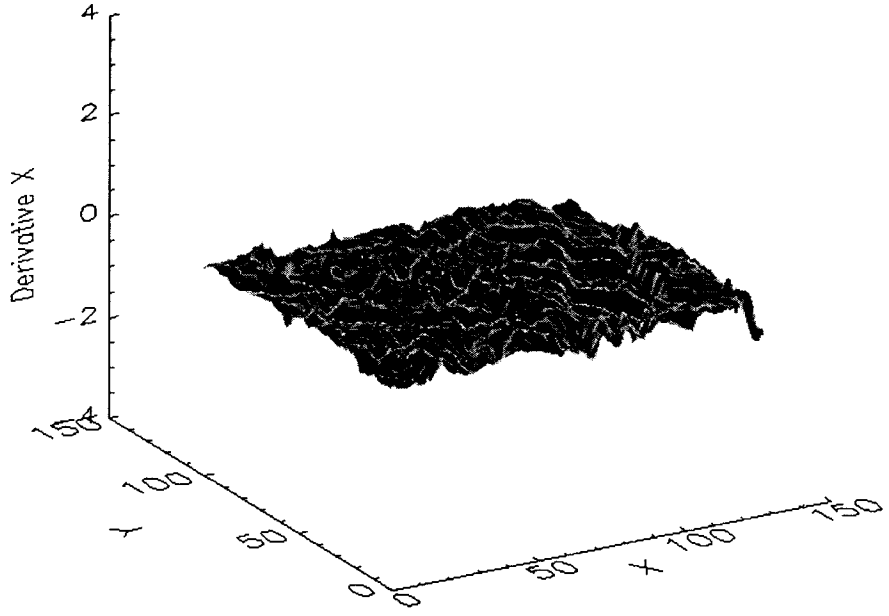

Figure 7-9(a) Estimates of X derivative

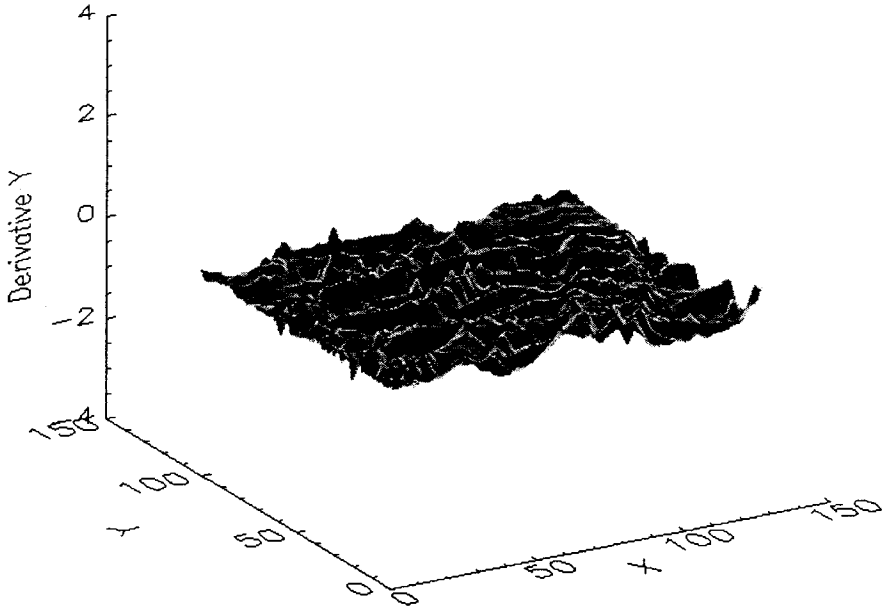

Figure 7-9(b) Estimates of Y derivative

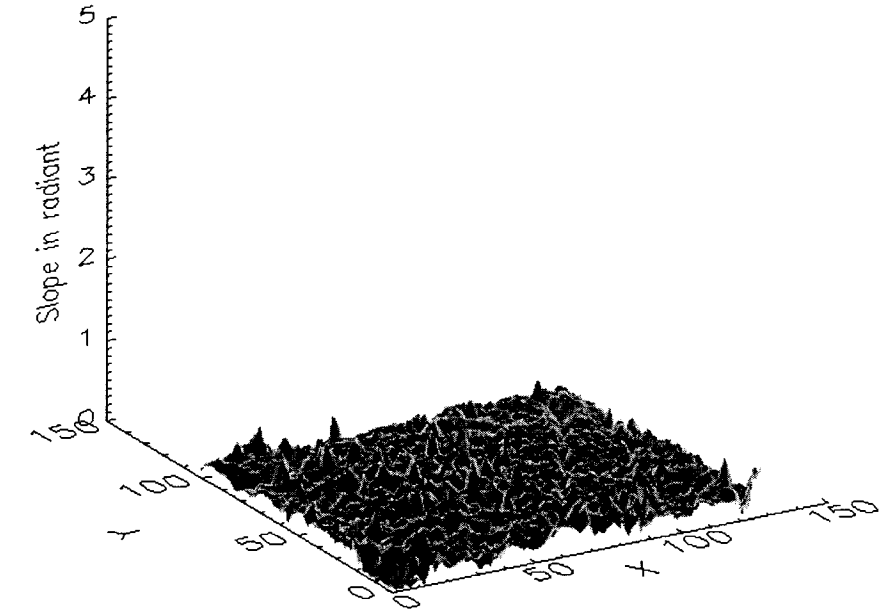

Figure 7-9 (d) Estimates of slope

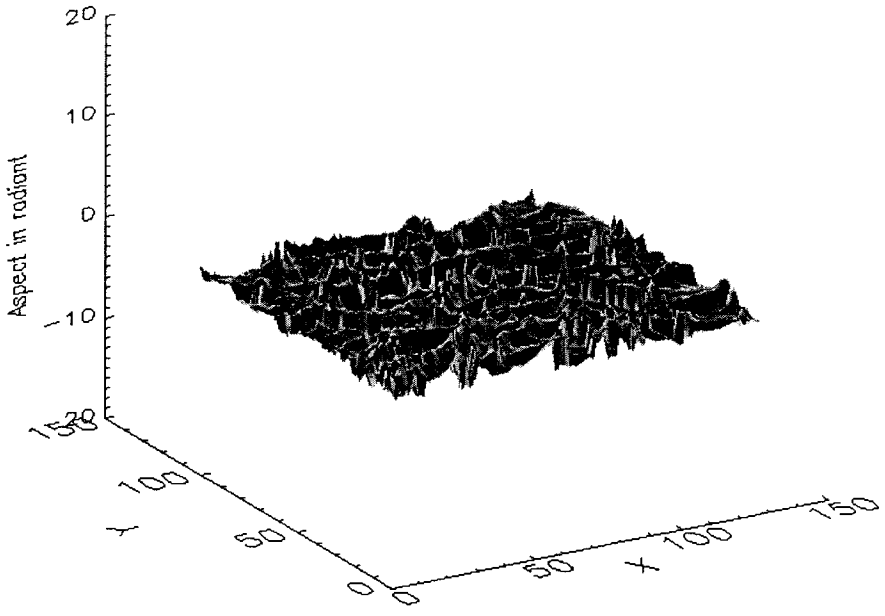

Figure 7-9(d) Estimates of aspect

Figure 7-9 The results of the Evans method using the 10m Katoomba DEM

Table 7-2 Comparison of errors remaining in the results of the 2-D Kalman filter and the Evans method using the 10m Katoomba DEM

	Minimum value	Maximum value	Mean value	Standard deviation	Improvement
X derivatives					
Errors in the Evans method	-0.83	0.56	0.07	**0.12**	---
Errors in Kalman filter	-0.21	0.29	0.01	**0.03**	**75%**
Y derivative					
Errors in the Evans method	-0.60	0.55	0.03	**0.14**	---
Errors in Kalman filter	-0.27	0.26	0.01	**0.03**	**79%**
Slope (radians)					
Errors in the Evans method	-0.23	0.50	0.15	**0.07**	---
Errors in Kalman filter	-0.22	0.28	0.02	**0.03**	**57%**
Aspect (radians)					
Errors in the Evans method	-3.09	3.29	0.10	**1.12**	---
Errors in Kalman filter	-3.29	3.28	0.12	**0.85**	**24%**

Compared with the ground truth, the standard deviations of the estimates of the X and Y derivatives derived by the Evans method are 0.12 and 0.14, which is about three to four times higher than those in the results of the 2-D Kalman filter. While generating the estimates of slope and aspect of the 10m Katoomba DEM, the standard deviation of the error remaining in the slope derived by the Evans method is 0.07 radians, which is twice that of the results of the 2-D Kalman filter. The aspect computation using the Evans method is also worse than the 2-D Kalman filter. The standard deviation of the aspect calculation usng the Evans method is 1.12 radians, compared to 0.85 radians in the 2-D Kalman filter result. The improvement of the 2-D Kalman filter over the Evans method, in terms of standard deviation, is about 75% in estimating X derivatives, 79% in

estimating Y derivatives, 57% and 24% in deriving slope and aspect, on the 10m Katoomba DEM.

7.4 Outlier Detection and Removal

7.4.1 Reliability of outlier detection and removal of the 2-D Kalman filter

As has been described in Section 5.3, the internal and external reliability of outlier detection in the 2-D Kalman filtering algorithm relates to the level of critical value ξ_α used in the relevant filtering process. Rewriting Eq. 5-20 into a full expression, the minimum detectable bias, in which the minimum acceptable power of test was set as 50%, the relevant effect on estimates of the terrain variables can be derived as:

$$\min\left|Z(i,j)-\mathbf{DS}^{-}(i,j)\right|=\xi_\alpha\sqrt{\mathbf{DP}^{-}(i,j)\mathbf{D}^{T}+R(i,j)} \qquad 7\text{-}5$$

$$\Delta\mathbf{S}_L==\mathbf{K}(i,j)\cdot\min\left|Z(i,j)-\mathbf{DS}^{-}(i,j)\right| \qquad 7\text{-}6$$

For instance, the critical value ξ_α was chosen as 2 in the outlier detection and removal of the 2-D Kalman filtering process over the 5m Katoomba DEM. Then, the minimum detectable biases and their possible impact on the derivation of the three terrain variables, can derived using Eq. 7-5 and Eq. 7-6 (shown in Figure 7-10 and Figure 7-11). In this case, the minimum detectable biases in the elevation estimates derived by the 2-D Kalman filtering process are in the range of 2.78m to 4.88m (see Table 7-3). Larger values mainly occur around isolated trees. This is due to the effect of the outliers, which reduce the accuracy of the estimates of their surrounding points. Once an outlier is detected, the relevant observation variance $R(i,j)$ would be amplified into a large value in order to remove it, and therefore, the variance of the estimates of the elevation of the surrounding DEM points will be enlarged.

The possible effect of the minimum detectable biases on the derivation of terrain variables of the 5m Katoomba DEM were also investigated (see Figure 7-11 and Table 7-4). The maximum effect of the minimum detectable biases is only 3.48m for estimates of elevation, and 0.16 for the estimates of X and Y derivatives.

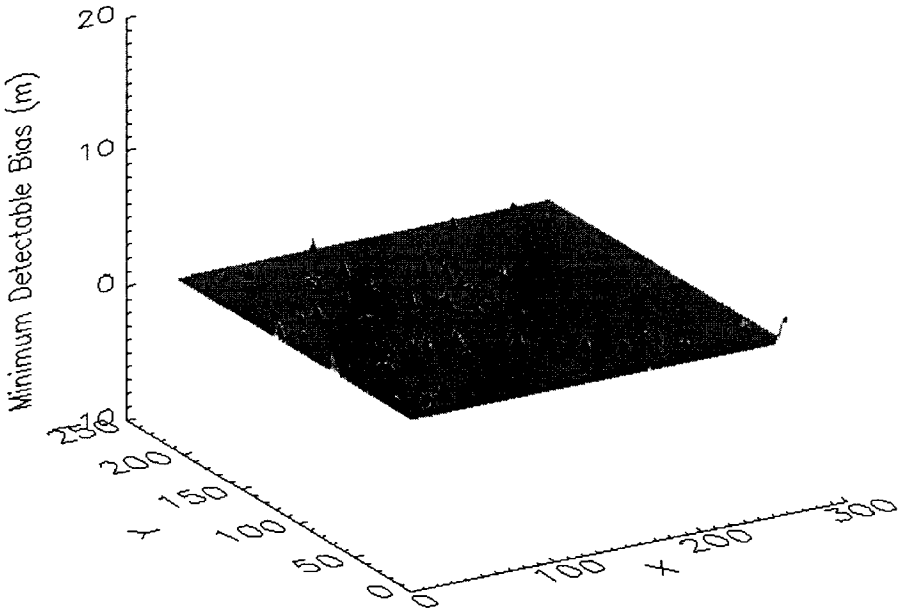

Figure 7-10 The minimum detectable biases for outlier detection in the 2-D Kalman filter using 5m Katoomba DEM ($\xi_\alpha = 2$)

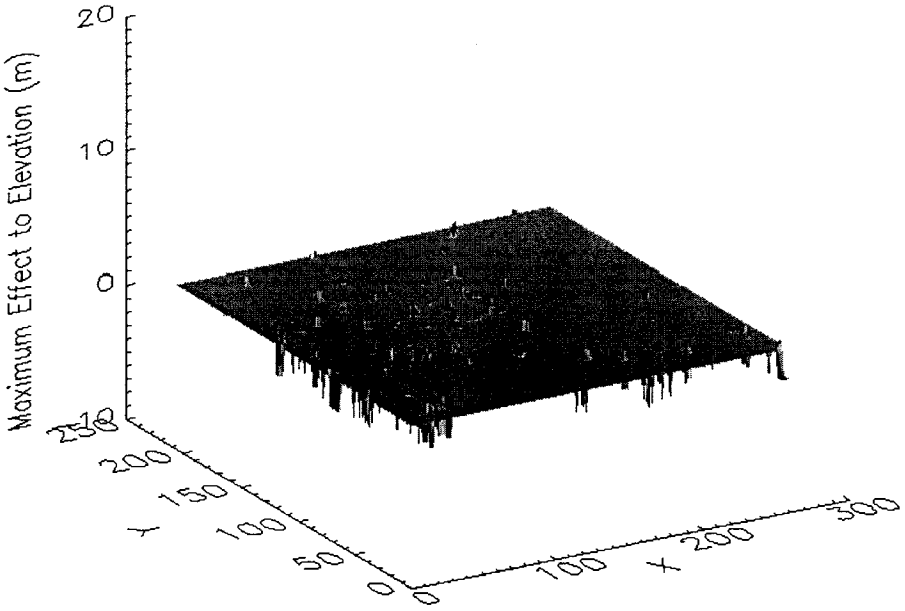

Figure 7-11(a) Effect on elevation

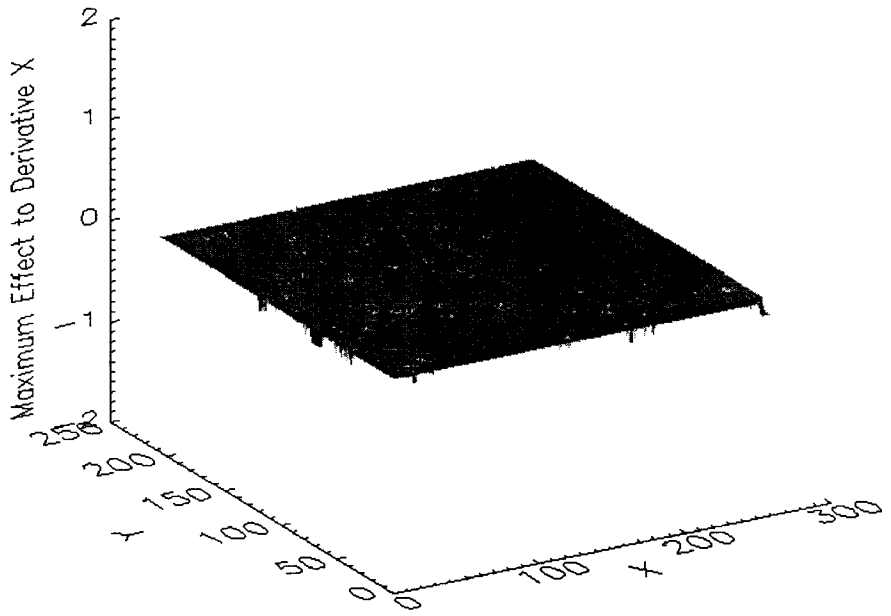

Figure 7-11(b) Effect on X derivative

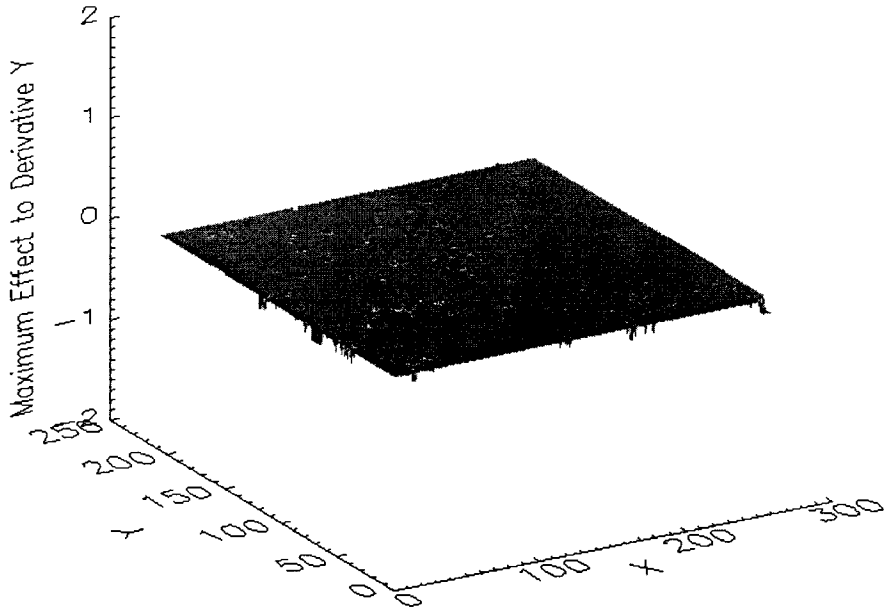

Figure 7-11(c) Effect on Y derivatives

Figure 7-11 Effect of the minimum detectable biases on the estimation of terrain variables using the 2-D Kalmna filtering process and the 5m Katoomba DEM

Table 7-3 **The Minimum detectable biases of outlier detection in the 2-D Kalman filter using the 5m Katoomba DEM ($\xi_\alpha = 2$)**

(unit in metres)

	Minimum value	Maximum value	Mean value	Standard deviation
minimum detectable bias	**2.78**	**4.88**	2.79	0.07

Table 7-4 **Effect of the minimum detectable biases on the derivation of terrain variables using the 2-D Kalman filtering algorithm and 5m Katoomba DEM ($\xi_\alpha = 2$)**

	Minimum value	Maximum value	Mean value	Standard deviation
Effect on elevation	0.00m	**3.48m**	2.24m	0.25m
Effect on X derivative	0.00	**0.16**	0.13	0.01
Effect on Y derivative	0.00	**0.16**	0.13	0.01

Further analysis of the innovation series and the minimum detectable biases of the 5m Katoomba DEM indicates that only one outlier in the 5m DEM was not detected and removed. The innovation series is 3.81m, which is less than the corresponding minimum detectable value, i.e. 3.94m. This point is located at the 5th column and 122nd row of the data, or $X = 5$ and $Y = 122$ of the $\mathbf{S}_1^+$ orientation in Figure 7-4, which is close to the left boundary. Its effect on the estimates of elevation is 2.26m, and 0.13 for the X and Y derivatives.

It can be concluded that the method of outlier detection and removal applied in the 2-D Kalman filtering algorithm is capable of detecting erroneous observations from a complex terrain surface, like the Katoomba data, with a high degree of reliability.

7.4.2 Outlier detection and removal in the 2-D Kalman smoothing process

If the 2-D Kalman smoother is applied to a DEM data, the outliers would be detected and removed four times. The results of the 2-D Kalman smoothing process would be the mean values of the four filtering results, weighted by the relevant variance covariance factors.

This can be examined in the results of the 5m Katoomba DEM. The original outliers of the 5m Katoomba DEM are plotted in Figure 7-12(a), in which the vertical axis represents the magnitude of outliers and the horizontal axis represents the number of outliers. The results of outlier detection and removal of the 2-D Kalman smoothing are plotted in Figure 7-12(b), in which the vertical axis represents the errors remained in the estimates of the outliers compared with the relevant ground truth, and the horizontal axis is the same as Figure 7-12(b). Similarly, the errors remained in the results of each of the four Kalman filtering processes are plotted in Figure 7-12(c), (d), (e) and (f).

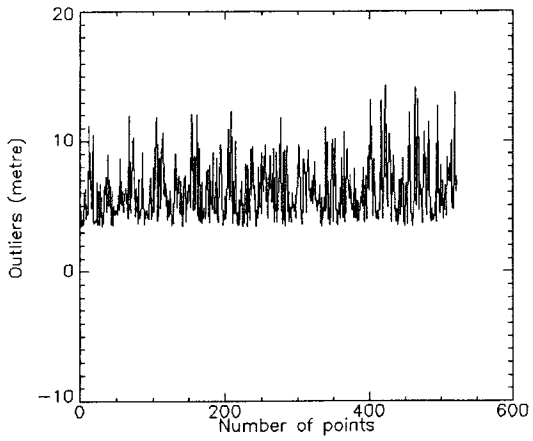

Figure 7-12(a) Original outliers

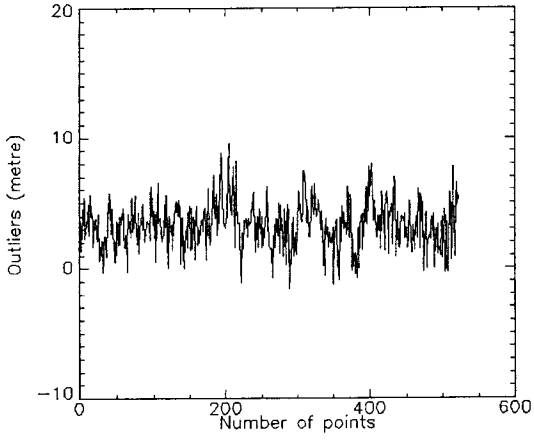

Figure 7-12(b) Smoothing result

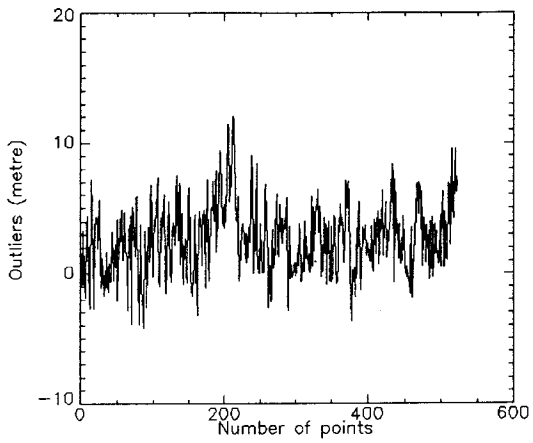

Figure 7-12(c) Filtering #1 result

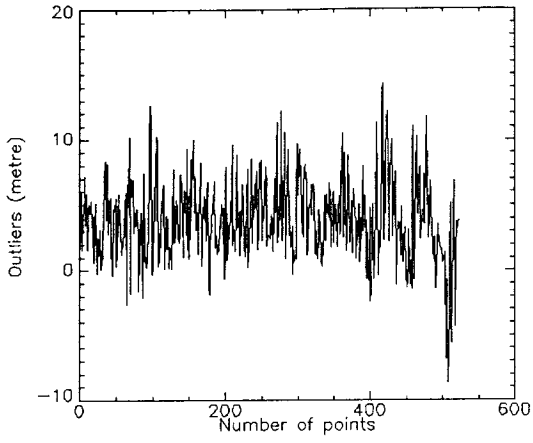

Figure 7-12(d) Filtering #2 result

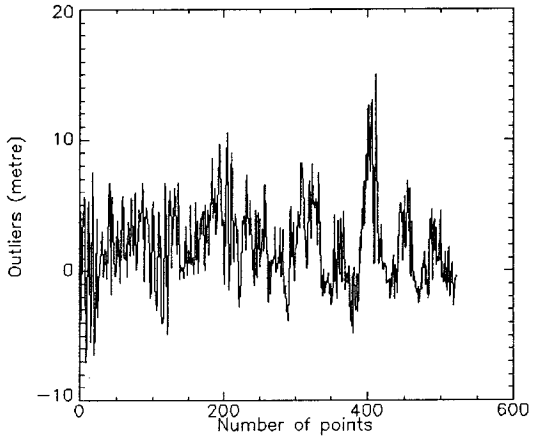

Figure 7-12(e) Filtering #3 result

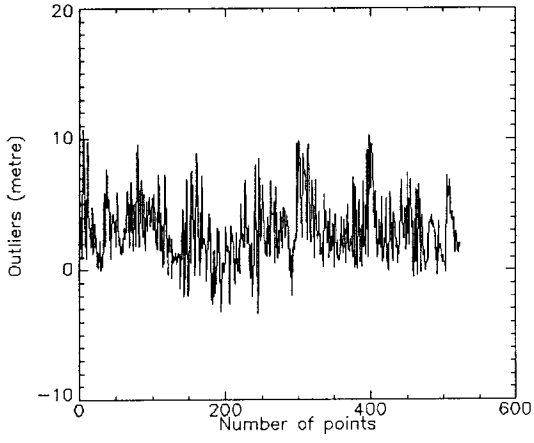

Figure 7-12(f) Filtering #4 result

Figure 7-12 Outlier detection and removal using the 2-D Kalman smoother and the 5m Katoomba DEM

The significant statistics of outlier detection and removal of the 2-D Kalman smoothing of the 5m Katoomba DEM are shown in Table 7-5. The improvement of the outlier detection and removal shown in the Table is evaluated in the mean value of the errors remained in the filtering/smoothing results compared with those of the original magnitude of the outliers in the 5m Katoomba DEM. The efficiency of outlier detection and removal is validated in the four filtering processes, and the best result was produced in the computation $\mathbf{S}_3^+$. This is probably because that the filter started with good

boundary conditions, compared with other three orientations, and therefore, produced more accurate predicted estimates of elevation at the positions where the outliers occur.

The overall efficiency of outlier detection and removal of the 2-D Kalman smoother is significant. The mean magnitude of the outliers had been reduced to nearly half of its original value, i.e. from 6.16m to 3.35m, and the improvement is about 46%, after applying the 2-D Kalman smoothing process (see Table 7-5).

Table 7-5 Efficiency of outlier detection and removal using the 2-D Kalman smoother on the 5m Katoomba DEM

(unit in metres)

	Mini value	Maxi value	Mean value	Standard deviation	Improve-ment
Outliers in 5m DEM	3.50	14.29	**6.16**	2.21	---
Errors remained in process #1	-4.20	12.04	**2.56**	2.85	**58%**
Errors remained in process #2	-8.70	14.26	**3.84**	3.07	**38%**
Errors remained in process #3	-7.07	15.00	**1.94**	3.23	**69%**
Errors remained in process #4	-3.40	10.70	**3.00**	2.51	**51%**
Errors remained in smoothing results	-1.60	9.56	**3.35**	1.79	**46%**

7.4.3 Efficiency of detecting and removing outliers of different magnitudes using the 2-D Kalman smoothing process

The power of the test is different for outliers with different magnitudes with a given critical value. It is expected that the taller the trees, the more powerful will be the test for detection and removal in the 2-D Kalman smoothing process. The isolated trees were separated into two groups based on their heights, i.e. 3.5 to 7m (see Figure 7-13(a)) and greater than 7m (see Figure 7-13(c)). After applying the 2-D Kalman smoother, the differences between the estimates of the elevation and the relevant ground

truth of outliers in each group were measured and displayed in Figure 7-13(b) and (d), where the vertical axis of Fig 7-13(b) and (d) represent these differences, while the vertical axis of Fig 7-13(a) and (c) represent the original magnitudes of the outliers. The magnitude of Figure 7-13(d) is significantly shifted closer to zero, compared to that of Figure 7-13 (b). This indicates a greater capability for outlier detection and removal by the 2-D Kalman filtering algorithm. The 2-D Kalman filtering algorithm reduced the mean value of the outliers greater than 7m from 9.00m to 4.13m, and from 4.98m to 3.02m for the outliers less than 7m. The improvement, evaluated in terms of mean value, is about 54% for the 7m over outlier group, and 39% for the 7m less outlier group.

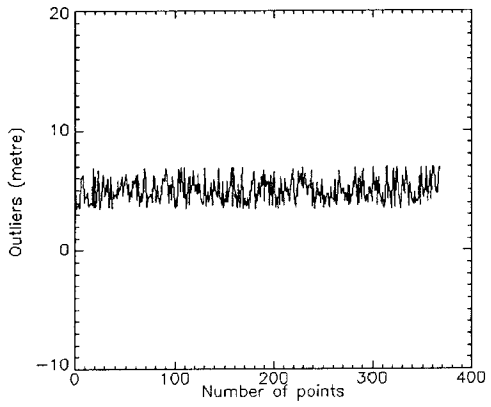

(a) 3.5m <= outlier <= 7.0m

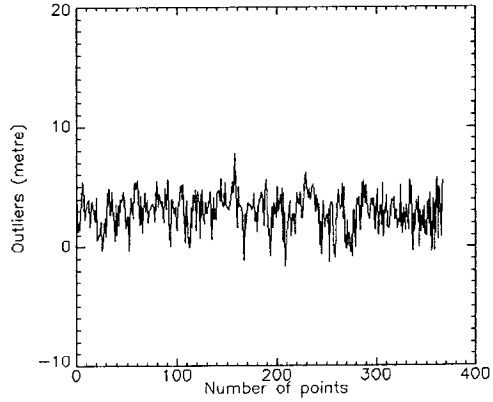

(b) 2-D Kalman smoothing result

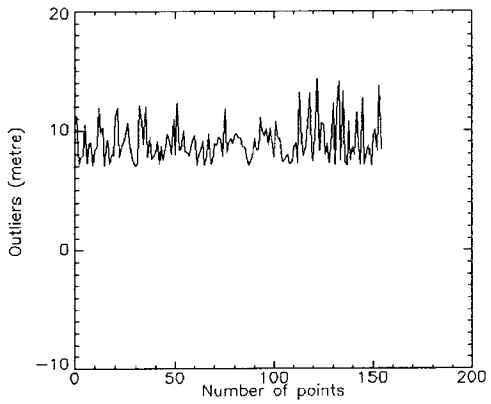

(c) outlier > 7m

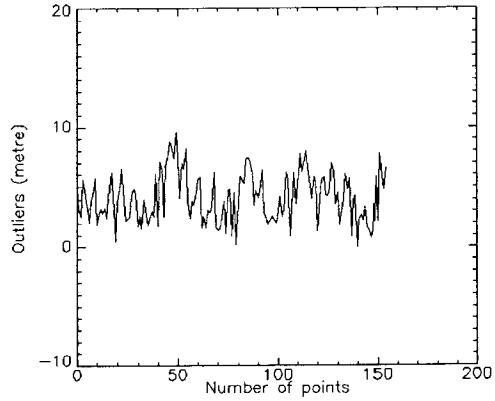

(d) 2-D Kalman smoothing result

Figure 7-13 Efficiency of outlier detection and removal of the 2-D Kalman filtering algorithm with different magnitudes of outliers using 5m Katoomba DEM ($\xi_\alpha = 2$)

Table 7-6 Comparing efficiency of outlier detection and removal with different outlier magnitudes of the 5m Katoomba DEM ($\xi_\alpha = 2$)

(unit in metres)

	Number of outliers	Mini value	Maxi value	Mean value	Standard deviation	Improve-ment
3.5 <= Outlier <= 7m	368	3.50	7.00	**4.98**	1.01	---
Errors in detection and removal	368	-1.60	7.80	**3.02**	1.59	**39%**
Outlier > 7m	155	7.01	14.29	**9.00**	1.65	**--**
Errors in detection and removal	155	-0.03	9.56	**4.13**	2.03	**54%**

7.4.4 Effect of DEM resolution on outlier detection and removal

The size of the canopy of the isolated trees found in the Katoomba mapping area varies from 5m by 5m to 20m by 20m. Due to the use of two DEM resolutions, the number of the outliers in the 5m and 10 Katoomba DEM are different, and the efficiency for outlier detection and removal is affected.

Comparing the results of the 5m and 10m Katoomba DEM derived by the 2-D Kalman smoothing process, the outliers in the 5m DEM were more efficiently detected and removed (see Figure 7-13 and Table 7-7) than those in the 10m DEM. The mean value of the errors remaining in the Kalman smoothing result for the 5m DEM is 3.35m, which is a reduction of about 46% in the mean value of the original outliers in the DEM. However, the errors remaining in the Kalman smoothing result for the 10m DEM have a mean value of 5.01m, which shows that the mean value of the outliers in the 10m DEM was reduced by only about 18% by the 2-D Kalman smoothing algorithm.

Table 7-7 Comparison of the results of outlier detection and removal using 5m and 10m Katoomba DEMs and the 2-D Kalman smoother

(unit in metres)

	Minimum value	Maximum value	Mean value	Standard deviation
Outliers in 5m DEM	3.50	14.29	**6.16**	2.21
Errors in 5m Kalman smoothing results	-1.60	9.56	**3.35**	1.79
Outliers in 10m DEM	3.51	3.26	**6.10**	2.11
Errors in 10m Kalman smoothing result	-2.58	10.28	**5.01**	2.03

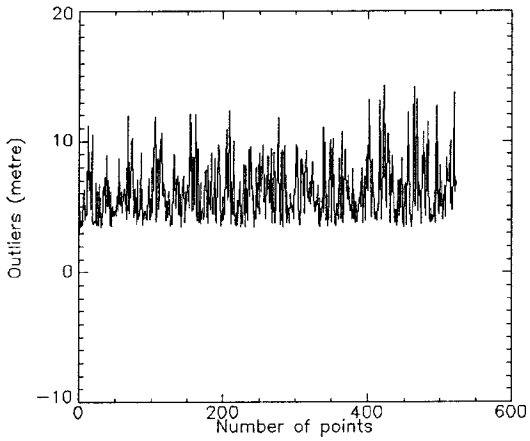

(a) Outliers in 5m Katoomba DEM

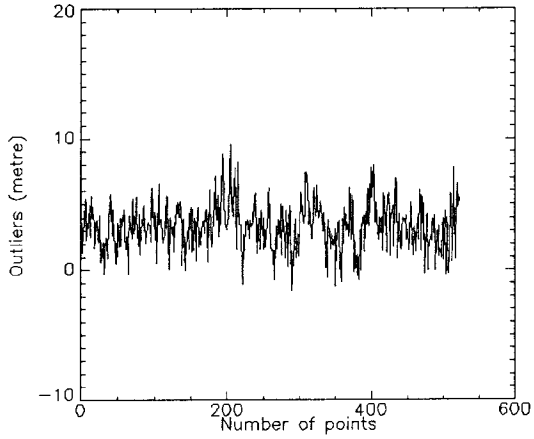

(b) Smoothing result of 5m DEM

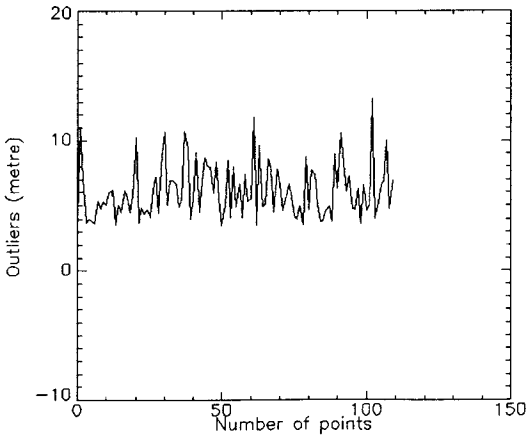

(c) Outliers in 10m Katoomba DEM

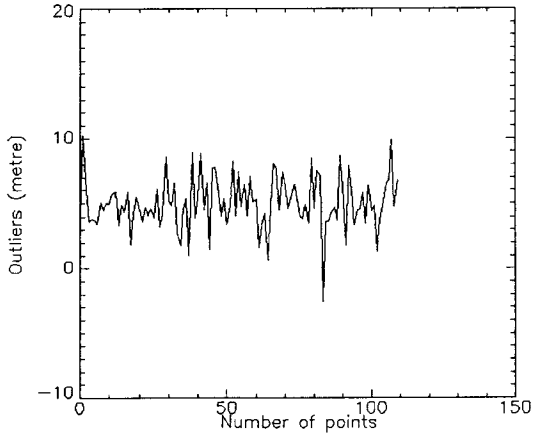

(d) Smoothing result of 10m DEM

Figure 7-13 Comparison of the results of the outlier detection and removal derived by the 2-D Kalman smoother on the 5m and 10m DEMs

It is necessary to mention that the ground truth used in this Section to evaluate the accuracy of outlier detection and removal of the 2-D Kalman filtering algorithm was derived by digital photogrammetrical method using the Helava software (Version 4.0.8). Initially, the isolated trees in the mapping area were manually checked on the stereo model to determine their size and height. Since there were too many outliers in 5m resolution DEM, the function of 'Eliminate trees/buildings' of the Helava software was used on the 5m Katoomba DEM to remove the effects of the isolated trees, which were defined as being taller than 3.5m and covering an area of 20m by 20m. Comparing the elevation differences between the Helava software smoothed 5m DEM and the original 5m DEM, those points with elevation differences greater than 3.5m were the isolated trees. The ground truth of each outlier is assumed to be the smoothed results obtained by the function 'Eliminate trees/buildings' of the Helava software. This was the only practical way of identifying all outliers in a DEM when the size and the height of the outliers are known. Therefore, the accuracy of ground truth data is dependent on the quality of the function of 'Eliminate trees/buildings' of the Helava software. The comparisons in this Section indicate that the mean value of the errors remaining after the outlier detection and removal of the 2-D Kalman filtering and smoothing are not as good as the results shown in Chapter 5 based on the artificial data, where they are so close to zero. In this respect, it is suggested that further study of the accuracy of 'Eliminate trees/buildings' function in the software be undertaken in the future, or use of another method to obtain the ground truth of the outliers.

7.5 Results of the 2-D Kalman Filter and 2-D Kalman Smoother

In Section 7.4.2 the results of outlier detection and removal derived by the 2-D Kalman filter and smoother were compared and analysed. In this Section, the estimates of terrain variables derived by the 2-D Kalman filter and smoother will be further examined to investigate the improvement in DEM random noise reduction by using the 2-D Kalman smoother.

The results of the 2-D Kalman filter and smoother on the 10m Katoomba DEM were compared. The Kalman smoothing results of the 5m Katoomba DEM were used as ground truth in the comparison. Comparing with the ground truth data, the errors in the

estimates of terrain variables derived by the 2-D Kalman filter and smoother on the 10m Katoomba DEM were measured and are summarized in Table 7-8. The errors in the estimates derived by the 2-D Kalman filter are the same as those listed in Table 7-1. The comparison shows that the results of the 2-D Kalman smoother reduces by 11% of the standard deviation for the estimates of elevation, and 33% for the estimates of the X and Y derivatives, compared with the results of the 2-D Kalman filter. The 2-D Kalman smoother also further reduces the effect DEM random noise on the calculation of slope surface, and improves by 33% in terms of standard deviation. Though the accuracy of the X and Y derivatives of the DEM had been considerably increased by the 2-D Kalman smoother, the improvement of DEM random noise reduction in the aspect computation is only about 4%. This is probably due to the complex pattern of the aspect surface in the mapping area.

Table 7-8 **Comparison of errors remaining in the estimates of terrain variables derived by the 2-D Kalman filter and smoother on the 10m Katoomba DEM**

	Mini value	Maxi value	Mean value	Standard deviation	Improve-ment
Elevation (m)					
Kalman filtering	-6.30	8.09	-0.01	**0.37**	---
Kalman smoothing	-4.78	6.40	0.00	**0.33m**	**11%**
X derivative					
Kalman filtering	-0.21	0.29	0.01	**0.03**	---
Kalman smoothing	-0.22	0.25	0.00	**0.02**	**33%**
Y derivative					
Kalman filtering	-0.27	0.26	0.01	**0.03**	---
Kalman smoothing	-0.27	0.24	0.00	**0.02**	**33%**
Slope (radians)					
Kalman filtering	-0.22	0.28	0.02	**0.03**	---
Kalman smoothing	-0.24	0.20	0.00	**0.02**	**33%**
Aspect (radians)					
Kalman filtering	-3.29	3.28	0.12	**0.85**	---
Kalman smoothing	-3.30	3.30	-0.01	**0.82**	**4%**

7.6 Conclusions

In this Chapter, some experimental results of applying 2-D Kalman filtering algorithm to DEMs derived from a real terrain surface are introduced. The DEM data used in this testing, generated by digital photogrammetric methods, covers approximately 1.3km by 1.1km of rugged terrain in the Katoomba area, New South Wales.

The results of the 2-D Kalman filtering algorithm on the Katoomba DEMs were examined from two respects: DEM outlier detection and removal, and DEM random noise reduction.

Outliers in the test data refer to the effects on elevation caused by isolated trees in the mapping area. Using photogrammetric methods, the elevation of isolated trees can be observed, and the relevant ground truth established. The method of outlier detection and removal developed in the 2-D Kalman filtering algorithm was investigated in terms of the reliability of outlier detection and removal, the effect of DEM resolution and outlier magnitude, and efficiency of the 2-D Kalman filter and Kalman smoother. The relevant results indicate that the method has a high level of reliability over rough and complex terrain surfaces. Only one outlier, which is located close to the boundary area, had not been detected by the method. The impact of this undetected outlier is 2.26m for the estimate of elevation, 0.13 for the estimates of X and Y derivatives. The experiments also indicate that the efficiency of outlier detection and removal is different for outliers with different magnitude. The results also demenstrated the impact of the DEM resolution on outlier detection and removal. Outliers can be more efficiently detected and removed in a denser resolution DEM, such as 5m Katoomba DEM, than those in a coarser DEM, such as the 10m Katoomba DEM, derived for the same mapping area.

The efficiency in DEM random noise reduction of the 2-D Kalman filtering algorithm was examined in two ways. One was to investigate the improvement of the 2-D Kalman filter, compared with the Evans method, in terms of DEM random noise reduction. The other was to further compare the accuracy of the 2-D Kalman smoothing process with the 2-D Kalman filter to investigate the improvement of the 2-D Kalman smoother over the 2-D Kalman filter. The Kalman smoothing results of the 5m Katoomba DEM were used as the bases for these comparisons. Compared with the Evans method, the 2-D Kalman filter is more efficient in reducing DEM random noise, and therefore produces better estimates of terrain variables over the same DEM data. The accuracy of the Evans method can be improved more than 70% for X and Y derivative, 50% for slope and 20% for aspect using the 2-D Kalman filter on the 10m Katoomba DEM. The comparison between the 2-D Kalman filtering and smoothing process indicates that, using the 2-D Kalman smoother, the accuracy of the terrain attributes can be further

improved more than 10% for elevation, 30% for X and Y derivatives, 30% for slope and about 4% for aspect over the 10m Katoomba DEM.

CHAPTER 8

CONCLUSIONS

8.1 Summary

In this thesis, the development of 2-D Kalman filtering algorithm for terrain surface modelling using grid DEMs is presented. The aim of the study was to improve the accuracy of the derivation of terrain topographic attributes from DEMs by reducing the effect of DEM random noise, and detecting and removing the effect of DEM outliers. This method can be used for GIS applications, which require accurate terrain topographic attributes that can be directly derived from a grid DEM. It can be used for analysis of:

- Vegetation type and distribution
- Potential energy
- Solar radiation
- Overland and subsurface flow velocity and runoff rate
- Soil erosion rates
- Soil properties
- Flow acceleration
- Drainage network
- Soil water content and surface saturation zones
- Precipitation
- Climate, etc.

The aims and objectives of this research have been achieved in the following respects:

- The stochastic terrain models were developed in this study based on terrain geometry and the relevant terrain modelling assumptions. The characteristics and the performances of the stochastic terrain models, over simulated and real DEM data, were investigated.

- All observations of a DEM data can be used to derive estimations of terrain variables in the 2-D Kalman smoother. Therefore, the efficiency of reducing the effect of DEM random noise has been greatly improved, compared with the current terrain modelling methods.

- The method for DEM outlier detection and removal was developed, based on the application of the 2-D Kalman filter, and detection theory. The reliability of outlier detection was also fully investigated. Some important aspects, such as the effect of terrain roughness and DEM resolution on the outlier detection and removal were further addressed.

- The developed 2-D Kalman filter is a recursive modelling process with significant computational efficiency, especially for the application of terrain surface modelling using grid DEMs.

- The developed 2-D Kalman smoother was also developed in the research. Therefore, the efficiency of reducing DEM random noise is further improved.

8.2 Conclusions

The following conclusions can be derived from this study:

- **Using linear differential relationships of the terrain attributes between the adjacent DEM points**

The stochastic models used in this study, which are two linear differential equations monitoring the terrain attributes between the adjacent DEM points, are the bases for establishing the dynamic models of the 2-D Kalman filter. They define the relevant assumptions about the characteristics of terrain topography. The linear differential relationships used in the current form only include the three most important terrain variables, i.e. elevation and two first partial derivatives of elevation. However, it is straightforward to include the estimates of more terrain variables, such as the two second order partial derivatives of elevation, and based on them, to calculate profile and plan curvatures of a DEM.

The experiments on the DEMs derived from Katoomba area, New South Wales show that the efficiency of DEM random noise reduction is significant when using the stochastic terrain models in the 2-D Kalman filter, compared with the results for other terrain methods, i.e. the Evans method, which use deterministic terrain models. The 2-D Kalman filter leads to an improvement in the accuracy of the first derivatives of terrain, slope and aspect, compared with the Evans method of more than 70% for X and Y derivatives, 50% for slope and 20% for aspect on the same 10m Katoomba DEM.

- **Integrating the predictions derived from the two orthogonal directions of the DEM to make it a Kalman filter in two dimensions**

The prediction of elevations from two orthogonal directions is the particular strategy applied in the Kalman recursive process that makes it successful for processing the 2-D DEM data. The strategy combines two predicted estimates derived from the orthogonal directions of the DEM, weighted by their variance-covariance matrices to produce $\mathbf{S}^-$ and the associated variance-covariance matrix $\mathbf{P}^-$. Therefore, the 2-D Kalman recursive process consists of nine equations rather than the conventional five equations.

- **Using differences between the predicted estimates of elevation and the relevant observations to detect DEM outliers**

In this thesis, the innovation series, which are the dispersions between the predicted estimates of elevation and the relevant observations of a DEM, were applied as a test statistic for outlier detection and removal. The internal reliability of outlier detection, in terms of minimum detectable bias, relates to the level of confidence of the detection, i.e. the critical value used in the detection, according to the binary hypothesis testing and the Neyman-Pearson strategy. The external reliability of outlier detection, in terms of the maximum effect of undetectable bias, is sensitive to the bias and the Kalman gain.

The experiments on the Katoomba DEMs indicate that the outliers in the Katoomba DEMs were successfully detected and removed with high reliability. A total of 523 outliers in the 5m Katoomba DEM were efficiently detected and removed by the developed method. Only one outlier in the DEM, which is close to the boundary area, was not detected by the method. The effect of the undetectable bias in the estimates of

terrain attributes is only about 2.26m for the elevation, and 0.13 for the X and Y derivatives. The mean value of the outliers in the 5m grid DEM were reduced from 6.16m to 3.35m using the 2-D Kalman smoothing process, which is about 56% of its original value. Due to the use of the coarser DEM resolution, outliers in the 10m Katoomba DEM were less efficiently detected and removed compared with those in the 5m Katoomba DEM. The mean magnitude of the outliers was reduced from 6.10m to 5.01m in the 10m Katoomba DEM by the 2-D Kalman smoothing process, which is only about 21% of its original value.

- **Smoothing a DEM by applying four times Kalman filtering processes with different orientations**

The developed 2-D Kalman smoothing algorithm applies the 2-D Kalman filter four times on a DEM with different orientations. The resulting four filtering results are assumed independent, for they are derived from the different filtering processes using different filtering information. The estimates of the terrain variables derived from the 2-D Kalman smoothing algorithm are a linear integration of the relevant four filtering estimates, weighted by their variance covariance matrices. The experiments over the Katoomba DEM show that, comparing with the results of the 2-D Kalman filter, the 2-D Kalman smoother can further improve the accuracy of the derivation of terrain attributes, by more than 10% for elevation, 30% for X and Y derivatives, 30% for slope and about 4% for aspect calculation over the 10m Katoomba DEM.

- **Terrain characteristics (roughness, breaklines, etc.) and DEM resolution may affect the determination of filtering parameters**

The model errors represent the accuracy of the predictions of the relevant estimates of terrain variables of a DEM point from its adjacent neighbours, which are affected by terrain roughness, breaklines and DEM resolution. Generally, over dense DEM data, which are derived from smooth terrain surfaces, the model errors are mainly a function of the DEM resolution and the second order of partial derivatives of elevation of the terrain surface. If the DEM is derived from a rough and complex terrain surface with many breaklines, the choice of the suitable model errors may be less effective, and therefore adaptive Kalman filtering techniques should be further developed.

8.3 Limitations and Recommendations for Future Studies

While significant achievements have been made with the 2-D Kalman filtering algorithm, further future studies are also recommended.

- **Integration of knowledge to more accurately model terrain topographic characteristics**

The limitations of the terrain surface modelling technique arise from insufficient understanding of terrain topographic characteristics in discretely grid DEMs. The stochastic terrain models in the 2-D Kalman filtering algorithm are based on a limited set of geometric characteristics of terrain. The application of additional terrain characteristics, such as hydrographic, biological and geomorphological characteristics of the landscape, may also influence the modelling of terrain topographical attributes, and therefore, should be considered in the establishment of the terrain models.

- **Developing adaptive 2-D Kalman filter**

Terrain roughness and irregularity may affect the implementation of the 2-D Kalman filtering algorithm, and the quality of the results. The current algorithm for 2-D Kalman filtering uses pre-fixed parameters to process a DEM, and is not able to adapt to the change of terrain characteristics in the DEM. An adaptive 2-D Kalman filter is suggested in future developments of the algorithm to make it adaptive to different terrain and landscape contents.

- **Modelling more terrain variables**

The current 2-D Kalman filtering algorithm only estimates the three most important terrain attributes, i.e. elevation, and the two first order of partial derivatives of elevation. It is straightforward to extend the dynamic model to include more terrain attributes, such as second order of the partial derivatives of elevation and the associated profile and plan curvatures.

- **Exploring the 2-D Kalman filtering algorithm on more DEM data**

Finally, more experiments are suggested to test the 2-D Kalman filtering algorithm on different landscape with different DEM resolutions. The results would be helpful for improving the flexibility of the 2-D Kalman filtering algorithm for modelling different types of terrain surfaces.

REFERENCES

Ackermann, F., 1978: Experimental Investigation into the Accuracy of Contouring from DTM, Photogrammetric Engineering and Remote Sensing, 44(12), pp1537-1548.

Ackermann, F., 1994: Digital Elevation Models - Techniques and Application, Quality Standards, Development, International Archives of Photogrammetry and Remote Sensing, 30, Part 4, pp421-432.

Al-garnl, A. M., 1995: The Forth Dimension in Digital Photogrammetry (DP), Photogrammetric Engineering and Remote Sensing, 61(1), pp57-62

Ayeni, O. O. 1982: Optimum Sampling for Digital Terrain Models: A Trend Towards Automation, Photogrammetric Engineering and Remote Sensing, 48(11), pp1687-1694.

Azimi-Sadjadi, M. R. and P. W. Wong, 1987: Two-Dimensional Block Kalman Filtering for Image Restoration, IEEE Transactions on Acoustic, Speech, and Signal Processing, ASSP-35(12), pp1736-1749.

Balce, A. E. 1987: Determination of Optimum Sampling Interval in Grid Digital Elevation Models (DEM) Data Acquisition, Photogrammetric Engineering and Remote Sensing, 53(3), pp323-330.

Bacher, U., 1998: Experimental Studies into Automated DTM Generation on the DPW770, International Archives of Photogrammetry and Remote Sensing, 32, Part 4, pp35-41.

Baltsavias, E. P., 1991: Multiphoto Geometrically Constrained Matching, Institut für Geodäsie und Photogrammetrie an der Eidgenössischen Technischen Hochschule Zürich, Mitteilungen Nr. 49.

Baltsavias, E. P. and C. Käser, 1998: DTM and Ortherimage Generation – a Thorough Analysis and Comparison of Four Digital Photgrammetric Systems, International Archives of Photogrammetry and Remote Sensing, 32, Part 4, pp42-51.

Band, L., 1986: Topographic Partition of Watershed with Digital Elevation Models, Water Resources Research, 22(1), pp15-24.

Band, L. E., R. Vertessy and R. Lammers, 1995: The Effect of Different Terrain Representations and Resolution on Simulated Watershed Processes, Advances in Geomorphometry – Proceedings of the Walter F. Wood Memorial Symposium, ISBN 3-443-21101-1, pp187-199.

Beasley, D.B. and L. F. Huggins, 1982: ANSWERS (Areal Nonpoint Source Watershed Environmental Response Simulation): User's Manual. U.S. EPA-905/9-82-001. Chicago, IL.

Blaszczynski, J. S., 1997: Landform Characterization with Geographical Information Systems, Photogrammetric Engineering and Remote Sensing, 63(2), pp183-191.

Bolstad, P. V. and T. Stowe, 1994: An Evaluation of DEM Accuracy: Elevation, Slope, and Aspect, Photogrammetric Engineering and Remote Sensing, 60(11), pp1327-1332.

Brändli, M, 1996: Chapter 7 Hierarchical Models for the Definition and Extraction of Terrain Features, In: Geographic Objects with Indeterminate Boundaries edited by P. A. Burrough and A. U. Frank, London: Taylor and Francis, ISBN 0-7484-0386-8, pp257-270.

Briggs, I. C., 1973: Machine Contouring Using Minimum Curvature, Geophysics, 39(1), pp39-48.

Brown, D. G. and T. J. Bara, 1994: Recognition and Reduction of Systematic Error in Elevation and Derivative Surfaces From 71/2-Minute DEMs, Photogrammetric Engineering and Remote Sensing, 60(2), pp189-194.

Brown, R. G. and P. Y. C. Hwang, 1992: Introduction to Random Signals and Applied Kalman Filtering (Second Edition), New York: John Wiley and Sons, INC., ISBN 0471-52573-1, p230-236, p259-261, p278-281, p288, p330-332, p342-349.

Burrough, P. A. and R. A. McDonnell, 1998: Principles of Geographical Information Systems, Oxford University Press, ISBN 0-19-823366-3, pp98-161, pp190.

Cao, C. and N. S. Lam, 1997: Understanding the Scale and Resolution Effects in Remote Sensing and GIS, In: Scale in Remote Sensing and GIS edited by D. A. Quattrochi and M. F. Goodchild, Boca Raton, Fla.: Lewis Publishers, ISBN 1-56670-104-X, pp57-72.

Carter, J. R., 1988: Digital Representations of Topographic Surfaces, Photogrammetric Engineering and Remote Sensing, 54(11), pp1577-1580.

Caspary, W. F., 1988: Concepts of Network and Deformation Analysis, Monograph 11, School of Surveying, University of New South Wales, Australia, pp85-96.

Chang, K. and B. Tsai, 1991: The Effect of DEM Resolution on Slope and Aspect Mapping, Cartography and Geographic Information Systems, 18(1), pp69-77.

Chorowicz, J., C. Ichoku, S. Riazanoff, Y. Kim and B. Cervelle, 1992: A Combined Algorithm for Automated Drainage Network Extraction, Water Resources Research, 28(5), pp1293-1302.

Crosetto, M. and B. Crippa, 1998: Optical and Radar Data Fusion for DEM Generation, International Archives of Photogrammetry and Remote Sensing, 32, Part 4, pp128-134.

Doyle, F., 1978: Digital Terrain Models: An Overview, Photogrammetric Engineering and Remote Sensing, 44(12), pp1481-1485.

Dozier, J. and A. H. Strahler, 1983: Ground Investigations in Support of Remote Sensing, In: Manual of Remote Sensing edited by R. N. Colwell, Falls Church, Virginia: American Sociaty of Photogrammetry.

Evans, I. S., 1972: General Geomorphometry, Derivative of Altitude, and Descriptive Statistics, In: Spatial Analysis in Geomorphology edited by R. J. Chorley, London: Methuen, ISBN 0416660703, pp22.

Evans, I. S., 1980: An Integrated System of Terrain Analysis and Slope Mapping. Zeitschrift für Geomorphologie, 36, pp274-295.

Faust, N. L., 1987: Automatic Data Capture for Geographic Information Systems: A Commentary, Photogrammetric Engineering and Remote Sensing, 53(10), pp1389-1390.

Florinsky, I. V., 1998: Accuracy of Local Topographic Variables Derived from Digital Elevation Models. International Journal of Geographical Information Science 12(1), pp47-61.

Förstner, W., 1981: Reliability and Discernability of Extended Gauss-Markov Models, Proceeding of Working Group III/1 of ISP Seminar on Mathematical Models of Geodetic/Photogrammetric Point Determination with Regard to Outliers and Systematic Errors, Stuttgart, Nov. 26-27, 1981, pp79-104.

Fraser, D. C. and J. E. Potter, 1969: The Optimum Linear Smoother as a Combination of Two Optimum Linear Filters, IEEE Transaction on Auto Control, AC-14(4), p387.

Freeman, T. G., 1991: Calculating Catchment Area with Divergent Flow Based on a Regular Grid, Computers and Geosciences, 17(3), pp413-422.

Garbrecht, J. and P. Starks, 1995: Note on the Use of USGE Level 1 7.5-Minute DEM Coverage for Landscape Drainage Analyses, Photogrammetric Engineering and Remote Sensing, 61(5), pp519-522.

Giles, P. T. and P. E. Franklin, 1996: Comparison of Derivative Topographic Surfaces of a DEM Generated from Stereoscopic SPOT Images with Field Measurements, Photogrammetric Engineering and Remote Sensing, 62(10), pp1165-1171.

Guth, P. L., 1995: Slope and Aspect Calculations on Grided Digital Elevation Models: Examples from a Geomorphometric Toolbox for Personal Computers. Advances in Geomorphometry - Proceedings of the Walter F. Wood Memorial Symposium, ISBN 3-443-21101-1, pp31-52.

Haralick, R., 1983: Ridges and Valleys on Digital Images, Computer Vision, Graphics, and Image Processing, 22, pp28-38.

Hawkins, D. H., 1980: Identification of Outliers, London; New York: Chapman and Hall, ISBN 0-412-21900-X, pp1-12.

Heerdegen, R. G. and M. A. Beran, 1982: Quantifying Source Areas Through Land Surface Curvature and Shape, Journal of Hydrology, 57(4), pp359-373.

Heipke, C. 1993: State-of-the-Art of Digital Photogrammetric Workstations for Topographic Applications, Integrating Photogrammetric Techniques with Scan Analysis and Machine Vision, SPIE Vol.1944, pp210-222.

Hodgson, M. E., 1995: What Cell Size Does the Computed Slope/Aspect Angle Represent? Photogrammetric Engineering and Remote Sensing, 61(5), pp513-517.

Holmgren, P, 1994: Multiple Flow Direction Algorithms for Runoff Modelling in Grid Based Elevation Models: an Empirical Evaluation, Hydrological Processes, 8, pp327-334.

Horn, B. K. P., 1981: Hill Shading and the Reflectance Map. Proceedings of the Institute of Elcctrical and Elcctronics Engineers, 69, pp14-47.

Hunter, G. J., and M. F. Goodchild 1997: Modeling the Uncertainty of Slope and Aspect Estimates Derived from Spatial Databases, Geographical Analysis, 29(1), pp35-49.

Huss, R. E. and M. A. Pumar, 1997: Effects of Database Errors on Intervisibility Estimation, Photogrammetric Engineering and Remote Sensing, 63(4), pp415-424.

Hutchinson, M. F., 1984: A Summery of Some Surface Fitting and Contouring Programs for Noisy Data, Consulting Report No. ACT 84/6, CSIRO Division of Mathematics and Statistics and Division of Water and Land resources.

Hutchinson, M. F., 1989: A New Procedure for Gridding Elevation and Stream Line Data with Automatic Removal of Spurious Pits, Journal of Hydrology, 106, pp211-232.

Kalman, R. E., 1960: A New Approach to Linear Filtering and Prediction Problems, ASME Journal of Basic Engineering, 82D, pp35-45.

Kalmar, J., G. Papp and T. Szabo, 1995: DTM-Based Surface and Volume Approximation, Geophysical Applications, Computers and Geosciences, 21(2), pp245-257.

Klinkenberg, B., 1988: Tests of Fractal Model of Topography, Ph.D. Dissertation, University of Western Ontario, Canada.

Kraus, K., and E. M. Mikhail, 1972: Linear Least-Squares Interpolation, Twelfth Congress of the International Society of Photogrammetry, Commission III, pp1016-1021.

Kraus, K., 1994: Visualization of the Quality of Surfaces and Their Derivatives, Photogrammetric Engineering and Remote Sensing, 60(4), pp457-462.

Kraus, K. and N. Pfeifer, 1998: Determination of Terrain Models in Wooded Areas with Airborne Laser Scanner Data, ISPRS Journal of Photogrammetry and Remote Sensing, 53, pp193-203.

Kubik, K. and A. G. Botman, 1976: Interpolation Accuracy for Topographic and Geological Surfaces, ITC Journal, 4, pp236-273.

Kubik, K., 1985: Report 2 Recommended Procedure for Data Capture and Processing, from Digital Elevation Model Data Base for Queensland (Internal Report).

Lam, N. S., 1983: Spatial Interpolation Methods: A Review, The American Cartographer, 10(2), pp129-149.

Lammers, R. B. and L. Band, 1990: Automatic Object Representation of Drainage Basins, Computers and Geosciences, 16(6), pp787-810.

Lapen, D. R. and L. Martz, 1993: The Measurement of Two Simple Topographic Indices of Wind Sheltering-Exposure from Raster Digital Elevation Models, Computers and Geosciences, 19(6), pp769-779.

Lee, J., 1994: Digital Analysis of Viewshed Inclusion and Topographic Features on Digital Elevation Models, Photogrammetric Engineering and Remote Sensing, 60(4), pp451-456.

Lee, J., P. K. Snyder and P. F. Fisher, 1992: Modeling the Effect of Data Errors on Feature Extraction from Digital Elevation Models, Photogrammetric Engineering and Remote Sensing, 58(10), pp1461-1467.

Li, Z., 1994: A Comparative Study of the Accuracy of Digital Terrain Models (DTMs) Based on Various Data Models, ISPRS Journal of Photogrammetry and Remote Sensing, 49(1), pp2-11.

Madani, M., 1993: How a Digital Photogrammetric Workstation is Compared to an Analytical Plotter? The International Society for Optical Engineering, State-of-the-Art Mapping, Orlando, Florida, USA, 13-15 April 1993, SPIE Vol.1943, pp266-276.

Maffini, G., M. Arno and W. Bitterlich, 1989: Observations and Comments on the Generation and Treatment of Error in Digital GIS Data, In: The Accuracy of Spatial Databases edited by M. F. Goodchild and S. Gopal, London: Taylor & Francis, ISBN 0-85066-847-6, pp55-68.

Makarovic, B., 1973: Progressive Sampling for Digital Terrain Models, ITC Journal, 3, pp397-416.

Makarovic, B., 1976: A Digital terrain Model System, ITC Journal, 1, pp57-83.

Makarovic, B., 1977: Composite Sampling for Digital Terrain Models, ITC Journal, 3, pp406-433.

Mark, D., 1984: Automated Detection of Drainage Networks from Digital Elevation Models, Cartographica, 21(2/3), pp168-178.

Martz, L. and E. D. Jong, 1988: Catch: A Fortrain Program for Measuring Catchment Area from Digital Elevation Models, Computers and Geosciences, 14(5), pp627-640.

Martz, L. W. and J. Garbrecht, 1992: Numerical Definition of Drainage Network and Subcathment Areas from Digital Elevation Models, Computers and Geosciences, 18(6), pp747-761.

McDonough, R. N. and A. D. Whalen, 1995: Detection of Signals in Noise (second edition), San Diego: Academic Press, Inc. ISBN 0-12-7448252-7, pp152-166.

Meisels, A., S. Raizman and A. Karniel., 1995: Skeletonising a DEM into a Drainage Network, Computers and Geosciencces, 21(1), pp187-196.

Minkler, G. and J. Minkler, 1993: Theory and Application of Kalman Filtering, Palm Bay, FL.: Magellan Book Company, ISBN 0-9621618-2-9, p41, p.78, pp160-164, p507.

Molnar, L., J. Wintner and B. Wöhrer, 1996: DTM System SCOP in a New Technological Generation, International Archives of Photogrammetry and Remote Sensing, 31, Part B4, pp569-574.

Moore, I. D., R. B. Grayson and A. R. Ladson, 1991: Digital Elevation Modelling: A Review of Hydrological, Geomorphological, and Biological Applications, Hydrological Processes, 5(1), pp3-30.

Moore, I. D., A. K. Turner, J. P. Wilson, S. K. Jenson and L. E. Band, 1993: GIS and Land-Surface-Subsurface Process Modelling, In: Environmental Modelling with GIS edited by M. F. Goodchild, B. O. Parks and L. T. Steyaert, New York: Oxford University Press, ISBN 0-19-508007-6, pp196-230.

Nakano, T., 1984: A Systematics of "Transient Fractals" of Rias Coastlines: an Example of Rias Coast from Kamaishi to Shizugawa, Northeastern Japan, Annual Report of Institute of Geoscience, the University of Tsukuba.

Nery, C. E., R. R. Rangel and L. A. V. Dias, 1994: Digital Elevation Models Interpolated by Linear, Akima and Beta-Spline Methods: A Comparison, International Archives of Photogrammetry and Remote Sensing, Vol. 30, Part 4, pp416-420.

O'Callaghan, J. F. and D. M. Mark, 1984: The Extraction of Drainage Networks from Digital Elevation Data, Computer Vision, Graphics, and Image Processing, 28, pp323-344.

O'Loughlin, E. M., 1986: Prediction of Surface Saturation Zones on Natural Catchments by Topographic Analysis, Water Rcsources Research, 22(5), pp794-804.

Padulo, P. and M. A. Arbib, 1974: System Theory, Philadelphia: W. B Saunders, p21-22.

Papo, H. B. and Gelbman, E., 1984: Digital Terrain Models for Slopes and Curvatures. Photogrammetric Engineering and Remote Sensing, 50(6), pp695-701.

Pennock, D. J., B. J. Zebarth and E. De Jong, 1987: Landform Classification and Soil Distribution in Hummocky Terrain, Saskatchewan, Canada, Geoderma, 40, pp297-315.

Peucker, T. K., 1980: The Impact of Different mathematical Approaches to Contouring, Cartographica, 17(3), pp73-95.

Pike, R. J., 1988: The Geometric Structure: Quantifying Landslide Terrain Types from Digital Elevation Models, Mathematical Geology, 20(5), pp491-511.

Polidori, L. and J. Chorowicz, 1993: Comparison of Bilinear and Brownian Interpolation for Digital Elevation Models, ISPRS Journal of Photogrammetry and Remote Sensing, 48(2), pp18-23.

Qian, J., R. W. Ehrrich and J. Campbell., 1990: DNESYS----an Expert System for Automatic Extraction of Drainage Networks from Digital elevation Data, IEEE Transaction on Geoscience and Remote Sensing, 28(1), pp29-45.

Quinn, P., K. Beven, P. Chevallier and O. Planchon, 1991: The Prediction of Hillslope Flow Paths for Distributed Hydrological Modelling Using Digital Terrain Models, Hydrological Processes, 5, pp59-79.

Rieger, W., 1996: Accuracy of Slope Information Derived from DEM-Data, International Archives of Photogrammetry and Remote Sensing, 31, Part 4, pp690-695.

Ritter, P., 1987: A Vector-based Slope and Aspect Generation Algorithm. Photogrammetric Engineering and Remote Sensing, 53(8), pp1109-1111.

RSMAS, 1995: SAR Interferometry and Surface Change Detection, RSMAS Technical Report TR 95-003, Rosenstiel School of Marine and Atmospheric Science, University of Miami, 97p.

Schut, G. H., 1976: Review of Interpolation Methods for Digital Terrain Models, The Canadian Surveyor, 30(5), pp389-412.

Schwarz, P. G., 1982: A Test of Personal Stereoscopic Measuring Precision, Photogrammetric Engineering and Remote Sensing, 48, pp375-381.

Seemuller, W. W., 1990: The Extraction of Ordered Vector Drainage Networks from Elevation Data, Computer vision, Graphics, and Image Processing, 47, pp45-58.

Shanholtz, V. O., C. J. Desai, N. Zhang, J. W. Kleene and C. D. Metz, 1990: Hydrologic/Water Quality Modelling in a GIS Environment, ASAE Paper 90-3033, St. Joseph, MI.

Sharpnack, D. A. and G. Akin, 1969: An Algorithm for Computing Slope and Aspect from Elevations, Photogrammetric Engineering and Remote Sensing, 35, pp247-248.

Shary, P. A., 1995: Land Surface in Gravity Points Classification by Complete System of Curvatures, Mathematical Geology, 27, pp373-390.

Shear J. C. and J. W. Allen, 1996: Softcopy Photogrammetry and Its Uses in GIS, International Archives of Photogrammetry and Remote Sensing, 31, Part B4, pp70-73.

Sibson, R., 1980: A Brief Description of Natural Neighbour Interpolation, In: Interpreting Multivariate Data edited by B. Barnett, Chichester: Wiley, IBSN 0471280399, pp21-26.

Sircar, J. K. and J. A. Cebrian 1991: An Automated Approach for Labeling Raster Digitized Contour Maps, Photogrammetric Engineering and Remote Sensing, 57(7), pp965-971.

Skidmore, A.K., 1989: A Comparison of Techniques for Calculating Gradient and Aspect from a Grided Digital Elevation Model, International Journal of Geographical Information Systems, 3(4), pp323-334.

Smith, T. R., C. Zhan and P. Gao, 1990: A Knowledge-Based Two Step Procedure for Extraction Channel Networks from Noisy DEM Data, Computers and Geosciences, 16(6), pp777-786.

Srinivasan, R., B. A. Engel, 1991: Effect of Slope Prediction Methods on Slope and Erosion Estimates, Applied Engineering in Agriculture, 7(6), pp779-783.

Tekalp. A. M., H. Kaufman and J. W. Woods, 1989: Edge-Adaptive Kalman Filtering for Image Restoration with Ringing Suppression, IEEE Transactions on Acoustic, Speech, and Signal Processing, 37(6), pp892-899.

Tempfli, K., 1980: Spectral Analysis of Terrain Relief for the Accuracy Estimation of Digital Terrain Models, ITC Journal, 1980-3, pp478-510.

Thapa, K. and J. Bossler, 1992: Accuracy of Spatial Data Used in Geographic Information Systems, Photogrammetric Engineering and Remote Sensing, 58(6), pp835-841.

Theobald, D., 1989: Accuracy and Bias Issues in Surface Representation, In: The Accuracy of Spatial Databases edited by M. F. Goodchild and S. Gopal, London: Taylor & Francis, ISBN 0-85066-847-6, pp99-106.

Todini, E. and M. Ferraresi, 1996: Influence of Parameter Estimation Uncertainty in Kriging, Journal of Hydrology, 175, pp555-566.

Torlegård, K., A. Östman and R. Lindgren, 1986: A Comparative Test of Photogrammetrically Sampled Digital Elevation Models, Photogrammetria, 41, pp1-16.

Travis, M.R., G. H. Elsner, W. D. Iverson, and C. G. Johnson, 1975: VIEWIT: Computation of Seen Areas, Slope, and Aspect for Land-Use Planning. US Department of Agriculture Forest Service General Technical Report PSW-11/1975. Pacific Southwest Forest and Range Experimental Station, Berkeley, CA.

Tribe, A., 1991: Automatic Recognition of Valley Heads from Digital Elevation Models, Earth Surface Processes and Landforms, 16, pp33-49.

Trinder, J. C., 1984: Precision of Stereoscopic Height Measurements, Photogrammetric Engineering and Remote Sensing, 52(1), pp75-79.

Trinder, J. C., B. E. Donnelly, V. K. Shettigara, 1994: A Study of Procedures and Tests on DEM Software For SPOT Images, International Achieves of Photogrammetry and Remote Sensing, 30, Part 4, pp449-456.

Trinder, J. C., 1996: Data Acquisition and Terrain Modelling, Teaching Notes GMAT 9532, School of Geomatic Engineering, University of New South Wales, Australia.

Walsh, S. J., 1989: Users Considerations in Landscape Characterization, In: The Accuracy of Spatial Databases edited by M. F. Goodchild and S. Gopal, London: Taylor & Francis, ISBN 0-85066-847-6, pp35-43.

Wang, P., 1998. Applying Two Dimensional Kalman Filtering on Digital Elevation Models, International Archives of Photogrammetry and Remote Sensing, 32, Part 4, pp649-656.

Wang, P., J. C. Trinder and S. Han, 1998a: A Two Dimensional Kalman Filtering Approach to Derivation of Terrain Surface Variables, 9th Australian Remote Sensing and Photogrammetry Conference, Proceedings CD-ROM, Volume 1, Paper no. 56, 14 pages.

Wang, P., J. C. Trinder and S. Han, 1998b: DEM Outlier Detection, Identification and Adaptation Using Digital Signal Processing Technology, Proceedings of 39th Australian Surveyors Congress, pp269-276.

Wang, P., J. C. Trinder and S. Han, 1999: A Two-Dimensional Kalman Filtering Algorithm for Terrain Surface Modelling Using Digital Elevation Models, submitted to ISPRS Journal of Photogrammetry and Remote Sensing.

Wang, P., J. C. Trinder and S. Han, 2000: Two-Dimensional Kalman Smoothing for Digital Terrain Modelling, to be published in the International Archives of Photogrammetry and Remote Sensing.

Watson, D. F. and G. M. Philip, 1985: A Refinement of Inverse Distance Weighted Interpolation, Geo-Processing, 2, pp315-327.

Wise, P., 1989: Spaceborne Radar Imagery-Its Acquisition, Processing and Cartographic Applications, Cartography, 18(1), pp9-20.

Wolock, D. M. and G. J. McCade Jr., 1995: Comparison of Single and Multiple Flow Direction Algorithms for Computing Topographic Parameters in TOPMODEL, Water Resources Research, 31(5), pp1315-1324.

Woods, J. W. 1981: Two-Dimensional Kalman Filtering, In: Two-Dimensional Digital Signal Processing I Linear Filter edited by T.S. Huang, Berlin: Springer-Verlag, ISBN 3-540-10348-1.

Woods, J. W. and V. K. Ingle, 1981. Kalman Filtering in Two Dimensions: Further Results, IEEE Transactions on Acoustic, Speech, and Signal Processing, ASSP-29(2), pp188-197.

Woods, J. W. and C. H. Radewan, 1977: Kalman Filtering in Two Dimensions, IEEE Transactions on Information Theory, IT-23(4), pp473-482.

Wu, W. and A. Kundu, 1992: Image Estimation Using Fast Modified Reduced Update Kalman Filter, IEEE Transactions on Signal processing, 40(4), pp915-926.

Xia, Z., 1993: The Uses and Limitations of Fractal Geometry in Digital Terrain Modelling, Ph.D. Dissertation, The City University of New York, New York City.

Xia, Z. and K. C. Clarke, 1997: Approaches to Scaling of Geo-Spatial Data, In: Scale in Remote Sensing and GIS edited by D. A. Quattrochi, M. F. Goodchild, Boca Raton, Fla.: Lewis Publishers, ISBN 1-56670-104-X, pp309-360.

Yoeli, P. 1984: Cartographic Contouring with Computer and Plotter, The American Cartographer, 11(2), pp139-155.

Zhang, W. and D. R. Montgomery, 1994: Digital Elevation Model Grid Size, Representation, and Hydrologic Simulations, Water Resource Research, 40(4), pp1019-1028.

Zevenbergen, L. W. and C. R. Thorne, 1987: Quantitative Analysis of Land Surface Topography, Earth Surface Processes and Landforms, 12, pp47-56.

Zhou, Q., 1992: Relief Shading Using Digital Elevation Models, Computers and Geosciences, 18(8), pp1035-1045.

ADDENDUM

The following comments and additional work have been submitted to satisfy the request by one of the examiners. The examiner's comments are given in *italics*.

1. Alternative methods

There are alternative methods for smoothing errors from a DEM, including wavelets, Fourier Analysis (mentioned on p 45), and commercial software (ANUDEM that utilizes splines complemented by a drainage forcing algorithm), as well as the Helava software that was used in this study. Why were these alternative approached not used and compared?

The 2-D Kalman filtering algorithm has been compared with alternative algorithms such as Horn (1981), Evans (1980), and Heerdegen and Beran's method (1981). However, there are many other methods (see Chapter 2 for a discussion), and it is not relevant to compare the approach developed in this Thesis with each of these. Indeed, this was not considered necessary given that Evans' method is believed to be the 'best' method currently available because it produces more smoothing of terrain attributes than any other of the existing methods (Florinsky 1998). That is why the performance of the new approach developed in this research to implement the 2-D Kalman filtering algorithm was only compared with the Evans method. Moreover, the research presented in this Thesis focused on developing a new terrain-modelling algorithm, not on an evaluation of all terrain modelling/DEM smoothing methods.

2. Derivation of method and formulae

The derivation of methods, and in particular equations, was difficult to follow in the thesis. It is definitely written for mathematically enabled readers (e.g. p 63).

The candidate has attempted to make it as easy as possible to introduce the development of the 2-D Kalman filtering algorithm, such as introducing the theory of one-dimensional (1-D) Kalman filtering in Chapter 3, giving full derivations of the formulae in Chapter 3, 4, 5, and 6, and providing simple examples to illustrate the derivation in Chapter 6. However, the Kalman filter is not easily understood, and the mathematics is even more difficult to follow in the two-dimensional case without a good grounding in mathematics. It is assumed that this research is of primary interest to those working in the field and they are "mathematically enabled". On p 63,

equations 4-27 to 4.29 are the straightforward extension of Eqs. 4-1 to 4-3 to include the second order partial derivatives of elevation by applying basic knowledge of Advanced Algebra as shown below:

$$H(i,j) = H(i-1,j) + H_x(i-1,j)dx + v_{H_b}(i,j) \qquad 4\text{-}1$$

$$H_x(i,j) = H_x(i-1,j) + v_{H_{x_b}}(i,j) \qquad 4\text{-}2$$

$$H_y(i,j) = H_y(i-1,j) + v_{H_{y_b}}(i,j) \qquad 4\text{-}3$$

$$H(i,j) = H(i-1,j) + H_x(i-1,j)dx + \frac{1}{2}H_{xx}(i-1,j)(dx)^2 + v_{H_{bb}}(i,j) \qquad 4\text{-}27$$

$$H_x(i,j) = H_x(i-1,j) + H_{xx}(i-1,j)dx + v_{H_{xbb}}(i,j) \qquad 4\text{-}28$$

$$H_y(i,j) = H_y(i-1,j) + H_{yx}(i-1,j)dx + v_{H_{ybb}}(i,j) \qquad 4\text{-}29$$

Is there a circular argument in Section 6.3, Eqs 6-3 to 6.7?

No, the argument is not circular. Explained in another way, the *Theorem* is that if all measurements have been used twice in least squares estimation, the estimated values will be the same, and their variance-covariance matrix will be scaled by a factor of ½.

Proof:

If the observation is used once:

$$v = A\delta x - l \qquad 1$$

$$\delta x' = (A^T P A)^{-1} A^T P l \qquad 2$$

$$D_x' = (A^T P A)^{-1} \qquad 3$$

where v is the residual, A is the design matrix, $\delta x'$ is the estimate and D_x' is the associated variance- covariance matrix, P is the variance of observation, and l is the observation.

If the observations is used twice:

$$\begin{bmatrix} v \\ v \end{bmatrix} = \begin{bmatrix} A \\ A \end{bmatrix} \delta x'' - \begin{bmatrix} l \\ l \end{bmatrix} \qquad 4$$

$$\delta x'' = \left\{ \begin{bmatrix} A \\ A \end{bmatrix}^T \begin{bmatrix} P & 0 \\ 0 & P \end{bmatrix} \begin{bmatrix} A \\ A \end{bmatrix} \right\}^{-1} \begin{bmatrix} A \\ A \end{bmatrix}^T \begin{bmatrix} P & 0 \\ 0 & P \end{bmatrix} \begin{bmatrix} l \\ l \end{bmatrix} \qquad 5$$

$$= (A^T P A)^{-1} A^T P l$$

$$D_x^{"} = \left\{ \begin{bmatrix} A \\ A \end{bmatrix}^T \begin{bmatrix} P & 0 \\ 0 & P \end{bmatrix} \begin{bmatrix} A \\ A \end{bmatrix} \right\}^{-1} \qquad 6$$
$$= \frac{1}{2}\left(A^T P A\right)^{-1}$$

where $\delta x^{"}$ is the estimate and $D_x^{"}$ is the associated variance- covariance matrix.

Based on Eqs. 1-6, the following equations can be derived:

$$\delta x^{"} = \delta x^{'} \qquad 7$$

$$D_x^{"} = \frac{1}{2} D_x^{'} \qquad 8$$

The application of the above *Theorem* forms the basis of the work presented in Section 6.3.

3. Hypothesis

Why are no research hypotheses proposed in the Introduction?

The 2-D Kalman filtering algorithm developed in this research consists of three parts which are based on different assumptions. If the assumptions for the three parts were given in the Introduction, it may cause confusion and might also be difficult to follow. Therefore, in the Thesis the assumptions of the 2-D Kalman filtering algorithm were introduced where they are most relevant, that is at each step of the algorithm development (the beginning of Chapters 4, 5, and 6) in order to make these more easily understood.

Some hypotheses are described but are not properly formulated (e.g. p 84).

Only two (not *some*) hypotheses have been used in this research for outlier which were formulated as the following equations on p 84, according to the theory of binary hypothesis testing:

$$\boldsymbol{H}_0 : \quad m = 0 \quad with \quad p_0(L(i,j)) \sim N(0, \quad 1) \qquad 5\text{-}14$$

$$\boldsymbol{H}_1 : \quad m = \delta \neq 0 \quad with \quad p_\delta(L(i.j)) \sim N(\delta, \quad 1) \qquad 5\text{-}15$$

where δ is a variable.

The synthesis (Introduction and Conclusion) list the main results, but do not summarize the work in the thesis in a coherent whole, nor show how the work contributes to the development of DEM derivation.

In section 1.5 (Chapter 1), a summary of 2-D Kalman filtering algorithm is presented. The three parts of the Kalman filtering algorithm to be developed, i.e. 2-D Kalman filter, outlier detection and removal, and Kalman smoother, were generally introduced together. In section 8.2 (Chapter 8), the contributions of the Kalman filtering algorithm to digital terrain modelling technique are given. Since the method proposed in the Thesis is a new modelling approach, compared with existing terrain modelling methods, the discussion focused on its unique way of establishing the terrain models, its capability to detect outliers, as well as its functionality for smoothing.

4. Dealing with outliers

During data acquisition, errors in the DEM caused by the presence of trees cannot be differentiated from rock outcrops. Are rock outcrops treated as outliers in the thesis? Are rock outcrops actually errors?

Outliers in this study refer to the outliers in the DEM observations, and may also refer to some specific DEM points, which may significantly effect the accuracy of DEM applications. For example, in the Katoomba DEM, where an isolated tree exists, the corresponding DEM points represent the height of the isolated tree, but not real terrain elevation. If these DEM points are used to compute gradients, slope and aspect of the terrain surface, the results obviously will be erroneous. In order to compute correct terrain variables, these isolated trees should be detected and removed. Hence they are treated as outliers. Whether a specific DEM point is an outlier should be based on DEM application. If the Katoomba DEM is not used to compute terrain attributes in this thesis, for example, identifying the height of isolated trees. The isolated trees would be the most important information in a DEM, and should not be removed. They do not constitute outliers.

The Blue Mountain DEM used in the thesis covers a 1320m by 1060m mapping area. Using photogrammetric means, the rock outcrops were not observed. They were not significant compared with isolated trees in this particular mapping area. Therefore, no special consideration was given in processing rock outcrops using the

Katoomba DEMs. If rock outcrops were significantly observed in the Katoomba DEMs, then further analysis of the characteristics of the outcrops and their impact on the derivation of terrain variables would need to be undertaken prior to determining whether or not they constitute outliers.

As the Blue Mountains area is forested, and the ground surface cannot be seen through the trees, why were there not more outliers?

The results of the 2-D Kalman filter depend on the quality of the input DEM data. Over forest or vegetation covered terrain, where the ground surface cannot be seen through the vegetation, the accuracy of the 2-D Kalman filter algorithm would not be high, for it cannot provide additional information than the input DEM does not contain. Under such circumstances, it is suggested that active sensors such as laser or radar (as mentioned in Section 2.1.1) be applied for DEM generation. The suitability of the 2-D Kalman filter over DEMs, generated using active sensors, needs to be further investigated but this lies beyond the scope of this research.

Why was a theoretical surface used to test the algorithm in all Chapters, except for Chapter 7 (a weak justification is given on p 66)? It would be appropriate to check the proposed Kalman Filtering methods using a real DEM.

In this Thesis, both real and simulated DEMs were used to test the algorithm. Real DEM data for the Katoomba area was used in Chapter 7, and the simulated DEMs were used in Chapters 4, 5 and 6. Using simulated data, rather than real data, to investigate the characteristics of a new algorithm is a usual way of proceeding in this kind of research. It is much easier to obtain the ground truth of terrain variables, not only elevation but also gradient, slope and aspect of each DEM point, from a simulated surface than a real terrain surface. They are very helpful in evaluating the accuracy of the 2-D Kalman filtering and other terrain modelling methods. This is described clearly on p 66.

Only one case study was used – this is surprising given the wide range of topographic landscapes, and the potential for the results to be an artifact of the data set used. In other words, there is concern that the results are empirical.

The primary objective of the research, and hence the most important contribution of this Thesis is the development of a new terrain modelling algorithm

using 2-D Kalman filtering technique. The results of experiments using simulated and real DEM data presented in the Thesis clearly show that the algorithm is better than the 'best' existing terrain modelling methods. The flexibility and reliability of the algorithm when applied to different landscapes is a very important issue, but is beyond the scope of this research and is left for further study. Some suggestions for further research are given in Chapters 4 and 8. An example is developing adaptive Kalman filters.

5. Error and testing of the Kalman Filter against the Evans method

There were no field checks of actual errors in the DEM. Field checked data points should be used to calculate error in the DEM. The improvement, if any, using the proposed Kalman filter should be reported. The candidate should answer the question whether the outliers are really outliers (see previous comments).

Field survey is not the only way of evaluating an algorithm. In this research, it would be very expensive and impractical, considering the testing area is 1320m by 1060m with appropriate sampling interval of 5m by 5m. In practice, there are alternative ways of evaluating algorithms, such as using data of higher accuracy as a basis for comparison, i.e. ground truthing to investigate the 'relative' improvements of algorithms. In this Thesis, the evaluation of the 2-D Kalman filtering algorithm with the Evans method was conducted using such an alternative approach. This indicated the 'relative' not 'absolute' improvement of Kalman filtering over the Evans method. It used DEMs for the same mapping area but at different resolutions, such as 5m (more accurate) and 10m (less accurate). The most accurate data (e.g. 5m DEM) were used as the basis for comparing the results of the two methods derived from the same data (e.g. 10m DEM). In this way, the comparison indicates 'relative' not the absolute improvement of one method against the other method. Whether a DEM point is an outlier or not is not only based on the accuracy of the observation of the point, but also based on DEM applications.

Variance is a measure of precision, not of accuracy. Normally scientists and engineers are more interested in differences in accuracy, not precision.

Accuracy *is* more interesting than precision in this research. Investigating the accuracy of an algorithm needs 'true' values as a basis for comparison. How are true values of terrain variables obtained? Field survey is one way of obtaining the 'true'

values of terrain variables but, as discussed above, that was impracticable in this research. Following the recommendations of Kubik (1985), the suitable DEM sampling spacing, which may accurately represent the landscape of the Katoomba area, is 5m. So it is appropriate to use 5m Katoomba DEM as the basis for testing to evaluate the accuracy of the terrain modelling results of the 10m Katoomba DEM in this research. Besides testing accuracy using real DEMs, artificial DEMs were also simulated for the algorithm testing, for which the real surfaces of terrain variables are known.

Even though the candidate consistently states the Kalman filter is more accurate, accuracy is not calculated. There is no statistical test of accuracy in the Thesis. Thus it is not possible to conclude that the Kalman filter is statistically different (see pp 66, 71,72, etc.). The efficiency of the Kalman filter technique is claimed to be higher than the other method, though this is never tested, and no data or results are presented to justify this conclusion (pp 137,148)

The accuracy of the Kalman filtering algorithm has been tested adequately in the following parts of Chapters 4, 5, 6 and 7:

1. The accuracy of Kalman filtering algorithm and the Evans method for random noise reduction over the simulated noisy DEM, against the true smoothing DEM in Section 4.5;
2. The accuracy of Kalman filtering algorithm for outlier detection and removal over the simulated noisy DEM, against the true smoothing DEM in Section 5.5;
3. The accuracy of Kalman smoother and filter over the simulated noisy DEM, against the true smoothing DEM in Section 6.4;
4. The accuracy of Kalman filtering algorithm for random noise reduction over the 10m Katoomba DEM, against the 5m Katoomba DEM for random noise reduction in Section 7.3;
5. The accuracy of Kalman filtering algorithm for outlier detection and removal over the 10m and 5m Katoomba DEM, against the photogrammetry means in Section 7.4;
6. The accuracy of Kalman smoother and filter over the 10m Katoomba DEM, against the 5m Katoomba DEM in Section 7.5.

   The conclusions were derived based on the above accuracy analysis.

The candidate should repeat the statistical testing (confirmatory tests) using acceptable methods, and rewrite the discussion and conclusions so that they reflect the actual results obtained.

The statistical testing used in the thesis is appropriate.

6. Assumptions of the Kalman Filter

The assumptions of the Kalman filter are not discussed in details. For example, one assumption that the input should be independent – is not met because DEM data exhibit spatial autocorrelation (pp35, 36). The assumption should be critically evaluated against the experimental set-up results.

The Kalman filtering algorithm is developed based on the comprehensive analysis of DEM characteristics, and the investigation of the limitations of current terrain modelling methods (see Chapter 2), which quite clearly are not experimental set-up results. The topographic relationship between DEM neighbouring points is related, and can be estimated and modelled. That is why terrain models can be established in Section 4.1. However, the noise of every DEM measurement can be assumed to be independent for it may be caused by various sources. The Kalman filter requires measurement noise to be independent (see pp 35 and 36), and the DEM application satisfies the requirement of the Kalman filter. In the view of t candidate, there is no conflict.

A discussion of the theoretical and practical advantages and disadvantages of the Kalman filter should be added, and the synthesis appropriately updated.

The theoretical and practical advantages and disadvantages of the Kalman filtering technique have been fully investigated in this research, and the details were presented throughout the Thesis, for example in Sections 3.3, 3.4, 3.5, 4.1, 4.3, 4.4, 5.1, 5.4, 6.1, and 6.3.

7. Statistical tests

Chapter 5 does not appear to be a contribution to the statistical literature, as claimed in the Introduction. The Chapter uses t-test and central limit theory to define the significance of the data range for the DEM data. If there is originality to the approach, then the originality should be described.

This is the first time, to the candidate's author's knowledge, that the method of DEM outlier detection and removal is developed, and it is also the first time that the reliability of detection has been investigated. The strength of the Thesis lies in the *originality* of the approach adopted in the research. Chapter 5 is one of the three new contributions developed in this thesis to the technology of digital terrain modelling.

References cited

Evans, I S (1980), An integrated system of terrain analysis and slope mapping, *Zeitschrift für Geomorphologie*, 36, 274-295.

Horn, B K P (1981), Hill shading and the reflectance map. *Proceedings of the Institute of Electrical and Electronics Engineers*, 69, 14-47.

Florinsky, I V (1998), Accuracy of local topographic variables derived from digital elevation models. *International Journal of Geographical Information Science*, 12(1), 47-61.

Heerdegen, R G and M A Beran (1981), Quantifying source areas through land surface curvature and shape, *Journal of Hydrology*, 57(4), 359-373.

Kubik, K (1985), Recommended procedures for data capture and processing, Report 2, *Digital Elevation Model Data Base for Queensland* (Internal Report).

Publications from the

SCHOOL OF SURVEYING AND SPATIAL INFORMATION SYSTEMS
(formerly: SCHOOL OF GEOMATIC ENGINEERING)

THE UNIVERSITY OF NEW SOUTH WALES
ABN 57 195 873 179

To order, write to:
Publications Officer, School of Surveying and Spatial Information Systems
The University of New South Wales, UNSW SYDNEY NSW 2052, AUSTRALIA

NOTE: ALL ORDERS MUST BE PREPAID. CREDIT CARDS ARE ACCEPTED.
SEE BACK PAGE FOR OUR CREDIT CARD ORDER FORM.

MONOGRAPHS

Australian prices include postage by surface mail and GST.
Overseas prices include delivery by UNSW's air-lifted mail service (~2-4 weeks to Europe and North America).
Rates for air mail through Australia Post on application.

(Prices effective October 2001)

		Price Australia (incl. GST)	**Price** Overseas
M1.	R. S. Mather, "The Theory and Geodetic Use of some Common Projections", (2nd edition), 125 pp, 1978.	$ 16.50	$ 15.00
M2.	R. S. Mather, "The Analysis of the Earth's Gravity Field", 172 pp, 1971.	$ 8.80	$ 8.00
M3.	G. G. Bennett, "Tables for Prediction of Daylight Stars", 24 pp, 1974.	$ 5.50	$ 5.00
M4.	G. G. Bennett, J. G. Freislich & M. Maughan, "Star Prediction Tables for the Fixing of Position", 200 pp, 1974.	$ 8.80	$ 8.00
M8.	A. H. W. Kearsley, "Geodetic Surveying", 96 pp, 1988.	$ 13.20	$ 12.00
M11.	W. F. Caspary, "Concepts of Network and Deformation Analysis", 183 pp, 2000.	$ 27.50	$ 25.00
M12.	F. K. Brunner, "Atmospheric Effects on Geodetic Space Measurements", 110 pp, 1988.	$ 17.60	$ 16.00
M13.	B. R. Harvey, "Practical Least Squares and Statistics for Surveyors", (2nd edition, reprinted with corrections), 319 pp, 1998.	$ 33.00	$ 30.00
M14.	E. G. Masters and J. R. Pollard (Eds.), "Land Information Management", 269 pp, 1991. (Proceedings LIM Conference, July 1991).	$ 22.00	$ 20.00
M15/1	E. G. Masters and J. R. Pollard (Eds.), "Land Information Management - Geographic Information Systems - Advance Remote Sensing Vol. 1", 295 pp, 1993 (Proceedings of LIM & GIS Conference, July 1993).	$ 33.00	$ 30.00
M15/2	E. G. Masters and J. R. Pollard (Eds.), "Land Information Management - Geographic Information Systems - Advance Remote Sensing Vol. 2", 376 pp, 1993 (Proceedings of Advanced Remote Sensing Conference, July 1993).	$ 33.00	$ 30.00
M16.	A. Stolz, "An Introduction to Geodesy", 2nd extended edition, 148 pp, 2000.	$ 24.20	$ 22.00
M17.	C. Rizos, "Principles and Practice of GPS Surveying", 565 pp, 1997.	$ 46.20	$ 42.00

UNISURV REPORTS - S SERIES

(Prices effective October 2001)

Australian Prices *:	S8 - S20		$11.00
	S29 onwards	Individuals	$27.50
		Institutions	$33.00
Overseas Prices **:	S8 - S20		$10.00
	S29 onwards	Individuals	$25.00
		Institutions	$30.00

* Australian prices include postage by surface mail and GST.

** Overseas prices include delivery by UNSW's air-lifted mail service (~2-4 weeks to Europe and North America). Rates for air mail through Australia Post on application.

S8. A. Stolz, "Three-D Cartesian Co-ordinates of Part of the Australian Geodetic Network by the Use of Local Astronomic Vector Systems", Unisurv Rep. S8, 182 pp, 1972.

S14. E. G. Anderson, "The Effect of Topography on Solutions of Stokes' Problem", Unisurv Rep. S14, 252 pp, 1976.

S16. K. Bretreger, "Earth Tide Effects on Geodetic Observations", Unisurv S16, 173 pp, 1978.

S17. C. Rizos, "The Role of the Gravity Field in Sea Surface Topography Studies", Unisurv S17, 299 pp, 1980.

S18. B. C. Forster, "Some Measures of Urban Residential Quality from LANDSAT Multi-Spectral Data", Unisurv S18, 223 pp, 1981.

S19. R. Coleman, "A Geodetic Basis for Recovering Ocean Dynamic Information from Satellite Altimetry", Unisurv S19, 332 pp, 1981.

S29. G. S. Chisholm, "Integration of GPS into Hydrographic Survey Operations", Unisurv S29, 190 pp, 1987.

S31. J. Soetandi, "A Model for a Cadastral Land Information System for Indonesia", Unisurv S31, 168 pp, 1988.

S33. R. D. Holloway, "The Integration of GPS Heights into the Australian Height Datum", Unisurv S33, 151 pp, 1988.

S35. B. Merminod, "The Use of Kalman Filters in GPS Navigation", Unisurv S35, 203 pp, 1989.

S36. A. R. Marshall, "Network Design and Optimisation in Close Range Photogrammetry", Unisurv S36, 249 pp, 1989.

S37. W. Jaroondhampinij, "A Model of Computerised Parcel-Based Land Information System for the Department of Lands, Thailand", Unisurv S37, 281 pp, 1989.

S38. C. Rizos (Ed.), D. B. Grant, A. Stolz, B. Merminod, C. C. Mazur, "Contributions to GPS Studies", Unisurv S38, 204 pp, 1990.

S39. C. Bosloper, "Multipath and GPS Short Periodic Components of the Time Variation of the Differential Dispersive Delay", Unisurv S39, 214 pp, 1990.

S40. J. M. Nolan, "Development of a Navigational System Utilizing the Global Positioning System in a Real Time, Differential Mode", Unisurv S40, 163 pp, 1990.

S41. R. T. Macleod, "The Resolution of Mean Sea Level Anomalies along the NSW Coastline Using the Global Positioning System", Unisurv S41, 278 pp, 1990.

S42. D. A. Kinlyside, "Densification Surveys in New South Wales - Coping with Distortions", Unisurv S42, 209 pp, 1992.

S43. A. H. W. Kearsley (ed.), Z. Ahmad, B. R. Harvey and A. Kasenda, "Contributions to Geoid Evaluations and GPS Heighting", Unisurv S43, 209 pp, 1993.

S44. P. Tregoning, "GPS Measurements in the Australian and Indonesian Regions (1989-1993)", Unisurv S44, 134 + xiii pp, 1996.

S45. W.-X. Fu, "A Study of GPS and Other Navigation Systems for High Precision Navigation and Attitude Determinations", Unisurv S45, 332 pp, 1996.

S46. P. Morgan et al, "A Zero Order GPS Network for the Australia Region", Unisurv S46, 187 + xii pp, 1996.

S47. Y. Huang, "A Digital Photogrammetry System for Industrial Monitoring", Unisurv S47, 145 + xiv pp, 1997.

S48. K. Mobbs, "Tectonic Interpretation of the Papua New Guinea Region from Repeat Satellite Measurements", Unisurv S48, 256 + xv pp, 1997.

S49. S. Han, "Carrier Phase-Based Long-Range GPS Kinematic Positioning", Unisurv S49, 185 + xi pp, 1997.

S50. M. D. Subari, "Low-cost GPS Systems for Intermediate Surveying and Mapping Accuracy Applications", Unisurv S50, 179 + xiii pp, 1997.

S51. L.-S. Lin, "Real-Time Estimation of Ionospheric Delay Using GPS Measurements", Unisurv S51, 199 + xix pp, 1997.

S53. D. B. Lemon, "The Nature and Management of Positional Relationships within a Local Government Geographic Information System", Unisurv S53, 273 + xvi pp, 1997.

S54. C. Ticehurst, "Development of Models for Monitoring the Urban Environment Using Radar Remote Sensing", Unisurv S54, 282 + xix pp, 1998.

S55. S. S. Boey, "A Model for Establishing the Legal Traceability of GPS Measurements for Cadastral Surveying in Australia", Unisurv S55, 186 + xi pp, 1999.

S56. P. Morgan and M. Pearse, "A First-Order Network for New Zealand", Unisurv S56, 134 + x pp, 1999.

S57. P. N. Tiangco, "A Multi-Parameter Radar Approach to Stand Structure and Forest Biomass Estimation", Unisurv S57, 319 + xxii pp, 2000.

S58. M. A. Syafi'i, "Object–Relational Database Management Systems (ORDBMS) for Managing Marine Spatial Data: ADCP Data Case Study", Unisurv S58, 123 + ix pp, 2000.

S59. X.-Q. Lu, "Strategies for Improving the Determination of Displacements of Sea Surface Temperature Patterns Using Consecutive AVHRR Thermal Images", Unisurv S59, 209 + xiii pp, 2000.

S60. G. Dickson, "GPS-Controlled Photography: The Design, Development and Evaluation of an Operational System Utilising Long-Range Kinematic GPS", Unisurv S60, 417 + x pp, 2000.

S61. J. Wang, "Modelling and Quality Control for Precise GPS and GLONASS Satellite Positioning", Unisurv S61, 171 + x pp, 2001.

S62. Y. Wang, "Knowledge-Based Road Extraction from Aerial Images", Unisurv S62, 178 + xi pp, 2001.

S63. L. Ge, "Development and Testing of Augmentations of Continuously-Operating GPS Networks to Improve their Spatial and Temporal Resolution", Unisurv S63, 230 + xvi pp, 2001.

S64. H.-Y. Chen, "A Study on Real-Time Medium-Range Carrier-Phase-Based GPS Multiple Reference Stations", Unisurv S64, 182 + xxiv pp, 2001.

S65. G. Y. K. Shea, "A Web-Based Approach to the Integration of Diverse Data Sources for GIS", Unisurv S65, 233 + xv pp, 2001.

S66. M. Mirbagheri, "Analysis of Interferometric SAR for Topographic Mapping", Unisurv S66, 135 + xvii pp, 2001.

S67. P. Wang, "Applying Two-Dimensional Kalman Filtering Techniques to Digital Elevation Models for Terrain Surface Modelling", Unisurv S67, 175 + xi pp, 2001.

Credit Card Orders / Payment

from / to

School of Surveying and Spatial Information Systems

The University of New South Wales

Name and postal address of ordering person/organisation:

_____

_____

_____

_____

_____

Date : _____

Day time phone number : _____

Credit Card debit for:

_____ $ _____

_____ $ _____

_____ $ _____

_____ $ _____

Total $ _____

Please debit my credit card: ☐ Mastercard ☐ Visa ☐ Bankcard

Card Name: _____ Signature: _____

Card No: | | | | | | | | | | | | | | | | Expiry Date : _____

Note: UNSW requires that you attach a photocopy of your credit card to this order.